FACULTY OF ENGINEERING
AND ARCHITECTURE

Design of Textile Antennas and Flexible WBAN Sensor Systems for Body-Worn Localization Using Impulse Radio Ultra-Wideband

Dries Van Baelen

Doctoral dissertation submitted to obtain the academic degree of
Doctor of Electronics and ICT Engineering Technology

Supervisors
Prof. Hendrik Rogier, PhD - Prof. Jo Verhaevert, PhD

Department of Information Technology
Faculty of Engineering and Architecture, Ghent University

April 2021

GHENT
UNIVERSITY

ISBN 978-94-6355-474-9
NUR 959
Wettelijk depot: D/2021/10.500/22

Members of the Examination Board

Chair

Prof. Em. Daniël De Zutter, PhD, Ghent University

Other members entitled to vote

Prof. Jan Doutreloigne, PhD, Ghent University
Prof. Sam Lemey, PhD, Ghent University
Prof. Nobby Stevens, PhD, KU Leuven
Prof. Johanna Virkki, PhD, Tampere University, Finland

Supervisors

Prof. Hendrik Rogier, PhD, Ghent University
Prof. Jo Verhaevert, PhD, Ghent University

Dankwoord

In de afgelopen zes jaren op de universiteit heb ik het genoegen gehad met talloze mensen kennis te mogen maken. Elk ervan heeft op zijn of haar eigen manier een stempel op mijn leven achtergelaten. Het is dan ook niet meer dan op zijn plaats dat zij daar een woord van dank voor verdienen.

In de eerste plaats wens ik mijn promotoren prof. Jo Verhaevert en prof. Hendrik Rogier te bedanken om me de kans te geven om met dit boeiende onderwerp bezig te zijn. Het is niet elke doctoraatsstudent gegund om een dergelijke mate van ondersteuning en betrokkenheid te mogen ervaren gedurende deze afgelopen jaren, waarvoor ik hen dan ook oprecht wil bedanken.

Moreover, I'd like to extend my gratitude to prof. Sam Lemey, prof. Johanna Virkki, prof. Nobby Stevens and prof. Jan Doutreloigne, the members of the examination board, for evaluating my dissertation and for providing their valuable comments that give this extra touch to the work.

In my time, I had the pleasure of being part of a pleasurable and constructive office environment, which in the first place is owed to the people populating it: I'd like to extend my thanks to the following people:

Kamil, who is verily one of the kindest people I know. His admirable work ethic should best be expressed on a logarithmic scale. Nick and Quinten, 'the lads' of the office. They understand the languages of risky humor, so much to my delight. Nicolas, also falling in previous category. I am glad it was him that I could host the DMC labs with. He now lost a bet concerning a dolphin. Laura, for being such a nice about neighbor. I wish you someone with a less chaotic desk structure in front of you in the upcoming years. Jelle, who therefore bears a heavy responsibility. He is probably the best bachelor's student I've counseled and I greatly appreciate his assistance in the last few months. Igor, creator of the finest salads, whose ever positive mind provides sunshine even on the most dreary of days. Seppe, who skipped my every SiSy lesson but then still aced the test with astonishing grades. By the way, it used to be handy to have those two likeminded chaps around if a coffee break discussion wouldn't go my way. Martijn, another man hailing from good soil. Some would describe him as a friendly and nice colleague. Others might opt to depict him as a reference repository in a variety of predominantly most useful information. And of course my *comrade* Olivier, with who I enjoyed so many enlightening discourses in predominant topics such as some war, subcultures from Roeselare, antenna engineering and so much other, though usually rather specific stuff.

Some people were not part of the office, but colored my time at the university, and in doing so, left a warm memory as well. Thank you to Arne, Thomas, Pieter,

Gert-Jan, Duygu, Hossein, Michiel, Simon, Arno, Jinchao and Dries. Among them, some are best not left unchecked in a boardgame. Others are best not left at the controls of the warp. Others are best not left without Gentse Strop, and others should best not be left alone on a folk ball. And then there's just those people who play the blues so well. Well, they all know who I mean.

Verder wil ik ook het overige ZAP van onze onderzoeksgroep bedanken, met name Patrick, Sam, Ann en Dries, voor de aangename samenwerking, hun vele advies en inzichten, of gewoon erg fijne babbels aan de lunchtafel en de koffie-automaat.

Dat sluit dan ook naadloos aan bij de collega's uit mijn tijd op Schoonmeersen. Bedankt aan Jan, voor de ontzettend fijne samenwerking rond Signalen & Systemen en de erg leerrijke en nu ook niet bepaald onaangename studiereizen naar Italië, Polen en Oostenrijk. Bedankt aan Luc, om feitelijk de eerste vonk te slaan voor mijn interesse in antennes, en om de wereld duidelijk te maken dat elektronica rook nodig heeft om te werken. Natuurlijk heb ik ook nog het genoegen om Dimitri, Jan D.B., Matthias, Gianni, Sanne, Maarten, Francis, David, Peter, Kathleen, Nele, Joren, Veronique, Patrick en Johnny te bedanken voor de vreselijk saaie koffie- en lunchpauzes waarvan je wilt dat ze zo snel mogelijk voorbij zijn. Heu ik bedoel, omgekeerd. Een persoon die ook thuishoort in die lijst is mijn spitsbroeder Robbe, een kerel om op te bouwen, maar desalniettemin nog steeds welverdiend recordhouder Dries in slappe lach doen gaan.

Zonder mensen die het nodige *fingerspitzengefühl* aan de dag leggen, geraakt men zelden ver. Daarom wil ik ook graag Matthias, Josse, Peter, Kristien en de mensen van het *A-team* bedanken voor hun bijstand en hun knowhow. Zonder hun bijdrage draait alles mank, en komen tal van praktische realisaties niet eens van de grond.

Ook Bart verdient een ereplaats, hij is de universele elektronicus die me zowat alles geleerd heeft over flexdesign. Zoals hij weet vind ik nog steeds dat we artikels mogen verzamelen voor de eerste editie van de JoID (impact factor 0), en mag de ringvaart om niet nader vermelde redenen gerust nog wat uitgediept worden.

Een dikke merci aan de mensen van Mol, waarmee het allemaal begon. Bedankt Alexander, Jasper, Jakob, Steven, Emiel, Stijn en hun wederhelften, voor al die mooie jaren die begonnen op de schoolbanken, verder gingen op het speelplein, en zich sindsdien feitelijk vooral rond terras, bord- en quiztafels afspelen, als het even kan. Laat ons er nog veel zo'n jaren bij doen.

Bijna dertien jaar Gent begint inmiddels ook te tellen. En die hadden nooit hetzelfde geweest zonder Mathias, Wietse, Ruben en Filip. Bedankt, om op iets meer dan tweewekelijkse basis mee de d20 uit te dagen en zo situaties voor het geestesoog te brengen waarvan het in alle eerlijkheid, het beste is dat ze binnenskamers blijven.

Het beste moet natuurlijk tot laatst gehouden worden. Zo ontzettend veel bedankt aan mijn ouders Jef en Rita, om me gemaakt te hebben tot wie ik ben. Om me al die kansen te geven, om me zo te steunen, maar in de eerste plaats gewoon om zo'n ontzettend fijne en warme mensen te zijn. Even ontzettend veel bedankt aan mijn broer Lieven, al meer dan zesentwintig jaar mijn beste vriend. En daar hoeven geen woorden aan toegevoegd te worden.

En tot slot, op eenzame hoogte staat de belangrijkste van allemaal. Ze is mijn baken en mijn rots in de branding, ze is iemand die me gelukkig maakt, en iemand die ik graag gelukkig maak. In het vakjargon een pracht van een vrouw genoemd. Zonder haar had het allemaal niet hetzelfde geweest. Bedankt om deel te zijn van mijn leven, Paulien. Ik zie u graag.

Gent, maart 2021
Dries Van Baelen

If you're afraid to do it, you shouldn't do it.
If you're doing it, you should not be afraid.

NAAR GHENGIS KHAN

Inhoudsopgave

Samenvatting

Al sinds mensenheugenis draagt de mens een scala aan werktuigen en toestellen met zich mee, die hem in staat stellen zaken uit te voeren die voorheen onmogelijk waren. In recentere tijden zijn elektronische apparaten toegevoegd aan dit assortiment, waarmee waardevolle sensor- en communicatiefunctionaliteiten binnen handbereik kwamen. Niet alleen werden deze apparaten systematisch kosteneffici ënter, maar in de eerste plaats ook kleiner. Een voor de hand liggend voorbeeld daarvan is de walkietalkie, die evolueerde richting de gsm, dewelke op zijn beurt weer vergroeide tot de smartphone. Inmiddels is elektronica dermate geëvolueerd dat het mogelijk is geworden om deze te integreren in tal van alledaagse voorwerpen. Deze kunnen daardoor niet alleen verbonden worden met het internet, maar ze worden er zo ook actief deel van. Dit fenomeen staat bekend als het *Internet of Things (IoT)*, ofwel *internet der dingen*. Het implementeren van sensor- en actuatorfunctionaliteiten in dagdagelijkse objecten en hen vervolgens aankoppelen aan het internet, biedt een schat van mogelijkheden voor tal van sectoren. Men dient zich enkel maar de mogelijkheden in medische, agrarische of industriële sectoren in te beelden om een idee te verkrijgen welke baanbrekende productiviteits- en functionaliteitswinsten deze technologie met zich meebrengt.

Nochtans is het succes van een dergelijk internet der dingen omgekeerd evenredig met de afstand tot diens eindgebruikers. Met andere woorden, het nut en het succes van dergelijke systemen hangt af van de mate waarin, en het gebruiksgemak waarmee eindgebruikers ermee kunnen interageren. *Smart Fabrics and Interactive Textiles (SFIT)*, vrij vertaald naar 'slimme stoffen en interactief textiel' vormen een beloftevolle technologie om deze kloof te overbruggen. In essentie komt dit neer op het toevoegen van functionaliteiten aan textiel door het integreren van elektronische schakelingen. Vooral de slimme stoffen die door de gebruiker gedragen worden, de zogenaamde *proximal textiles*, zijn ideaal geplaatst om waardevolle sensordata op en rond de gebruiker te verwerven, om de gebruiker informatie mee te delen, of om diens wensen en noden door te sturen aan actoren in zijn omgeving.

Desalniettemin blijven er nog tal van uitdagingen bestaan vooraleer de Smart Textile-industrie in staat is om de opschaling door te voeren die vereist is voor een marktdoorbraak. Met aanvaarding door de consument en daarbij ook diens gebruiksgemak in het achterhoofd, horen dergelijke systemen in de eerste plaats op een discrete en comfortabele wijze in de kledingstukken geïntegreerd te worden. Zulke systemen zouden dus ook plooibaar moeten zijn, waarbij rigide onderdelen zoals hardplastieken behuizingen en klassieke printplaten zo veel mogelijk vermeden dienen te worden. Voor tal van werken uit de literatuur is dit momenteel niet het geval: vele publicaties presenteren een rigide systeem met storende

vormfactor, bevestigd aan een stoffen houder, als een draagbaar systeem. Sommige voorgestelde prototypes bevatten nog steeds een aanzienlijk aantal rigide componenten. Nog andere publicaties gaan de flexibiliteitsuitdagingen die komen kijken bij de realisatie van de achterliggende infrastructuur uit de weg, door enkel het textielgedeelte van het systeem te ontwikkelen. Er is een duidelijke nood aan fabricagetechnieken voor de productie van complete flexibele draagbare systemen.

Massaproductie van dergelijke systemen vereist productieprocessen die goedkoop zijn, die machinaal uitgevoerd kunnen worden, en die betrouwbare en nauwkeurige resultaten geven. De afgeleverde eindproducten moeten wasbaar zijn, maar dienen ook bestand te zijn tegen de uitdagende omstandigheden die komen kijken bij het functioneren op een menselijk lichaam. Dit omvat onder meer het behoud van prestatie en het vermijden van beschadigingen als gevolg van bewegingen en vervormingen die eigen zijn aan kledingstukken, zoals buiging, samendrukking en verschuivingen van het kledingstuk ten opzichte van het lichaam. De materialen die gebruikt worden in slimme stoffen moeten bovendien na compressie hun oorspronkelijke vorm terug aannemen. Verder dient de invloed van een variërende luchtvochtigheid op de elektromagnetische materiaaleigenschappen beperkt te blijven en dienen deze eigenschappen nauwkeurig gekarakteriseerd te worden.

Aangezien stroomvoorziening zoals een batterij een groot deel van de in kledij beschikbare massa en plaats inneemt, is het des te meer aangewezen dat slimme draagbare systemen hun beschikbaar vermogen op efficiënte wijze besteden. Het wisselen van batterijen is niet evident in een kledingstuk en in het geval waar de batterij verweven zit in het textiel, zo goed als onmogelijk. Anderzijds vormt het opladen van een dergelijke batterij wel een haalbare kaart, ook al dient dit zo min mogelijk te gebeuren om het gebruiksgemak niet in de weg te staan. De antenne van het slimme draagbare systeem moet zeer efficiënt zijn. Daarom dienen de gebruikte textielmaterialen weinig elektromagnetische verliezen te vertonen, opdat ze door middel van energie-efficiënte antennetopologieën succesvol toegepast kunnen worden tot een efficiënte antenne.

Tot slot worden best antennetopologieën gebruikt die slechts weinig koppeling met het menselijk lichaam ervaren. Dit verzekert de prestaties van de antenne met betrekking tot bijvoorbeeld diens impedantie-aanpassing en stralingspatroon in het geval wanneer deze op het menselijk lichaam gedragen wordt. Daarbij zorgt een lage mate van koppeling er ook voor dat er minder energie verloren gaat aan absorptie in de menselijke weefsels. Dit resulteert niet alleen in het efficiënter functioneren van de antenne, ook de stralingsblootstelling van het lichaam van de gebruiker, meestal gekarakteriseerd door de *Specific Absorption Rate (SAR)*, wordt beperkt. Om aan de opgelijste vereisten tegemoet te komen blijken slotantennes met een achterliggende substraatgeïntegreerde golfgeleidercaviteit (in het Engels: *Substrate Integrated Waveguide (SIW) cavity-backed slot antennas*) erg interessante kandidaten te zijn, in het bijzonder naar koppeling met het menselijk lichaam toe. Ze zullen dan ook uitvoerig ingezet worden doorheen dit proefschrift.

In Hoofdstuk 2 wordt een nieuwe fabricagemethode voorgesteld voor de productie

van mechanisch flexibele, breedbandige SIW-slotantennes, volledig uitgevoerd in textiel. Deze fabricagemethode kan vlot geautomatiseerd worden en leidt tot minder afwijkingen in de uitlijning tussen de verschillende antennelagen. Bovendien zijn er minder productiestappen nodig in vergelijking met eerder gepubliceerde methodes om dergelijke breedbandige slotantennes te realiseren. De op deze manier gefabriceerde slotantennes zijn daarenboven plooibaar en bevatten geen rigide onderdelen, met uitzondering van de voedingspin. Verder resulteren ze in aanzienlijk lichtere antennes met kleinere afmetingen dan de antennes opgebouwd met behulp van de voorgaande fabricagemethodes, dewelke gebruik maken van rigide metalen zeilogen. Tot slot is dit fabricageproces geschikt voor het realiseren van grote geleidende textieloppervlakken en veroorzaakt het geen samendrukking van het substraat, zoals wel het geval is bij sommige fabricageprocessen gebaseerd op borduren. Als voorbeeld is een prototype gefabriceerd voor alle *unlicensed national information infrastructure (UNII)*-radiobanden. Dit prototype dekt de vereiste impedantiebandbreedte van 5.15 GHz tot 5.85 GHz volledig af, waardoor het gekwalificeerd wordt als ultrabreedbandige antenne (UWB-antenne). Daarbij vertoont deze een antennewinst groter dan 5.5 dBi en een stralingsefficiëntie groter dan 70 % over de gehele frequentieband. De belangrijkste troef is de geschiktheid om gedragen te worden op het menselijk lichaam, gezien zowel zijn stralingspatroon als zijn impedantie-aanpassing behouden blijven wanneer het prototype op de torso of de rechterbovenarm gedragen wordt. Dit geldt bovendien ook wanneer de antenne in de vrije ruimte gebogen wordt over tal van kromtestralen voorkomend op het menselijk lichaam. Zoals in het algemeen ook verwacht kan worden van antennetopologieën gebaseerd op een caviteit, kan geconcludeerd worden dat de koppeling van deze antenne met het menselijk lichaam inderdaad beperkt is.

In Hoofdstuk 3 wordt dit fabricageproces toegepast op een breedbandige slotantenne voor lokalisatie met behulp van impulsradio-ultrabreedband *(Impulse Radio Ultra-Wideband (IR-UWB))*. De antenne is ontworpen voor de kanalen 2 en 3 van de IEEE802.15.4a-standaard, die zich respectievelijk uitstrekken van 3744 MHz tot 4243.2 MHz en van 4243.2 MHz tot 4742.4 MHz. Voor een antenne voor lokalisatie, dienen oriëntatie-afhankelijke antenneparameters zoals de pulsvervorming en de verschuiving van het fasecentrum van de antenne geminimaliseerd te worden. De pulsvervorming wordt gekwantificeerd door de System Fidelity Factor (SFF), waarbij een te lage SFF een nauwkeurige ontvangst van het signaal in de weg staat. De verschuiving van het fasecentrum veroorzaakt een lokalisatiefout (*Distance Estimation Error (DEE)*) als gevolg van een faseverschil (en daardoor ook tijdsverschil) op het signaal toekomend bij de ontvanger. Het antenne-ontwerp voorgesteld in dit hoofdstuk voldoet aan beide doelstellingen voor alle oriëntaties relevant voor positiebepaling. De SFF ligt boven de voor lokalisatiescenario's gangbare grens van 90%, terwijl de DEE kleiner is dan 10 cm, hetgeen impliceert dat de lokalisatiefout geïntroduceerd door de antenne kleiner is dan de lokalisatiefout veroorzaakt door commerciële lokalisatie-IC's zoals de DW1000. De metingen tonen aan dat de impedantie-aanpassing en het stralingspatroon van de antenne stabiel zijn in tal van scenario's: op de torso of de rechterbovenarm, of

in de vrije ruimte gebogen over op het menselijk lichaam courant voorkomende kromtestralen. Bij de kleinste kromtestraal van 4 cm dekte de antenne niet meer de volledige band af. De antenne is met andere woorden geschikt om op het lichaam gedragen te worden. IR-UWB-lokalisatiesignalen zijn zeer resistent tegen multipadeffecten en vertonen bovendien een aanzienlijke lokalisatienauwkeurigheid. Gezien UWB-signalen op de frequenties die voorgeschreven worden door de IEEE802.15.4-standaarden bovendien ook doorheen muren propageren, is de technologie uitermate geschikt voor lokalisatie binnenhuis. Bovendien werkt IR-UWB-lokalisatie door afstandsmetingen uit te voeren tussen modules onderling. Hierdoor is er geen vaste externe lokalisatie-infrastructuur nodig indien enkel de afstand tussen deze modules bepaald dient te worden.

De metingen van de SFF en de DEE zijn beschreven in Hoofdstuk 4, door de transferfunctie te meten van het systeem bepaald door twee prototypes van deze antenne en het tussenliggende kanaal. Voor alle voor positiebepaling relevante oriëntaties voldoen de SFF en de DEE aan de eerder geformuleerde criteria voor IR-UWB-positiebepaling. De belangrijkste bijdrage van Hoofdstuk 4 is echter de integratie van een volledige en flexibele sensormodule op de achterkant van deze antenne, die de implementatie van IR-UWB-lokalisatie-elektronica en andere sensoren in op het menselijk lichaam gedragen textiel aantoont, en dit door de integratie van componenten zoals een eenvoudige temperatuurs-, luchtvochtigheids- en luchtdruksensor en het complexere DW1000-lokalisatie-IC op de achterzijde van de antennecaviteit. De sensormodule is uitgevoerd op een flexibel polyimidesubstraat en heeft dezelfde afmetingen als de antenne, hetgeen discrete en draagbare integratie in kledij faciliteert. Door de transceiver van de DW1000, die het voedende element van de antenne is, in continuegolfmodus te plaatsen, werd aangetoond dat het vermogenspatroon van de sensormodule van dezelfde vorm is als het stralingspatroon van de alleenstaande textielantenne. Het integreren van een PCB op de achterkant van de antenne heeft een beperkte invloed op diens stralingspatroon. Als gevolg van het directieve stralingspatroon van de antenne en schaduweffecten veroorzaakt door het lichaam van de drager, is het echter onmogelijk om met behulp van slechts één sensormodule lokalisatie in alle richtingen rondom de gebruiker mogelijk te maken. Om dit te realiseren moet het sensorsysteem op minstens zes verschillende posities rondom het lichaam van de gebruiker geplaatst worden. In een worstcasescenario waar het systeem 16 pakketten per seconde verzendt, voorziet een flexibele batterij van 5 V en 200 mAh het systeem van een gebruiksautonomie van 13.3 uur, zonder de slaapmodus van eender welke component te benutten. Dit is een pessimistische waarde, aangezien vermogensbesparende maatregelen de gebruiksduur van het systeem nog gevoelig kunnen verhogen. Voorbeelden hiervan zijn het gebruik van de slaapmodus van de verschillende componenten en het implementeren van UWB-MAC-protocollen die de UWB-radio periodiek uitschakelen. Deze sensormodule kan dus toegepast worden als een draagbaar lokalisatiesysteem, geschikt voor de integratie in op het lichaam gedragen textiel.

Summary

Since time immemorial, man has been carrying tools and devices to perform tasks that would otherwise be beyond its reach. In the most recent era, electronic appliances have joined this group, adding valuable sensing and communication capabilities. These devices systematically became not only more cost-effective, but in particular, smaller, as for example walkie talkies became cell phones, which on their turn transformed into smartphones. Electronics have evolved to a degree where they can be integrated in a plethora of everyday objects, and where these can be connected to the internet, making them an active participant in it. This phenomenon is better known as the Internet of Things (IoT). Implementing sensing and actuating functionalities into everyday objects and connecting them to the internet indeed offers nigh boundless possibilities for many sectors, since one should only imagine opportunities in the medical sector or in industry to recognize the groundbreaking productivity and functionality gains.

The success of such an internet of things on the other hand is directly related to its proximity to its end users, together with the ability of these end users to interact with it. A promising candidate technology to bridge this gap is the use of smart fabrics and interactive textiles (SFIT), which essentially involves the enhancement of functionalities offered by textile by the integration of electronics. In particular, textiles that are worn by the user are in pole position to collect sensor data on and immediately around a human person, to pass on information to the user, and to convey the user's needs or wishes to actors in its environment.

However, numerous challenges remain before the smart textile industry can perform the scale-up necessary for a broad market breakthrough. First of all, keeping consumer adoption and ease of use in mind, such systems should be integrated in the garment in an unobtrusive and comfortable way. They should be mechanically flexible, and therefore, they should avoid stiff segments such as rigid plastic casings or classic printed circuit boards. Many systems presented in literature as a wearable do not meet this goal, as many works consist of a lumpy rigid device affixed to a textile brace. In some works, the proposed prototype still contains a notable amount of rigid segments. Other authors only realize the flexible, textilized part, whereby the flexibility challenges encountered in the realization of the backbone are evaded. This only exemplifies the still existing need for manufacturing techniques that lead to flexible, wearable systems.

Mass production of such systems requires production processes that are cheap, machinable, and that provide reliable and accurate results. The fabricated end products should not only be washable, they also need to be robust and resilient against the hardships involved with body-deployed operation. Bending, compres-

sion and shifting of the system are commonplace in such circumstances, and should not impede proper operation of the system. Furthermore, the materials used in smart textile design need to recover from compression, they should experience little influence from varying air humidity levels, and they should have well-characterized electromagnetic properties.

Smart wearable systems should be power-efficient, since battery infrastructure takes up a large portion of a body-worn system's mass and space budget. On the other hand, battery exchanging procedures are difficult on a garment and, if the battery is sufficiently interwoven with the garment, probably impossible. Battery recharging, on the other hand, is feasible but its frequency should be kept to a minimum to improve ease of use. Nevertheless, the goal for the antenna part of the smart wearable to be highly efficient remains intact. Therefore, the selected textile materials should be low-loss, so that energy-efficient antenna topologies may be applied to good results.

Finally, antenna topologies should be chosen that exhibit a low coupling with the human body. This asserts the performance of the antenna in body-worn scenarios, with respect to its radiation pattern and impedance matching. Furthermore, such antennas experience significantly less effect from the deployment position or the morphology of the body they are worn on. Also, a low coupling between the antenna and the body implies a reduction in the amount of energy lost to human body tissues. This not only increases the antenna's efficiency in practice, but it also assists in achieving the goal of reducing the dose of radiation absorbed by the wearer's body (as is often characterized by the specific absorption rate (SAR)). To meet these listed requirements, cavity-backed slot antennas implemented in Substrate Integrated Waveguide (SIW) technology prove to be most interesting candidates, particularly in regard with coupling to the human body. They will be employed extensively throughout this dissertation.

In Chapter 2, a novel fabrication method for the manufacturing of mechanically flexible, all-textile cavity-backed slot antennas has been proposed. The fabrication method is machinable, significantly reducing the opportunities for misalignments in comparison with manufacturing processes presented in literature. Furthermore, fewer fabrication steps are required with respect to these methods. Cavity-backed slot antennas realized in this way are mechanically flexible and contain only the antenna feed as rigid part. Furthermore, they require a smaller footprint and are more lightweight in comparison with manufacturing methods employing rigid metal eyelets as vertical SIW cavity structures. Moreover, the manufacturing process is suitable for the implementation of large conductive surfaces, and it incurs no substrate compression, as opposed to some manufacturing techniques relying on embroidery. As a demonstration, a prototype has been fabricated for operation in all unlicensed national information infrastructure (UNII) radio bands. The prototype covers the required impedance bandwidth from 5.15 GHz to 5.85 GHz and therefore qualifies as an ultra-wideband antenna. It exhibits a gain larger than 5.5 dBi and a radiation efficiency of at least 70% over the entire frequency band.

The antenna's main asset is its suitability for body deployment, as both its radiation pattern and its impedance bandwidth are maintained when on the torso or the upper arm, or when the antenna deployed in free space is bent over several radii commonly encountered on the human body. Therefore it can be concluded that the coupling with the human body is indeed low, as can generally be expected from the cavity topology.

In Chapter 3, this production process has been applied to design a cavity-backed slot antenna for localization through impulse-radio ultra-wideband (IR-UWB) in Channel 2 and Channel 3 of the IEEE802.15.4a standard (3744 MHz - 4243.2 MHz and 4243.2 MHz - 4742.4 MHz, respectively). To qualify for positioning, the antenna's orientation-specific parameters such as its pulse deformation and its phase center shift need to be minimized. The former impedes proper and accurate reception of the signal, whereas the latter gives rise to a distance estimation error as a result of phase (and therefore time) shifts of the incoming pulse (DEE). The antenna design meets the goals for both, for all relevant orientations: the pulse deformation is quantified by the System Fidelity Factor (SFF), which is larger than the 90% commonly required for localization. The antenna's DEE is lower than 10 cm, which implies that the localization error introduced by the antenna remains smaller than the error caused by commercial localization IC's such as the DW1000. The impedance matching and the radiation pattern of the antenna have been measured to remain stable in diverse body deployment scenarios, such as when deployed on the torso or upper right arm of a test person, or when the antenna has been bent in free space over bending radii commonly found on the human body. Only when subjected to the smallest bending radius (i.e. $r = 4$ cm), the intended UWB band is no longer fully covered. Concluding, this antenna qualifies for use in a body deployment scenario. IR-UWB is a most desirable technology for body-worn localization, as it offers an excellent localization accuracy and it exhibits a high immunity to multipath effects. Since UWB signals at the frequencies prescribed in IEEE802.15.4 also propagate through walls, the technology is particularly suitable for indoor localization. Moreover, IR-UWB localization operates through ranging with other nodes, so it requires no external fixed localization infrastructure if only the distance to other nodes is to be determined.

The SFF and DEE of this antenna have been measured in Chapter 4 by acquiring the transfer function of the system composed by two prototypes of the aforementioned antenna, combined with the free space channel in between them. For all orientations relevant to body-worn positioning, the resulting SFF and DEE comply to the goals for localization stated earlier, thereby acknowledging the suitability of the antenna for IR-UWB localization purposes. The main contribution of Chapter 4 however, is the integration of a comprehensive, mechanically flexible sensor node on the back side of the antenna, which acts as a proof of concept for the implementation of IR-UWB localization electronics and other sensors in body-worn textile. This is demonstrated by the integration of components such as a basic temperature, air pressure and relative humidity sensor, and the more complex DW1000 localization IC to the back side of the antenna cavity. The sensor node is realized

on a mechanically flexible polyimide substrate and has the same dimensions as the textile antenna, which allows for unobtrusive and wearable integration of the system into body-worn textiles. The transceiver of the DW1000 forms the feeding element of the antenna. By configuring it in continuous wave mode, it is revealed that the power pattern of the sensor system is very similar to the radiation pattern of the standalone antenna. Hence, the radiation characteristics of the antenna experience very little influence from the presence of the PCB on the antenna's back side. However, due to the directive radiation pattern and the body shadowing effect, one single sensor node is unable to provide localization coverage in all directions around the user. To obtain this, the sensor system should be deployed on at least six locations around the wearer's body. In a worst-case testing scenario where the system transmits 16 packets per second, a 5 V, 200 mAh flexible battery provides the system an autonomy of 13.3 hours, even without the use of any component's sleep mode. This is a pessimistic value, since the application of power saving measures such as sleep modes and the implementation of UWB MAC protocols which periodically disable the UWB radio can significantly raise the autonomy of the system. Given this, it can be concluded that this sensor system is suitable for localization through IR-UWB, and that it acts as a proof-of-concept for the integration of electronics into body-worn textiles.

List of Abbreviations

5G	Fifth-generation
DC	Direct current
DEE	Distance estimation error
DoP	Dilution of precision
ECG	Electrocardiogram
EMC	Electromagnetic compatibility
ENIG	Electroless nickel plated gold
FTBR	Front-to-back ratio
GNSS	Global navigation satellite system
GPS	Global positioning system
IC	Integrated circuit
IEEE	Institute of electrical and electronics engineers
IoT	Internet of things
IR-UWB	Impulse radio ultra-wideband
IRS	Internal revenue service
MAC	Medium access control
PC	Personal computer
PCB	Printed circuit board
PDA	Personal digital assistant
RF	Radio-frequency
RFID	Radio frequency identification
RSSI	Received signal strength indicator
SAR	Specific absorption rate
SDS-TWR	Symmetric double-sided two-way ranging
SFF	System fidelity factor
SFIT	Smart fabrics and interactive textiles
SIW	Substrate integrated waveguide
SMA	SubMiniature version A
SPI	Serial peripheral interface
TDoA	Time difference of arrival
ToA	Time-of-arrival
TWR	Two-way ranging
UART	Universal asynchronous receiver-transmitter
UHF	Ultra-high frequency
UNICEF	United nations children's fund
UNII	Unlicensed national information infrastructure

UWB	Ultra-wideband
VLC	Visible light communication
WBAN	Wireless body-area network
WiPos	Wireless positioning
WPT	Wireless power transfer
WSN	Wireless sensor network

List of Symbols

$\|.\|$	Modulus of a complex number
$\Omega/\square$	Ohm per square
r	Bending radius
α	Angle between user anterior direction and tripod direction
ϕ	Angle between user anterior direction and antenna broadside
θ_{tripod}	Angle between antenna broadside and tripod direction
θ_{wall}	Angle between antenna broadside and wall-mounted anchor direction
f	Frequency
S	Scattering parameter

List of Publications

Articles in international journals

- D. Van Baelen, S. Lemey, J. Verhaevert, and H. Rogier, “A Novel Manufacturing Process For Compact, Low-Weight and Flexible Ultra-Wideband Cavity Backed Textile Antennas,” *MATERIALS*, vol. 11, no. 1, pp. 1—17, 2018.
- D. Van Baelen, Q. Van den Brande, S. Lemey, J. Verhaevert, and H. Rogier, "Foldable All-Textile Cavity-Backed Slot Antennas for Personal UWB Localization," *Radio Science*, vol. 55, no. 3, pp. 1–11, 2020.
- D. Van Baelen, N. Macoir, Q. Van den Brande, E. De Poorter, S. Lemey, J. Verhaevert, and H. Rogier, "Fully Flexible Textile Antenna-Backed Sensor Node for Body-Worn UWB Localization," *Sensors*, vol. 21, no. 5, pp. 1–20,2021.

Articles in conference proceedings

- J. Verhaevert and D. Van Baelen, “Localization at Room Resolution with Bluegiga Bluetooth Low Energy,” *2016 LOUGHBOROUGH ANTENNAS & PROPAGATION CONFERENCE (LAPC)*, Loughborough, United Kingdom, pp. 1–5, 2016.
- H. Rogier, D. Van Baelen, S. Lemey, S. Agneessens, M. Rossi, and J. Verhaevert, “Some Techniques for Mass Production of Textile Wireless Systems,” *2018 2ND URSI ATLANTIC RADIO SCIENCE MEETING (AT-RASC)*, Meloneras, Spain, pp. 1–4, 2018.
- D. Van Baelen, S. Lemey, J. Verhaevert, and H. Rogier, “Improved Fabrication Methodology for Foldable All-Textile Cavity-Backed Slot Antennas,” *2019 URSI ASIA-PACIFIC RADIO SCIENCE CONFERENCE (AP-RASC)*, New Delhi, India, 2019.
- D. Van Baelen, Q. Van den Brande, S. Lemey, J. Verhaevert, and H. Rogier, “Mechanically Flexible All-Textile Cavity-Backed Slot Antenna for Body-Worn UWB Localization,” presented at the 28th URSI Benelux Forum, Brussels, Belgium, pp. 1–1, 2019.

Design of textile antennas and flexible WBAN sensor systems for body-worn localization using Impulse Radio Ultra-Wideband

1 Introduction

1.1 Context

One of the first known cases of the use of wearable electronics is found deep down in the thirties of the previous century, where mob boss Al Capone was under scrutiny by undercover IRS agent Michael Malone. Malone must have been quite terrified when Capone put his hand on the agent's back, right at the spot where his colleagues had strapped an entire tape recorder under his clothing. Fortunately for Malone, Capone didn't have the slightest idea what was going on and the operation gathered evidence which was later used in court to bring the mob boss to justice.

Throughout modern history, people have been carrying all kinds of devices on their bodies and garments, be they are hidden or not. One can think of walkie talkies, personal radios, pagers, cell phones, GPS trackers and so on. These devices became smaller and increased in functionalities: cell phones such as Motorola DynaTAC, considered clumsy according to modern standards, gradually evolved into lightweight devices small enough to fit in one's pocket [1]. In the meantime, the portable but not exactly wearable personal digital assistants (PDA's) were created, providing functionalities that consumers nowadays would simply attribute to the smartphone. In a sense, PDAs even became the first smartphones, ever since the IBM Simon was released, the first PDA boasting mobile phone functionality [2].

Ever since, portable multi-purpose communication devices have been conquering the world, resulting in an industry with an annual revenue exceeding 400 billion U.S. dollars since half a decade by now [3]. Clearly, the decrease in device size and weight cannot be separated from the many improvements in battery technology. Not only did batteries achieve higher energy densities with respect to both mass and volume, also mechanically flexible batteries have emerged and have reached

the commercial stage [4]–[6]. Devices such as fitbits, activity trackers and smartphones are now present in everyday life [7]–[9], and the number of applications provided by these devices ever shrinking in size only seems to increase.

As the 5G network, now finally taking root, unleashes the Internet of Things (IoT) [10], [11], myriads of new functionalities become available in which wearables find their place. The essential idea behind the IoT is to connect every device or item to the internet, and to make them active participants in it. By cooperation between the sensors and actuators present in these smart devices, numerous new functionalities can be introduced. In intelligent homes, lighting and household appliances can be remote controlled, thermostats automatically adjust to better suit inhabitants' needs, doors open, plants notify when they need to be watered, clothes indicate when they should be washed, objects can be located when lost... Summarizing, household applications alone offer a plethora of functionalities [12]–[16]. Application of the principles underlying to the IoT in industry, logistics, transportation and agriculture will lead to a whole new world of novel functionalities and new possibilities, and furthermore opens the door to tremendous efficiency gains [17]–[20]. It should be no surprise that IoT is considered one of the key enablers for the so-called fourth industrial revolution [21], [22]. By 2019, 7.6 billion devices were already connected to the internet, a number which is expected to increase threefold by 2030 [23].

An essential requirement for the Internet of Things is the ability of its users to interface with it. Since a wealth of information about the user's intentions or situation, consciously or unconsciously, is present on the human body, at least some of the infrastructure that brings the Internet of Things to its users, and vice versa, should be deployed on the users' bodies. This naturally leads us back to the use of wearables. Expansion opportunities in this sector are ample. It should come as no surprise that the wearable technology market grew to the size of 37.10 billion USD in 2020, which is expected to reach more than 104 billion dollars by 2027 [24].

Truly, wearable electronics have come a long way since Michael Malone's time.

1.2 Motivation

An idea behind the IoT is bringing electronics closer into people's lives by integrating them in all kinds of objects. While the IoT certainly encompasses integration of electronics into everyday surfaces such as armchairs, curtains, walls and floorboards [25]–[29], the gap to the user can be bridged by the introduction of electronics in the user's clothing [30]. In this way, body-worn smart textiles become the practical link that extends the functionalities of human minds and bodies, by bringing the IoT closer to its users' daily lives than any other device [30], [31]. Integrating electronics in textile materials is also known under the name of Smart Fabrics and Interactive Textiles (SFIT).

Although integration in clothing forms a direct link to reach intuitive interfacing with a wearable electronic system, various challenges arise that are not present or already have been solved in conventional rigid electronic systems. From an economic point of view, wearable textile systems should be cheap and reliably mass producible, which implicates a need for suitable fabrication processes and an obviously necessary scale-up of the market's revenue [29], [32]. From the user's perspective, such systems need to be wearable: they should be lightweight and conveniently sized, preferably with a flexibility similar to the surrounding textile. With social acceptance in mind, the systems need to be unobtrusive and blend in with the garment, so as to make them an integral part of our everyday outfits [33]–[35]. Furthermore, interfacing with the system should be possible in an intuitive way [36], [37]. Another point of interest is the consideration which information should be conveyed to the user. Systems that bluntly provide all the information they have available, impede the user's effectiveness instead of enhancing it [38]. Therefore, it is necessary for smart textile systems to become aware of their context, so they can assert the relevance of the information they show [33]. If smart textiles have the right sensor data available and can connect with a low-latency high-data-rate communication network such as 5G, they become able to provide the right content to the right person at the right time to the right place in the right format [39]. A smart textile can also be implemented to do more than just provide advantages for the individual wearing it. By gathering and mapping sensor data such as for example air quality, noise pollution or, water quality (which is one of the examples given in UNICEF's Wearable for Good challenge [40]), the entire society can benefit.

Aside from economical, societal or user-centered considerations, body-worn smart textiles also pose a number of interesting technical challenges. Such systems need to be robust and resilient. Furthermore, they should be easy to maintain, implying that since clothes are prone to get dirty, they should be washable [41]. Body-worn systems also need to guarantee their functionalities under any reasonable circumstances. This includes taking into account the proximity of (and in many applications even the contact with) the human body, and this for the entire spectrum of body morphologies. A good way to achieve this is the reduction of electromagnetic coupling with the human body [42], [43]. It also helps fulfilling the goal of reducing the dose of radiation absorbed in the user's body tissues (which is often expressed as Specific Absorption Rate (SAR)) [44]. Body-worn systems should be able to cope with moving parts of the body. They need to perform efficiently under bending and also should suffer no significant adverse effect from garment displacement (such as an arm shifting in a sleeve). Furthermore, body-worn textile systems should be power-efficient, since power infrastructure such as batteries often spend a major portion of the mass and space budgets of any wearable. Thereby, the occurrence of battery charging or changing procedures should be minimized as much as possible. Consequentially, the antenna infrastructure of these systems should possess a high antenna efficiency, which translates into a need for low-loss textile materials and efficient antenna topologies. Textiles show some notewor-

thy differences with traditional rigid substrates. Compression or changes in the moisture content of an air-containing substrate such as a textile greatly affect its dielectric permittivity. Therefore, fabrics should be chosen that recover from compression [45]. Furthermore, the mass of the absorbed water in the textile material, as characterized by its moisture regain [46], should be low to obtain stable antenna characteristics [47]. Finally, antenna topologies should be chosen that experience as little influence as possible from the mechanical deformations described above.

A number of issues have been discussed which still impede smart textiles and wearable fabrics from taking their rightful place in the Internet of Things. Summarizing, smart textiles need to become cheap and mass-producible. They need to cope with the consequences of being worn on the human body and need to be energy-efficient, flexible and resistant against moisture, all this while maintaining their functionality. Furthermore, the coupling between the system and the human body should be minimized. Context-aware systems and appliances satisfying all these requirements will permit the market breakthrough of smart textiles, allowing them to finally properly plug in the user into the Internet of Things.

1.3 State-of-the-art

In the previous years, significant research efforts have been made to identify and address the issues arising with wearable textile electronics. As mentioned in Section 1.2, the production of smart textiles should be performed accurately and reliably. Since substrate compression or moisture absorption can significantly impact antenna performance by altering the substrate's dielectric permittivity, extensive investigations have been performed to identify and characterize suitable materials, and to quantify possible deviations in their properties [45], [48]–[51]. Statistical analysis methods have been applied to characterize uncertainties resulting from material properties or manufacturing inaccuracies. This allows the designer to make better informed decisions during antenna design, producing better results.

Throughout the years, many different fabrication methods have been proposed for the production of flexible antennas. Numerous works have been published where conductive inks have been patterned to antenna shapes by industrially established fabrication methodologies. An example of this is screen printing, where a squeegee applies conductive ink to the substrate by pressing it through a mask [52]–[54]. Another technology is inkjet printing, where conductive ink droplets are dispensed through a nozzle onto the substrate by means of a piezo or heat element [54]–[57]. A final example is flexography, where the substrate is squeezed through two rollers, one of which is patterned with ink carrying holes that deliver their contents to the substrate [56]. Although these fabrication methods offer high accuracies and high fabrication throughputs, they can only be applied to create planar structures through the use of liquid ink. The role of the conductive material has been filled by diverse materials. [57] and [58] report stretchable materials such as liquid metals in stretchable substrates, carbon nanotube films, silver flakes embedded in

silicone, silver-based fluorine rubber, polymer-zirconia nanocomposites, and polymeric nanocomposites such as MXene inks. These materials are well-suited for use in flexible systems, although they are not necessarily well-suited for use on textile. Furthermore, the conductivity and especially the washability of these materials remains a point of attention. Currently, these materials are only suitable for the creation of planar structures. Although, it will become clear throughout this dissertation that taking avail of the third dimension offers many promising possibilities, as in this way, the fabrication of cavity antennas becomes possible. These antennas which will prove to be most suitable to meet the requirements encountered throughout the dissertation.

However, the conductive layers can also be realized in alternative ways: some authors employ embroidery by knitting conductive threads such as the Liberator-20 or the Elektrisola E-thread to a textile substrate by means of an assistant yarn. By using a computerized process together with a sufficiently thin thread, accuracies up to scales of 0.1 mm have been achieved [59], [60]. Furthermore, embroidery machines are common in industry [61], and no glue of any kind is necessary [62]. However, the realization of extended conductive surfaces with this procedure is time-consuming, and care must be taken that the conductivity of the thread does not vanish after repeated washing cycles [63], [64]. Furthermore, the direction of the electric current in embroidered surfaces is nonuniform [65]–[67]. Generally, the losses present in embroidered patches are higher than in metallic materials [61] or woven fabrics such as copper coated taffeta [48] due to the reliance on mechanical contact between the metallic embroidered wires. Moreover, mechanical stretching has a detrimental impact on the sheet resistivity of the embroidered textile [68], while the materials discussed in [57], [58] have been specifically developed to maintain their conductivity when stretched. To improve the sheet resistivity, the embroidery can be performed double-layered, or higher embroidery densities can be selected. However, this only increases the production process' time consumption even more. Finally, embroidering in this fashion only allows the creation of planar structures.

Other approaches implement horizontal conductive surfaces by gluing woven conductive textiles, also known as *e-textiles*, to a textile substrate material. For this, e-textiles such as Pure Copper Taffeta, Shieldit Super or Zelt have been characterized and implemented as the conductive parts of textile antennas [48], [69]–[71]. This method allows fast fabrication, and it is particularly suitable for the realization of larger planar structures. Therefore, it allows to place a large ground plane between the user's body and the antenna, which provides significant isolation between both. In this methodology, special care must be taken to avoid misalignment of the antenna planes during fabrication. Furthermore, delamination of the antenna's textile layers is a common issue.

Instead of using an extensive ground plane, Substrate Integrated Waveguide (SIW) cavity-backed slot antennas isolate the human body from the antenna by confining their electromagnetic field inside the antenna cavity. The authors from [72], [73]

have implemented the vertical walls of the cavity antenna by means of conductive yarns, which have been stitched through the substrate to form a conductive vertical wall. However, such a knitting process exerts significant mechanical strain on the thread, which adds requirements to the tensile strength of the selected E-thread [74]. Also, the substrate around the seam experiences a significant compression [73], which changes the structure of the antenna and provokes a redesign to obtain the same characteristics as the non-compressed antenna. To obtain accurate results, the exact degree of compression needs to be characterized well. Last, the resistivity of the vertical walls is dependent on the yarn density and is higher than in metallic materials or woven conductive fabrics [43]. Other authors such as [42], [75]–[80] implement the vertical walls of SIW cavities by punching tubular brass eyelets through the substrate. When implemented on a flexible substrate, this SIW structure can be bent while still the electromagnetic goals are fulfilled. Specifically, since these cavity topologies confine the electromagnetic field inside the cavity, there is no more need for a large ground plane to realize the desired isolation between the antenna and the wearer's body. The pressing of these eyelets is automatable, and their height can be adjusted so that the surrounding substrate is only minimally compressed. However, since brass eyelets are rigid and heavy structures, this methodology is not fully consistent with unobtrusiveness and wearability goals. Furthermore, there is a risk of cracks in the electrotextile close to the eyelets.

During everyday use, body-worn textile systems will be exposed to water and dirt. Not only should the system experience no adverse effect from this, some form of washing is necessary. However, this might cause delamination of the textile layers, or compromise system functionality due to interactions with circuitry or antenna materials. Solutions have been proposed in which the conductive textile layer of the system is protected by a thermoplastic polyurethane coating [41], [81]–[83] or by an epoxy film [84]. UHF RFID tags employing conductive inks as a conductive layer have been successfully protected by screen printing of polymer thick films [52].

In the last decade, a plethora of sensor functionalities for wearables have been realized for use in a diverse range of sectors. Published systems include medical sensors, monitoring figures such as electrodermal activity [85], gait freeze in Parkinson's disease patients [86], cardiac and respiratory rhythm [87], electrocardiograms [88] and oxygen saturation [89]. Examples for paramedical systems contain fall detection [90], [91] or joint flexion detection [92]. Many of these systems are not flexible, or only partially. Often, these systems consist of a bulky, rigid box, which is attached to the body by means of a stretchable textile brace. In other cases, the sensor part itself is flexible indeed, or at least comfortably and unobtrusively wearable, but the circuitry driving the system or providing external communication are implemented in a rigid accessory. Widespread commercial adoption of these systems calls for a more comfortable and unobtrusive manner of wearing than what can be offered by previous examples. Hence, some further degree of textilization is required.

Most electronic components integrated in textile are implemented on a flexible substrate such as a polyimide foil. Yet, design on a flexible substrate comes with additional challenges such as the avoidance of tears in inner corners of the conductor material, or the breaking of soldering joints. The standard PCB design rules are therefore insufficient to produce reliable and robust circuitry. However, the design of electronic systems on flexible substrates is a well-established technology, for which detailed reference works can be consulted [93], [94]. When using these, a significant miniaturization can be obtained by integrating the circuitry on the back side of the textile antenna, as demonstrated in [95]–[98]. Other publications investigated placing singular electronic components on plastic strips, which are then woven into a mesh of both conductive and nonconductive textiles to realize the desired circuit topology [89], [99]–[101].

With the eye on applications, among the many functionalities that may be offered through a wearable system, indoor localization is a particularly valuable capability. To realize this, a plethora of technologies already exist [102], [103]. To some applications, a localization accuracy in the order of several meters is acceptable, although for most indoor applications, a finer accuracy is required. Fine localization accuracies, down to the order of 10 cm, are particularly interesting to body-worn systems, since this significantly enhances the system's context awareness. In this way, applications such as navigation aid for the visually impaired or the provision of relevant extra information at a particular work in a museum become feasible.

Currently, an accuracy in the order of 10 cm is only achieved by acoustic systems, visible light communication (VLC) positioning systems, positioning cameras and ultra-wideband positioning [103]. Acoustic systems require the addition of specific hardware such as microphones and speakers, or ultrasonic transmitters and receivers, which may pose integrability challenges. Furthermore they suffer from sound pollution [102]. Although image based camera positioning systems can reach excellent accuracies down to 1 cm, they require a line of sight and offer limited coverage [103]. On the other hand, signal strength-based positioning systems employing visible light have attained sub-cm ranging accuracies [104]. However, many challenges are still present in this technology, which need to be addressed before such systems may reliably provide localization in indoor environments: the authors in [105] note that the algorithms required to obtain such localization accuracies induce significant computational delays which impede real-time operation of such systems. Furthermore, the technology suffers from ambient noise [105] and multipath reflections [106]–[108]. Moreover, since visible light cannot permeate walls, such systems can only operate when they are situated in the same room, which may be an asset or a disadvantage, depending on the use case.

Solutions to these matters can be found in Impulse-Radio Ultra-Wideband technology (IR-UWB), as defined in the IEEE802.15.4 standard [109]. Prominent features of this standard are its low-power operation and a high node density, qualities which are particularly suitable for body-worn applications in IoT-scenarios. In IR-UWB technology, ranging is performed by use of short time-domain pulses which

use a large bandwidth. In this way, the flanks of the pulse in the time-domain are steep, allowing very accurate timestamping. This results in commercially available accuracies in the order of 10 cm [110]. Because of the short time duration of the pulses, these systems are very resistant against multipath effects [111], [112]. Furthermore, the noise-like power levels employed in UWB localization cause little interference with other technologies, and they are able to pass through walls without significantly impeding the localization accuracy [113]–[117]. To allow the receiving device to correctly interpret a given packet as an IEEE802.15.4 packet, the pulse distortion introduced by the system in between the transmitting Integrated Circuit (IC) and the receiving IC should be minimized. A valuable characteristic to quantize this is the System Fidelity Factor (SFF), as defined in [118]. Although many antenna designs intended for UWB operation exist, they often do not take this pulse deformation into account [119]–[121]. This requirement, together with the comparatively high cost with respect to localization technologies such as Bluetooth or ZigBee, form the primary drawbacks of this technology [102].

Not every positioning methodology is suited for body-worn localization. Methodologies using proximity do not reach the accuracy required in body-worn scenarios. Received signal strength indicator (RSSI)-based methods are prone to multipath fading and environmental noise, and lead to mediocre localization accuracies. Furthermore, they may require a preliminary mapping of the space, which needs to be updated everytime there is a variation in the layout of the monitored space [102]. Methods using time difference of arrival (TDoA) are very power efficient, although they particularly suffer from body shadowing effects that cause a poor dilution of precision (DoP) [122]. Furthermore, TDoA requires synchronization of the anchor infrastructure. Time of arrival (ToA)-based methods suffer from the same issue, and furthermore require synchronization of the wearable sensor system and the anchors. However, IR-UWB is ideally suited to implement two-way ranging (TWR) schemes, which require no synchronisation of the tag with the anchor modules. More advanced two-way ranging schemes such as symmetric double-sided ranging (SDS-TWR) thereby exhibit a high resilience against clock induced ranging errors [123], [124]. Furthermore, TWR schemes require no fixed anchor infrastructure, as they can simply determine the range with respect to another node.

1.4 Novel contributions and outline of this work

The goal of this dissertation is to improve the wearability and to extend the functionalities of smart textile systems, so as to bring the SFIT state-of-the-art closer to full maturity and pave the way for broad market adoption. Where state-of-the-art systems often resign on full mechanical flexibility by combining a flexible part with a lumpy rigid backbone, or only realize the flexible part of the system, omitting the other elements, the goal of this work is to realize a design paradigm for systems on textile that can be fully integrated with garments and that demonstrate

integrability of diverse sensor functionalities. More in detail, an antenna should be demonstrated that satisfies the prerequisites for deployment on a human body. Such an antenna should exhibit a high isolation to the human body, while it still meets wearability constraints concerning mechanical flexibility, weight and form factor.

As of today, no complete body-worn textile systems implementing positioning exist. Nevertheless, if a smart system is to be able to properly assess its current situation and context, it would benefit greatly from an accurate estimation of its location. The capabilities of wearable smart textiles should therefore be enhanced with the highly accurate UWB localization functionality. To achieve this, an antenna should be demonstrated that satisfies demands concerning pulse distortion, but still is in accordance with wearability constraints applicable for body-worn systems. Furthermore, the integration of complex sensor electronics for UWB localization with a textile antenna system needs to be realized. It should be demonstrated that such a system not only qualifies for all goals mentioned before, but also that it is cost-effective and energy-efficient.

In Chapter 2, a novel fabrication methodology for the realization of full-textile cavity-backed slot antennas has been presented. Such antennas consist of a metallic cavity filled by a dielectric substrate. By providing a slot in the top plane of the metal, an aperture is provided through which the antenna radiates. However, since cavities are notoriously narrowband resonant structures, a broadbanding technique based on the coupling between two SIW half-mode cavity resonators has been applied to obtain an antenna structure with a relative bandwidth larger than 20%.

The fabrication methodology causes a significant reduction in the chance of antenna plane misalignments. Furthermore, the process is machinable and in comparison with previous manufacturing methods, fewer fabrication steps are required. Moreover, the vertical walls of the antenna cavity now consist entirely out of electrotextile slabs. In comparison with embroidery methodologies, the conductivity of the vertical walls is now sufficiently large to avoid unnecessary antenna losses. Furthermore, this methodology causes no substrate compression. With respect to the antennas fabricated by means of metal eyelets, this fabrication methodology produces significantly more lightweight antennas, as it does not contain any rigid parts except for the feeding pin.

As a proof of concept, an antenna has been designed and realized for the unlicensed national information infrastructure (UNII) radio bands, thereby covering the [5.15–5.85] GHz band. A first prototype has been realized which is fed through an SMA connector. An even more lightweight prototype was then manufactured by implementing the probe feed by means of a metal pin, soldered to the center conductor of an ultra-small Hirose U.FL connector. As a substrate, a closed cell expanded rubber foam also found in firefighter suits has been selected. The resulting prototypes exhibit a gain higher than 5 dBi and an impedance match with respect to 50Ω lower than -10 dB, over the entire [5.15–5.85] GHz frequency band. Fur-

thermore, the antenna's radiation efficiency exceeds 70% in this frequency range.

Cavity-backed slot antennas in SIW are suitable for body-worn deployment scenarios as a result of their directive radiation pattern and their low coupling with the human body. Furthermore, since body-worn deployment scenarios such as integration in clothing involve bending of the textile antenna, this flexing motion causes the vertical walls of the electrotextile to crumple, which induces a risk of delamination of the electrotextile. By providing openings in the vertical walls, space is provided where the antenna is allowed to crumple. This makes the antenna an SIW cavity.

The antenna topology proves to be suitable for deployment on a human body, since measurements on the prototypes show that both its impedance matching and its radiation pattern experience limited influence from proximity of the human body, or from bending over bending radii commonly encountered in worn garments. Furthermore, changes in the humidity of the surrounding air prove to have no impact on the investigated prototypes.

In Chapter 3, the production process from the previous chapter has been applied to create a cavity-backed slot antenna for body-worn localization through IR-UWB in Channels 2 and 3 of the IEEE802.15.4a standard (3744 MHz - 4243.2 MHz and 4243.2 MHz - 4742.4 MHz, respectively). This resulted in a highly-efficient UWB-antenna with a fractional bandwidth of 27.9% and a radiation efficiency higher than 78% in both channels. Both the antenna's radiation pattern and impedance matching have been measured to exhibit an excellent resilience against proximity of the human body. Furthermore, bending of the antenna over the radii investigated in Chapter 3 has limited effect on the impedance matching of the antenna, since the antenna's impedance matching goal is met over all bending radii equal or larger than 7.5 cm. Even when the antenna is bent along its E-axis over a bending radius as small as 4 cm, the impedance matching is preserved.

Since the antenna is designed for localization through IR-UWB, specific attention must be paid to its time-domain characteristics. First, to allow a localization IC to recognize an incoming pulse, the pulse distortion of the entire system consisting of the transmit antenna, the receive antenna and the channel in between them, must be kept low. This is quantified by the System Fidelity Factor (SFF), which is defined in [118] as the normalized maximum of the cross-correlation between the signal as presented on the port of the transmitting antenna, and the signal as obtained on the port of the receiving antenna. The antenna has been designed through co-optimization of the frequency characteristics of the single antenna element on the one hand, and the SFF on the other hand. The time index t_{max} at which the maximum of this cross-correlation is found, is directly related to the time-of-flight of the pulse, but it is dependent on the orientation of the used antennas, which gives rise to a distance estimation error (DEE) when comparing any value for t_{max} with the value acquired in the broadside direction. Over all relevant directions for body-worn positioning, this DEE is found to be smaller than 5 cm, which is even less than the 10 cm positioning error introduced by localization IC's such as Decawave's

DW1000 [110]. Furthermore, an SFF larger than 94% is obtained, which is better than the 90% generally required for localization purposes. The favorable values for the SFF and DEE, together with the antenna's stable frequency domain parameters in the presence of the human body, qualify the design as a suitable candidate for body-worn localization through IR-UWB.

In Chapter 4, a mechanically flexible polyimide PCB has been integrated on the back plane of the antenna elaborated in Chapter 3, to form a comprehensive flexible sensor node for integration in body-worn textiles. The sensor electronics in the system may be refitted at will, although for this proof of concept, an environmental sensor, together with Decawave's DW1000 localization IC are chosen. The antenna and the PCB have been co-optimized to realize a comprehensive sensor node for IR-UWB localization in compliance with the IEEE802.15.4a standard. As required for integration with the flexible PCB, the through-hole connector used as the antenna feed in previous chapters has been replaced by a 1 mm diameter pin which pierces both the antenna and the flexible PCB. The antenna cavity is completed by soldering the pin to the PCB's RF feed line on the one end, and to the slot plane of the textile antenna on the other end. To compensate for the change in pin diameter required for integration with the flexible PCB, a minor redesign has been performed on the antenna from Chapter 3.

Flexible circuit design guidelines have been followed to ensure robust functionality of the design. Examples of this are the alignment of vias and component edges to control the locations of lines where the PCB should or should not bend, the tapering of a signal line at the interconnection with a via, and the gradual bending of inner corners in the metal [93].

To measure the SFF and the DEE, a system is considered that consists of two identical prototypes of the standalone antenna elaborated in Chapter 3. Here, the ports of the system are formed by the connectors of the transmit antenna and the receive antenna, respectively. Through measurement of the transfer function of the system for all orientations of the receive antenna, the impulse response of the system can be obtained. For the input pulse for the system, the default output pulse of the DW1000 IC when operating in IEEE802.15.4a Channel 2 is selected. Through convolution of this signal with the system's impulse response, the signal as seen on the receive antenna's connector is acquired. This permits the calculation of the SFF of the system. The measured SFF significantly exceeds the 90% goal commonly used for localization, and this for all orientations relevant to body-worn localization. From the aforementioned calculations, the DEE with respect to the antenna's broadside orientation has been found to be smaller than 5 cm for every orientation of the receive antenna, and is thus smaller than the 10 cm error introduced by the DW1000 IC itself [110]. Therefore, the antenna's time domain characteristics prove to be suitable for use in a localization system.

To obtain an assessment of the radiation pattern of the textile antenna fed by the PCB, the DW1000 IC, which hosts a transceiver, has been configured to transmit in continuous wave mode in IEEE802.15.4a Channel 2. In this way, the system's

power pattern has been recorded in free space, whose shape shows excellent similarity with the radiation pattern of the antenna discussed in Chapter 3.

Due to the shadowing effect of the wearer's body, and the radiation pattern of the antenna optimized to counter this, not every direction around the user can be serviced by the same antenna.

The sensor node has been outfitted on a belt, which can be shifted around the test subject's waist to investigate diverse body-deployment positions in all surrounding directions. The test subject has been rotated so that diverse orientations of the sensor node's textile antenna with respect to a tripod mounted anchor can be investigated. When examining a scenario with 6 different body deployment positions, some of them were shadowed by the test subject's arms, although data for adjacent investigated positions suggests the viability of a configuration with 6 body deployment positions. Finally, by deploying the sensor system on 8 body deployment positions, all directions around the user are serviced, with ample of redundancy.

With wearability in mind, the system should spend energy in an efficient way, since batteries take up a significant part of the weight and space budget available in any body-worn system. As a reference, the system's autonomy equals 13.3 hours on a 5V, 200 mAh flexible battery. When applying power saving measures, the autonomy can be raised significantly. Therefore, it can be concluded that this system is suited for body-worn localization by means of IR-UWB, thereby acting as a proof of concept for the integration of electronics into flexible wearable textile systems.

References

[1] "Radio Telephone System", Patent US3906166A, Sep. 1975.

[2] D. Aamoth, "First Smartphone Turns 20: Fun Facts About Simon", *Time*, 2020.

[3] S. O'Dea. (2020). "Global Smartphones Sales Revenue Statista", [Online]. Available: https://www.statista.com/statistics/237505/global-revenue-from-smartphones-since-2008/.

[4] D. Wang, C. Han, F. Mo, Q. Yang, Y. Zhao, Q. Li, G. Liang, B. Dong, and C. Zhi, "Energy Density Issues of Flexible Energy Storage Devices", *Energy Storage Materials*, vol. 28, 264–292, 2020.

[5] K. K. Fu, J. Cheng, T. Li, and L. Hu, "Flexible Batteries: From Mechanics to Devices", *ACS Energy Letters*, vol. 1, no. 5, 1065–1079, 2016.

[6] Shenzhen Grepow Battery Co., Ltd. (Aug. 2020). "A Review of Flexible Battery Manufacturers", [Online]. Available: https://www.grepow.com/article/detail/a-review-of-flexible-battery-manufacturers.html.

[7] B. Reeder and A. David, "Health at Hand: A Systematic Review of Smart Watch Uses for Health and Wellness", *Journal of Biomedical Informatics*, vol. 63, 269–276, 2016.

[8] S. P. Wright, T. S. Hall Brown, S. R. Collier, and K. Sandberg, "How Consumer Physical Activity Monitors Could Transform Human Physiology Research", *American Journal of Physiology-Regulatory, Integrative and Comparative Physiology*, vol. 312, no. 3, R358–R367, 2017, PMID: 28052867.

[9] "A Review of Activity Trackers for Senior Citizens: Research Perspectives, Commercial Landscape and the Role of the Insurance Industry", *Sensors*, vol. 17, no. 6, p. 1277, 2017.

[10] G. A. Akpakwu, B. J. Silva, G. P. Hancke, and A. M. Abu-Mahfouz, "A Survey on 5G Networks for the Internet of Things: Communication Technologies and Challenges", *IEEE Access*, vol. 6, pp. 3619–3647, 2018.

[11] M. R. Palattella, M. Dohler, A. Grieco, G. Rizzo, J. Torsner, T. Engel, and L. Ladid, "Internet of Things in the 5G Era: Enablers, Architecture, and Business Models", *IEEE Journal on Selected Areas in Communications*, vol. 34, no. 3, pp. 510–527, Mar. 2016.

[12] L. C. De Silva, C. Morikawa, and I. M. Petra, "State of the Art of Smart Homes", *Engineering Applications of Artificial Intelligence*, vol. 25, no. 7, 1313–1321, 2012.

[13] M. Chen, J. Yang, X. Zhu, X. Wang, M. Liu, and J. Song, "Smart Home 2.0: Innovative Smart Home System Powered by Botanical IoT and Emotion Detection", *Mobile Networks and Applications*, vol. 22, no. 6, 1159–1169, 2017.

[14] G. Lobaccaro, S. Carlucci, and E. Löfström, "A Review of Systems and Technologies for Smart Homes and Smart Grids", *Energies*, vol. 9, no. 5, p. 348, 2016.

[15] A. Brush, M. Hazas, and J. Albrecht, "Smart Homes, Inhabited", *IEEE Pervasive Computing*, vol. 17, no. 3, 78–82, 2018.

[16] R. Teng and T. Yamazaki, "Load Profile-Based Coordination of Appliances in a Smart Home", *IEEE Transactions on Consumer Electronics*, vol. 65, no. 1, 38–46, 2019.

[17] A. Zanella, N. Bui, A. Castellani, L. Vangelista, and M. Zorzi, "Internet of Things for Smart Cities", *IEEE Internet of Things Journal*, vol. 1, no. 1, pp. 22–32, Feb. 2014.

[18] S. Latif, H. Afzaal, and N. A. Zafar, "Modeling of Sewerage System Using Internet of Things for Smart City", in *2017 International Conference on Frontiers of Information Technology (FIT)*, 2017, pp. 46–51.

[19] A. H. Alavi, P. Jiao, W. G. Buttlar, and N. Lajnef, "Internet of Things-Enabled Smart Cities: State-of-the-Art and Future Trends", *Measurement*, vol. 129, 589–606, 2018.

[20] M. Aboelmaged, Y. Abdelghani, and M. A. Abd El Ghany, "Wireless IoT Based Metering System for Energy Efficient Smart Cites", in. 2017.

[21] M. Xu, J. David, and S. Kim, "The Fourth Industrial Revolution: Opportunities and Challenges", *International Journal of Financial Research*, vol. 9, p. 90, Feb. 2018.

[22] J.-M. Frangos. (2020). "The Internet of Things Will Power the Fourth Industrial Revolution. Here's How", [Online]. Available: `https://www.weforum.org/agenda/2017/06/internet-of-things-will-power-the-fourth-industrial-revolution/`.

[23] (2020). "Internet of Things (IoT) Connected Devices Worldwide in 2019 and 2030 | Statista", [Online]. Available: `https://www.statista.com/statistics/1183457/iot-connected-devices-worldwide-2019-2030/`.

[24] Grandviewresearch.com. (2021), [Online]. Available: `https://www.grandviewresearch.com/industry-analysis/wearable-technology-market`.

[25] O. Caytan, S. Lemey, S. Agneessens, D. Vande Ginste, P. Demeester, C. Loss, R. Salvado, and H. Rogier, "Half-Mode Substrate-Integrated-Waveguide Cavity-Backed Slot Antenna on Cork Substrate", *IEEE Antennas and Wireless Propagation Letters*, vol. 15, pp. 162–165, 2016.

[26] H. F. Khalili, S. Lemey, O. Caytan, T. Deckmyn, S. Agneessens, D. V. Ginste, and H. Rogier, "Biodegradable Dual Semicircular Patch Antenna Tile for Smart Floors", *IEEE Antennas and Wireless Propagation Letters*, vol. 18, no. 2, 368–372, 2019.

[27] R. Gonçalves, J. Reis, E. Santana, N. B. Carvalho, P. Pinho, and L. Roselli, "Smart Floor: Indoor Navigation Based on RFID", in *2013 IEEE Wireless Power Transfer (WPT)*, May 2013, pp. 103–106.

[28] M. Contigiani, E. Frontoni, A. Mancini, and A. Gatto, "Indoor People Localization and Tracking Using an Energy Harvesting Smart Floor", in *2014 IEEE/ASME 10th International Conference on Mechatronic and Embedded Systems and Applications (MESA)*, Sep. 2014, pp. 1–5.

[29] P. Brauner, J. van Heek, A. K. Schaar, M. Ziefle, N. A.-h. Hamdan, L. Ossmann, F. Heller, J. Borchers, K. Scheulen, T. Gries, H. Kraft, H. Fromm, M. Franke, C. Wentz, M. Wagner, M. Dicke, C. Möllering, and F. Adenau, "Towards Accepted Smart Interactive Textiles", in *HCI in Business, Government and Organizations. Interacting with Information Systems*, F. F.-H. Nah and C.-H. Tan, Eds., Cham: Springer International Publishing, 2017, pp. 279–298.

[30] J. Lee, D. Kim, H.-Y. Ryoo, and B.-S. Shin, "Sustainable Wearables: Wearable Technology for Enhancing the Quality of Human Life", *Sustainability*, vol. 8, no. 5, p. 466, 2016.

[31] S. Mann, ""Smart Clothing": Wearable Multimedia Computing and "Personal Imaging" to Restore the Technological Balance between People and Their Environments", in *Proceedings of the Fourth ACM International Conference on Multimedia*, ser. MULTIMEDIA '96, New York, NY, USA: Association for Computing Machinery, 1997, 163–174.

[32] G. Tröster, "Smart Clothes—The Unfulfilled Pledge?", *IEEE Pervasive Computing*, vol. 10, no. 2, pp. 87–89, Apr. 2011.

[33] M. Stoppa and A. Chiolerio, "Wearable Electronics and Smart Textiles: A Critical Review", *Sensors*, vol. 14, no. 7, 11957–11992, 2014.

[34] K. Cherenack and L. Van Pieterson, "Smart Textiles: Challenges and Opportunities", *Journal of Applied Physics*, vol. 112, no. 9, p. 091 301, 2012.

[35] S. Agneessens, S. Lemey, and H. Rogier, "Recent Advances in Materials and Technologies for Body-Centric and IoT Antenna Systems", in *2017 IEEE MTT-S International Microwave Workshop Series on Advanced Materials and Processes for RF and THz Applications (IMWS-AMP)*, Sep. 2017, pp. 1–3.

[36] H. P. Profita, J. Clawson, S. Gilliland, C. Zeagler, T. Starner, J. Budd, and E. Y.-L. Do, "Don't Mind Me Touching My Wrist: A Case Study of Interacting with on-Body Technology in Public".

[37] P. Holleis, A. Schmidt, S. Paasovaara, A. Puikkonen, and J. Häkkilä, "Evaluating Capacitive Touch Input on Clothes", in *Proceedings of the 10th International Conference on Human Computer Interaction with Mobile Devices and Services*, ser. MobileHCI '08, Amsterdam, The Netherlands: Association for Computing Machinery, 2008, 81–90.

[38] D. Norman. (Sep. 2013). "The Paradox of Wearable Technologies", [Online]. Available: `https://www.technologyreview.com/2013/07/24/83237/the-paradox-of-wearable-technologies/`.

[39] D. Evans. (2014). "Wearable to Aware-able: Contact, Connection, Context - Cisco Blogs", [Online]. Available: `https://blogs.cisco.com/digital/wearable-to-aware-able-contact-connection-context`.

[40] (2020). "Wearables for Good Challenge", Unicef.org, [Online]. Available: `https://www.unicef.org/innovation/media/1416/file`.

[41] M. L. Scarpello, I. Kazani, C. Hertleer, H. Rogier, and D. Vande Ginste, "Stability and Efficiency of Screen-Printed Wearable and Washable Antennas", *IEEE Antennas and Wireless Propagation Letters*, vol. 11, 838–841, 2012.

[42] S. Agneessens and H. Rogier, "Compact Half Diamond Dual-Band Textile HMSIW On-Body Antenna", *IEEE Transactions on Antennas and Propagation*, vol. 62, no. 5, 2374–2381, 2014.

[43] F. Liu, Z. Xu, D. C. Ranasinghe, and C. Fumeaux, "Textile Folded Half-Mode Substrate-Integrated Cavity Antenna", *IEEE Antennas and Wireless Propagation Letters*, vol. 15, pp. 1693–1697, 2016.

[44] R. Abd-Alhameed, K. Khalil, J. Mustafa, P. Excell, and R. Alias, "Sar and Radiation Performance of Balanced and Unbalanced Mobile Antennas Using a Hybrid Computational Electromagnetics Formulation", *IEE Proceedings - Science Measurement and Technology*, vol. 151, no. 6, 440–444, 2004.

[45] M. Rossi, S. Agneessens, H. Rogier, and D. V. Ginste, "Stochastic Analysis of the Impact of Substrate Compression on the Performance of Textile Antennas", *IEEE Transactions on Antennas and Propagation*, vol. 64, no. 6, 2507–2512, 2016.

[46] W. Morton and J. Hearle, "7 - equilibrium Absorption of Water", in *Physical Properties of Textile Fibres (Fourth Edition)*, ser. Woodhead Publishing Series in Textiles, W. Morton and J. Hearle, Eds., Fourth Edition, Woodhead Publishing, 2008, pp. 178 –194.

[47] C. Hertleer, A. Van Laere, H. Rogier, and L. Van Langenhove, "Influence of Relative Humidity on Textile Antenna Performance", eng, *TEXTILE RESEARCH JOURNAL*, vol. 80, no. 2, pp. 177–183, 2010.

[48] R. Salvado, C. Loss, R. Gonçalves, and P. Pinho, "Textile Materials for the Design of Wearable Antennas: A Survey", *Sensors*, vol. 12, no. 11, 15841–15857, 2012.

[49] F. Declercq, H. Rogier, and C. Hertleer, "Permittivity and Loss Tangent Characterization for Garment Antennas Based on a New Matrix-Pencil Two-Line Method", *IEEE Transactions on Antennas and Propagation*, vol. 56, no. 8, pp. 2548–2554, Aug. 2008.

[50] M. L. Scarpello, D. V. Ginste, and H. Rogier, "Design of a Low-cost Steerable Textile Antenna Array Operating in Varying Relative Humidity Conditions", *Microwave and Optical Technology Letters*, vol. 54, no. 1, 40–44, 2012.

[51] M. Rossi, S. Agneessens, H. Rogier, and D. Vande Ginste, "Assembly-Line-Compatible Electromagnetic Characterization of Wearable Antenna Substrates", *IEEE Antennas and Wireless Propagation Letters*, vol. 16, pp. 1365–1368, 2017.

[52] J. Virkki, T. Björninen, T. Kellomäki, S. Merilampi, I. Shafiq, L. Ukkonen, L. Sydänheimo, and Y. Chan, "Reliability of Washable Wearable Screen Printed UHF RFID Tags", *Microelectronics Reliability*, vol. 54, no. 4, 840–846, 2014.

[53] I. Kazani, M. L. Scarpello, C. Hertleer, H. Rogier, G. De Mey, G. Guxho, and L. Van Langenhove, "Washable Screen Printed Textile Antennas", eng, in *Advances in Science and Technology*, P Vincenzini and C Carfagna, Eds., vol. 80, Montecatini Terme, Italy: TRANS TECH PUBLICATIONS LTD, 2013, pp. 118–122.

[54] L. Roselli, N. B. Carvalho, F. Alimenti, P. Mezzanotte, G. Orecchini, M. Virili, C. Mariotti, R. Gonçalves, and P. Pinho, "Smart Surfaces: Large Area Electronics Systems for Internet of Things Enabled by Energy Harvesting", *Proceedings of the IEEE*, vol. 102, no. 11, pp. 1723–1746, Nov. 2014.

[55] Y. Al-Naiemy, T. A. Elwi, H. R. Khaleel, and H. Al-Rizzo, "A Systematic Approach for the Design, Fabrication, and Testing of Microstrip Antennas Using Inkjet Printing Technology", *ISRN Communications and Networking*, vol. 2012, 1–11, 2012.

[56] S. P. Sreenilayam, I. U. Ahad, V. Nicolosi, V. Acinas Garzon, and D. Brabazon, "Advanced Materials of Printed Wearables for Physiological Parameter Monitoring", *Materials Today*, vol. 32, 147–177, 2020.

[57] S. Ali, C. Sovuthy, M. Imran, S. Socheatra, Q. Abbasi, and Z. Abidin, "Recent Advances of Wearable Antennas in Materials, Fabrication Methods, Designs, and Their Applications: State-of-the-Art", *Micromachines*, vol. 11, no. 10, p. 888, 2020.

[58] K. N. Paracha, S. K. Abdul Rahim, P. J. Soh, and M. Khalily, "Wearable Antennas: A Review of Materials, Structures, and Innovative Features for Autonomous Communication and Sensing", *IEEE Access*, vol. 7, 56694–56712, 2019.

[59] A. Kiourti, C. Lee, and J. L. Volakis, "Fabrication of Textile Antennas and Circuits With 0.1 mm Precision", *IEEE Antennas and Wireless Propagation Letters*, vol. 15, 151–153, 2016.

[60] A. Kiourti and J. L. Volakis, "High-Geometrical-Accuracy Embroidery Process for Textile Antennas With Fine Details", *IEEE Antennas and Wireless Propagation Letters*, vol. 14, 1474–1477, 2015.

[61] M. El Gharbi, R. Fernández-García, S. Ahyoud, and I. Gil, "A Review of Flexible Wearable Antenna Sensors: Design, Fabrication Methods, and Applications", *Materials*, vol. 13, no. 17, p. 3781, 2020.

[62] T. Kaufmann, I. Fumeaux, and C. Fumeaux, "Comparison of Fabric and Embroidered Dipole Antennas", in *2013 7th European Conference on Antennas and Propagation (EuCAP)*, 2013, pp. 3252–3255.

[63] B. Ivšić, D. Bonefačić, and J. Bartolić, "Performance of Embroidered Conductive Yarn in Textile Antennas and Microstrip Lines", in *2015 9th European Conference on Antennas and Propagation (EuCAP)*, 2015, pp. 1–4.

[64] M. Toivonen, T. Bjorninen, L. Sydanheimo, L. Ukkonen, and Y. Rahmat-Samii, "Impact of Moisture and Washing on the Performance of Embroidered UHF RFID Tags", *IEEE Antennas and Wireless Propagation Letters*, vol. 12, 1590–1593, 2013.

[65] R. Seager, S. Zhang, A. Chauraya, W. Whittow, Y. Vardaxoglou, T. Acti, and T. Dias, "Effect of the Fabrication Parameters on the Performance of Embroidered Antennas", *IET Microwaves, Antennas Propagation*, vol. 7, no. 14, pp. 1174–1181, 2013.

[66] D. Vital, J. Zhong, S. Bhardwaj, and J. L. Volakis, "Loss-Characterization and Guidelines for Embroidery of Conductive Textiles", in. 2018.

[67] J. H. Choi, Y. Kim, K. Lee, and Y. C. Chung, "Various Wearable Embroidery RFID Tag Antenna Using Electro-thread", in. 2008.

[68] Y. Liu, L. Xu, Y. Li, and T. T. Ye, "Textile Based Embroidery-Friendly RFID Antenna Design Techniques", in. 2019.

[69] C. Hertleer, A. Tronquo, H. Rogier, and L. Van Langenhove, "The Use of Textile Materials to Design Wearable Microstrip Patch Antennas", *Textile Research Journal*, vol. 78, no. 8, 651–658, 2008.

[70] A. Dierck, S. Agneessens, F. Declercq, B. Spinnewyn, G.-J. Stockman, P. Van Torre, L. Vallozzi, D. Vande Ginste, J. Vanfleteren, T. Vervust, and H. Rogier, "Active Textile Antennas in Professional Garments for Sensing, Localisation and Communication", *International Journal of Microwave and Wireless Technologies*, vol. 6, no. 3-4, pp. 331–341, 2014.

[71] C. Hertleer, H. Rogier, L. Vallozzi, and L. Van Langenhove, "A Textile Antenna for Off-Body Communication Integrated Into Protective Clothing for Firefighters", *IEEE Transactions on Antennas and Propagation*, vol. 57, no. 4, pp. 919–925, Apr. 2009.

[72] T. Kaufmann and C. Fumeaux, "Wearable Textile Half-Mode Substrate-Integrated Cavity Antenna Using Embroidered Vias", *IEEE Antennas and Wireless Propagation Letters*, vol. 12, pp. 805–808, 2013.

[73] F. X. Liu, T. Kaufmann, Z. Xu, and C. Fumeaux, "Wearable Applications of Quarter-Wave Patch and Half-Mode Cavity Antennas", *IEEE Antennas and Wireless Propagation Letters*, vol. 14, pp. 1478–1481, 2015.

[74] Z. Wang, L. Z. Lee, D. Psychoudakis, and J. L. Volakis, "Embroidered Multiband Body-Worn Antenna for GSM/PCS/WLAN Communications", *IEEE Transactions on Antennas and Propagation*, vol. 62, no. 6, 3321–3329, 2014.

[75] S. Agneessens, "Coupled Eighth-Mode Substrate Integrated Waveguide Antenna: Small and Wideband With High-Body Antenna Isolation", *IEEE Access*, vol. 6, 1595–1602, 2018.

[76] R. Moro, S. Agneessens, H. Rogier, and M. Bozzi, "Circularly-Polarised Cavity-Backed Wearable Antenna in SIW Technology", *IET Microwaves, Antennas & Propagation*, vol. 12, no. 1, 127–131, 2018.

[77] R. Moro, S. Agneessens, M. Bozzi, and H. Rogier, "Wearable Textile Antenna in Substrate Integrated Waveguide Technology", *Electronics Letters*, vol. 48, no. 16, 985–987, 2012.

[78] S. Agneessens, S. Lemey, T. Vervust, and H. Rogier, "Wearable, Small, and Robust: The Circular Quarter-mode Textile Antenna", *IEEE Antennas and Wireless Propagation Letters*, vol. 14, pp. 1482–1485, 2015.

[79] S. Agneessens, S. Lemey, R. Moro, M. Bozzi, and H. Rogier, "The Next Generation Textile Antennas Based on Substrate Integrated Waveguide Technology", in *2014 XXXITH URSI GENERAL ASSEMBLY AND SCIENTIFIC SYMPOSIUM (URSI GASS)*. 2014.

[80] R. Moro, S. Agneessens, H. Rogier, A. Dierck, and M. Bozzi, "Textile Microwave Components in Substrate Integrated Waveguide Technology", *IEEE Transactions on Microwave Theory and Techniques*, vol. 63, no. 2, pp. 422–432, Feb. 2015.

[81] B. Karaguzel, C. R. Merritt, T. Kang, J. M. Wilson, H. T. Nagle, E. Grant, and B. Pourdeyhimi, "Flexible, Durable Printed Electrical Circuits", *The Journal of The Textile Institute*, vol. 100, no. 1, 1–9, 2009.

[82] I. Kazani, F. Declercq, M. L. Scarpello, C. Hertleer, H. Rogier, D. Vande Ginste, G. De Mey, G. Guxho, and L. Van Langenhove, "Performance Study of Screen-Printed Textile Antennas after Repeated Washing", *Autex Research Journal*, vol. 14, no. 2, 47–54, 2014.

[83] X. Chen, H. He, Y. Lu, H. Lam, L. Ukkonen, and J. Virkki, "Fabrication and Reliability Evaluation of Passive UHF RFID T-shirts", in. 2018.

[84] S. Wang, N. L. Chong, J. Virkki, T. Björninen, L. Sydänheimo, and L. Ukkonen, "Towards Washable Electrotextile UHF RFID Tags: Reliability Study of Epoxy-Coated Copper Fabric Antennas", *International Journal of Antennas and Propagation*, vol. 2015, 1–8, 2015.

[85] C. Kappeler-Setz, F. Gravenhorst, J. Schumm, B. Arnrich, and G. Tröster, "Towards Long Term Monitoring of Electrodermal Activity in Daily Life", *Personal and Ubiquitous Computing*, vol. 17, no. 2, 261–271, 2013.

[86] S. Mazilu, U. Blanke, A. Calatroni, E. Gazit, J. M. Hausdorff, and G. Tröster, "The Role of Wrist-Mounted Inertial Sensors in Detecting Gait Freeze Episodes in Parkinson's Disease", *Pervasive and Mobile Computing*, vol. 33, 1–16, 2016.

[87] A. Kiaghadi, S. Z. Homayounfar, J. Gummeson, T. Andrew, and D. Ganesan, "Phyjama: Physiological Sensing via Fiber-Enhanced Pyjamas", *Proceedings of the ACM on Interactive, Mobile, Wearable and Ubiquitous Technologies*, vol. 3, no. 3, 1–29, 2019.

[88] V. Toral, A. García, F. Romero, D. Morales, E. Castillo, L. Parrilla, F. Gómez-Campos, A. Morillas, and A. Sánchez, "Wearable System for Biosignal Acquisition and Monitoring Based on Reconfigurable Technologies", *Sensors*, vol. 19, no. 7, p. 1590, 2019.

[89] C. Zysset, N. Nasseri, L. Büthe, N. Münzenrieder, T. Kinkeldei, L. Petti, S. Kleiser, G. A. Salvatore, M. Wolf, and G. Tröster, "Textile Integrated Sensors and Actuators for Near-infrared Spectroscopy", *Opt. Express*, vol. 21, no. 3, pp. 3213–3224, Feb. 2013.

[90] S. K. Gharghan, S. S. Fakhrulddin, A. Al-Naji, and J. Chahl, "Energy-Efficient Elderly Fall Detection System Based on Power Reduction and Wireless Power Transfer", *Sensors*, vol. 19, no. 20, p. 4452, Oct. 2019.

[91] C. Kamyod, "Low-Cost Falling Detection System", in *In Proceedings of the 2018 15th International Conference on Electrical Engineering/Electronics, Computer, Telecommunications and Information Technology (ECTI-CON)*, Chiang Rai, Thailand, 18–21 July 2018, pp. 784–787.

[92] V. Mishra and A. Kiourti, "Wearable Electrically Small Loop Antennas for Monitoring Joint Flexion and Rotation", *IEEE Transactions on Antennas and Propagation*, vol. 68, no. 1, 134–141, 2020.

[93] J. Fjelstad, *Flexible Circuit Technology*, 4th ed., Seaside, OR USA: BR Publishing, Inc., 2011.

[94] C. Coombs and H. Holden, *Printed Circuits Handbook*, seventh. McGraw-Hill Publishing Company, 2017.

[95] P. Vanveerdeghem, H. Rogier, J. Knockaert, P. Van Torre, and C. Stevens, "Flexible Dual-Diversity Wearable Wireless Node Integrated on a Dual-Polarised Textile Patch Antenna", *IET Science, Measurement & Technology*, vol. 8, no. 6, 452–458, 2014.

[96] A. Dierck, H. Rogier, and F. Declercq, "A Wearable Active Antenna for Global Positioning System and Satellite Phone", *IEEE Transactions on Antennas and Propagation*, vol. 61, no. 2, pp. 532–538, 2013.

[97] S. Lemey, S. Agneessens, P. Van Torre, K. Baes, J. Vanfleteren, and H. Rogier, "Wearable Flexible Lightweight Modular RFID Tag With Integrated Energy Harvester", *IEEE Transactions on Microwave Theory and Techniques*, vol. 64, no. 7, 2304–2314, 2016.

[98] O. Caytan, S. Lemey, S. Agneessens, and H. Rogier, "Siw Antennas As Hybrid Energy Harvesting and Power Management Platforms for the Internet of Things", *International Journal of Microwave and Wireless Technologies*, vol. 8, no. 4-5, 767–775, 2016.

[99] C. Zysset, T. Kinkeldei, N. Münzenrieder, L. Petti, G. Salvatore, and G. Tröster, "Combining Electronics on Flexible Plastic Strips With Textiles", English, *Textile Research Journal*, vol. 83, no. 11, pp. 1130–1142, Jul. 2013, Copyright - Copyright Textile Research Institute Jul 2013; Document feature - Illustrations; Photographs; ; Graphs; Last updated - 2017-11-20.

[100] T. Kinkeldei, C. Zysset, N. Münzenrieder, and G. Tröster, "An Electronic Nose on Flexible Substrates Integrated Into a Smart Textile", *Sensors and Actuators B Chemical*, vol. 174, 81–86, 2012.

[101] W. Zeng, L. Shu, Q. Li, S. Chen, F. Wang, and X.-M. Tao, "Fiber-Based Wearable Electronics: A Review of Materials, Fabrication, Devices, and Applications", *Advanced Materials*, vol. 26, no. 31, 5310–5336, 2014.

[102] F. Zafari, A. Gkelias, and K. K. Leung, "A Survey of Indoor Localization Systems and Technologies", *IEEE Communications Surveys Tutorials*, vol. 21, no. 3, pp. 2568–2599, 2019.

[103] Z. Wang, Z. Yang, and T. Dong, "A Review of Wearable Technologies for Elderly Care that Can Accurately Track Indoor Position, Recognize Physical Activities and Monitor Vital Signs in Real Time", *Sensors*, vol. 17, no. 2, p. 341, 2017.

[104] W. Raes, L. D. Strycker, and N. Stevens, "Design and Accuracy Evaluation of a RSS-Based Visible Light Positioning Implementation", in. 2018.

[105] J. Luo, L. Fan, and H. Li, "Indoor Positioning Systems Based on Visible Light Communication: State of the Art", *IEEE Communications Surveys & Tutorials*, vol. 19, no. 4, 2871–2893, 2017.

[106] H. Hosseinianfar and M. Brandt-Pearce, "Performance Limits for Fingerprinting-Based Indoor Optical Communication Positioning Systems Exploiting Multipath Reflections", *IEEE Photonics Journal*, vol. 12, no. 4, 1–16, 2020.

[107] Y. Almadani, M. Ijaz, W. Joseph, S. Bastiaens, S. Rajbhandari, B. Adebisi, and D. Plets, "A Novel 3D Visible Light Positioning Method Using Received Signal Strength for Industrial Applications", *Electronics*, vol. 8, no. 11, p. 1311, 2019.

[108] W. Gu, M. Aminikashani, P. Deng, and M. Kavehrad, "Impact of Multipath Reflections on the Performance of Indoor Visible Light Positioning Systems", *Journal of Lightwave Technology*, vol. 34, no. 10, 2578–2587, 2016.

[109] "IEEE Standard for Local and Metropolitan Area Networks–Part 15.4: Low-Rate Wireless Personal Area Networks (LR-WPANs)", *IEEE Std 802.15.4-2011 (Revision of IEEE Std 802.15.4-2006)*, pp. 1–314, Sep. 2011.

[110] *DW1000 IEEE802.15.4-2011 UWB Transceiver*, 2.19, Decawave Limited, Adelaide Chambers, Peter Street, Dublin, D08 T6YA, Ireland, 2017.

[111] D. Dardari, A. Conti, U. Ferner, A. Giorgetti, and M. Z. Win, "Ranging With Ultrawide Bandwidth Signals in Multipath Environments", *Proc. IEEE*, vol. 97, no. 2, pp. 404–426, 2009.

[112] M. Z. Win and R. A. Scholtz, "On the Robustness of Ultra-Wide Bandwidth Signals in Dense Multipath Environments", *IEEE Commun. Lett.*, vol. 2, no. 2, pp. 51–53, 1998.

[113] R. Kshetrimayum, "An Introduction to UWB Communication Systems", *IEEE Potentials*, vol. 28, no. 2, pp. 9–13, Mar. 2009.

[114] M. Sharma, *Ultra Wideband Wearable Sensors for Motion Tracking Applications*, Ph.D. Thesis, Queen Mary University of London, London, UK, 2015.

[115] M. Delamare, R. Boutteau, X. Savatier, and N. Iriart, "Static and Dynamic Evaluation of an UWB Localization System for Industrial Applications", *Science*, vol. 2, no. 2, p. 23, 2020.

[116] A. Alarifi, A. Al-Salman, M. Alsaleh, A. Alnafessah, S. Al-Hadhrami, M. A. Al-Ammar, and H. S. Al-Khalifa, "Ultra Wideband Indoor Positioning Technologies: Analysis and Recent Advances", *Sensors*, vol. 16, no. 5, p. 36, 2016.

[117] A. Yassin, Y. Nasser, M. Awad, A. Al-Dubai, R. Liu, C. Yuen, R. Raulefs, and E. Aboutanios, "Recent Advances in Indoor Localization: A Survey on Theoretical Approaches and Applications", *IEEE Communications Surveys & Tutorials*, vol. 19, no. 2, 1327–1346, 2017.

[118] G. Quintero, J.-F. Zürcher, and A. K. Skrivervik, "System Fidelity Factor: A New Method for Comparing UWB Antennas", *IEEE Trans. Antennas Propag.*, vol. 59, no. 7, pp. 2502–2512, 2011.

[119] Z. Zhang and Z. Pan, "Design of Reconfigurable Bandwidth Filtering Antenna and Its Applications in IR/UWB System", *Electronics*, vol. 9, no. 1, p. 163, 2020.

[120] M. Koohestani, A. A. Moreira, and A. K. Skrivervik, "Fidelity Concepts Used in UWB Systems", in *In Proceedings of the 2014 IEEE Antennas and Propagation Society International Symposium (APSURSI)*. Memphis, TN, USA, 2014.

[121] M. Koohestani, A. A. Moreira, and A. K. Skrivervik, "System Fidelity Factor Evaluation of Wearable Ultra-Wideband Antennas for On-Body Communications", *IET Microwaves, Antennas & Propagation*, vol. 9, no. 10, pp. 1054–1058, 2015.

[122] R. B. Langley, "Dilution of Precision", *GPS World*, pp. 52–59, 1999.

[123] *DW1000 User Manual*, 2.12, Decawave Limited, Adelaide Chambers, Peter Street, Dublin, D08 T6YA, Ireland, 2017.

[124] Nanotron Technologies GmbH, *Symmetrical Multipath Method for Determining the Distance Between Two Transceivers*, 2015.

2

A Novel Manufacturing Process for Compact, Low-Weight and Flexible Ultra-Wideband Cavity Backed Textile Antennas

Dries Van Baelen, Sam Lemey, Jo Verhaevert and Hendrik Rogier

Published in Materials

A novel manufacturing procedure for the fabrication of ultra-wideband cavity-backed substrate integrated waveguide antennas on textile substrates is proposed. The antenna cavity is constructed using a single laser-cut electrotextile patch, which is folded around the substrate. Electrotextile slabs protruding from the laser-cut patch are then vertically folded and glued to form the antenna cavity instead of rigid metal tubelets to implement the vertical cavity walls. This approach drastically improves mechanical flexibility, decreases the antenna weight to slightly more than 1 g and significantly reduces alignment errors. As a proof of concept, a cavity-backed substrate integrated waveguide antenna is designed and realized for ultra-wideband operation in the [5.15 - 5.85] GHz band. Antenna performance is validated in free space as well as in two on body measurement scenarios. Furthermore, the antenna characteristics are characterized when the prototype is bent at different curvature radii, as commonly encountered during deployment on the human body. Also the effect of humidity content on antenna performance is studied. In all scenarios, the realized antenna covers the entire operating frequency band, meanwhile retaining a stable radiation pattern with a broadside gain above 5 dBi, and a radiation efficiency of at least 70%.

2.1 Introduction

In the most recent years, numerous applications have arisen that would benefit greatly from Smart Fabrics and Interactive Textiles (SFIT) technologies. These applications include, among others, on-body communication nodes for first responders [1], [2], medical implant communication infrastructure [3], [4], personal locator beacons implemented in life jackets [5], [6] and Internet of Things (IoT)-applications [7]–[9]. To achieve a deep market penetration of such systems, consumer requirements concerning wearability need to be satisfied. This can be achieved through textilization of the aforementioned components.

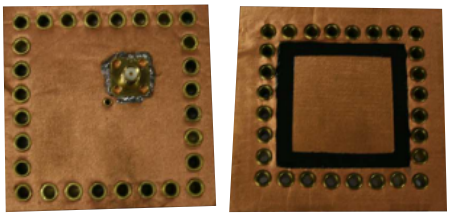

(a) Textile SIW cavity antenna using electrotextile and long-sail eyelets [10].

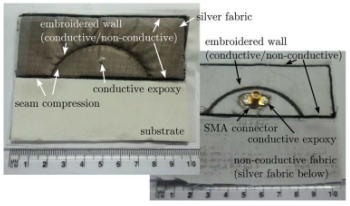

(b) Semi-circular half-mode SIW cavity antenna with embroidered vertical walls [11].

Figure 2.1: Some previous SIW antenna fabrication methods employing electrotextiles.

Up to now, some textile systems have been demonstrated that address a number of issues arising with wearable communication systems. The work in [10], displayed in Figure 2.1a, discusses the first full-textile substrate integrated waveguide (SIW) antenna based on a conductive coated fabric and metal long sail eyelets. The antenna exhibits low coupling to the human body, yet long sail eyelet punching requires contact pressure to create good contact between different electrotextile layers, which causes compression of the foam substrate. Furthermore, this antenna employs metal long sail eyelets as vertical walls of the SIW cavity, resulting in a heavier and larger antenna structure [8], [12] addresses some of these issues, as one-piece tube eyelets, henceforth called "tubelets", are used [8], [9], [13] instead of two-part long sail eyelets used in [10], thereby removing the concern of compression due to the additional part of the latter. Furthermore, the use of two resonant modes results in a broader bandwidth. In [13], both metal tubelets and conductive coated fabrics are used, offering the same advantages as in [8]. This antenna topology provides a very high degree of miniaturization, and exhibits two modes. Thereby, it demonstrates the effectiveness of the antenna at higher frequencies. All fabrication methods until now require two electrotextile layers, an antenna substrate layer and a significant amount of tubelets to implement the antenna cavity. This results in an elaborate manufacturing procedure with a high number of fabrication steps, as, first, three layers of material need to be patterned; next, judicious alignment between all layers should be guaranteed; and, finally,

multiple rows of tubelets need to be inserted at the correct positions. Figure 2.1b from [11] also implements the cavity top and bottom planes by a conductive coated fabric, but utilizes embroidery to construct the vertical cavity walls. This results in a fully textilized design that is more efficient than antennas where the cavity top and bottom planes are realized by embroidery [14]. Furthermore, as the thin electrotextile threads substitute the vias, the antenna size is reduced even further. However, the vertical wall conductivity is low and rather inaccurate, which impedes reproducibility, and special attention has to be paid to the stitch direction with respect to current flow [15].

This chapter proposes a novel production method to implement SIW technology in textile materials. Now, the antenna cavity is constructed out of a single laser-cut electrotextile layer that is folded around the antenna substrate, thereby implementing all cavity walls without requiring additional tubelet punching or embroidery steps and the corresponding alignment issues. As a result, the fabrication procedure requires fewer manufacturing steps, and yields highly efficient, fully textilized antennas that are not only easier to design, but are also more conveniently fabricated at higher accuracy. Furthermore, these antennas are lightweight, more compact and mechanically more flexible as a result of substituting the heavy metal tubelets by electrotextile slabs. Since ripping of the electrotextile around the metal tubelets has now been avoided, the robustness of the antenna increases. Even further miniaturization is obtained by using a Hirose ultra-small surface mount coaxial connector (U.FL connector) [16] instead of a rather bulky SubMiniature version A (SMA) connector [9], [10], [17].

A representative design is discussed to demonstrate the novel fabrication process. Therefore, an antenna for operation in the [5.15 - 5.85] GHz band has been developed and fabricated, based on the hybrid cavity mode operation principle introduced in [18]. The antenna covers the entire frequency band, and maintains a stable radiation pattern with a broadside gain above 5 dBi and a radiation efficiency of at least 70%, measured both in free space and realistic on body conditions.

This chapter is organized as follows. In Section 2.2, the antenna topology and antenna operation principle are discussed. Specific attention is paid to the choice of materials. In Section 2.3, the manufacturing process is elaborated. Four essential fabrication steps are described to construct the antenna. Section 2.4 shows the influence of essential design parameters on the behavior of the antenna and thus motivates the chosen antenna parameter values. Measurements were performed both in free space and realistic on-body operating conditions. These are discussed in Section 2.5.

2.2 Antenna Design and Material Selection

In this section, the antenna design principle and the figures of merit to which it has to comply are discussed. Furthermore, an insight is given in the utilized antenna materials.

2.2.1 Antenna Design

Design Goals

The antenna will be designed for operation in all unlicensed national information infrastructure (UNII) radio bands. As such, ultra-wideband (UWB) antenna operation is required with an impedance bandwidth extending from 5.15 GHz to 5.85 GHz. This means that the magnitude of the reflection coefficient $|S_{1,1}|$ should remain below -10 dB and an antenna efficiency of at least 70% should be achieved over the entire band, while maintaining stable radiation characteristics. The first requirement will guarantee that at most 10% of the maximally available power is reflected back by the antenna and, therefore, 90% of that power is injected into the antenna. In the presence of losses, this power will either be radiated or dissipated into heat. A radiation efficiency of at least 70% will ensure that maximally 30% of the power injected into the antenna is transferred into heat, while minimally 70% is radiated. Meeting these requirements in the considered frequency band of operation allows, for example, to set up wireless communication using the 802.11ac protocol. From the end user's perspective, the antenna system needs to be highly flexible, robust (and thus also resistant against crumpling), lightweight, and invisibly integrated. From the system engineer's perspective, this means that the radiation characteristics of the antenna need to be stable when the antenna is subject to bending over different curvature radii, an effect that is commonly encountered when the antenna is worn on the human body. Furthermore, when deploying an antenna on the human body, part of the radiated power will be absorbed and transformed into heat in the body itself, in addition to the power dissipated in the antenna itself. Hence, the antenna's radiation efficiency will typically decrease when the antenna is placed on the human body. Therefore, we require that the antenna radiates its energy mainly within half a hemisphere pointing away from the body, such that power absorbed by the human body is minimized. In doing so, the decrease in antenna efficiency by deploying the antenna on the human body will be minimized and a high and stable radiation efficiency can be obtained, which is of high importance given the limited available power in on-body applications. For the end user's safety, such an antenna topology that exhibits low coupling to the human body will also reduce the wearer's radiofrequency-field exposure. The front-to-back ratio of the antenna is a very suitable figure of merit to indicate the isolation between the human body and the antenna, as it describes the amount of power radiated away from the human body with respect to the power radiated towards the human body. This ratio is characterized in free space conditions, since the power radiated towards the body cannot be measured in actual deployment conditions, because this power is directly absorbed by the body. Therefore, in free-space conditions, we require a front-to-back ratio of at least 6 dB, meaning that the antenna radiates four times more power away from the body than towards the body. In this respect, one typically defines the antenna's directivity as the power radiated by the antenna along a certain direction over the power radiated by an isotropic antenna, in which the same amount of power is injected. In contrast

to the directivity, the antenna gain also takes losses in the antenna into account. The antenna gain is found by multiplying the directivity by the antenna's radiation efficiency.

Antenna Topology

In order to fulfill the design goals, a cavity-backed slot antenna topology is chosen. Such antennas are composed of a metallic cavity, filled with a dielectric material, in which a slot is cut out, as seen in Fig. 2.2. The metal walls ensure that the electromagnetic waves only radiate through this slot, being in the hemisphere along the positive Z-axis. Therefore, if the human body is located within the opposite hemisphere, along negative Z values, it will be shielded from radiation, thereby fulfilling the radiation exposure constraint. To achieve mechanical flexibility, a closed-cell expanded-rubber foam is chosen as dielectric substrate, whereas the metal walls of the cavity are implemented in a conducting electrotextile. However, radiating cavities are typically very narrowband, as only one resonant cavity mode is excited [19]. To remedy this, the cavity bandwidth enhancement technique proposed in [18] is applied, providing a -10 dB impedance bandwidth that covers the entire desired frequency band, as explained below.

Operation Principle

Fig. 2.2 schematically illustrates the adopted bandwidth enhancement technique, where two half-mode cavities are brought together to achieve ultra-wideband behavior: Since the field distribution of the TE_{110} mode inside a rectangular cavity is symmetrical, the horizontal symmetry plane of the cavity can be considered as a virtual magnetic wall (Fig. 2.2 step 1) [18]. If now two differently dimensioned half-mode cavities are placed in close proximity within a single antenna footprint, they exhibit a strong coupling to each other. This strong coupling causes mode bifurcation [20], yielding two distinct resonances at frequencies that are controlled by the dimensions of each subcavity and their respective spacing W_s (step 2). Since both resonance frequencies are reasonably close to each other, thorough computer-aided optimization of the aforementioned resonance frequencies allows the coupled half-mode cavities to cover the entire frequency band of operation. At both sides of the radiating slot, electrotextile strips are added to keep both half-mode cavities together, as shown in step 3. These strips will also be used to further tune coupling between both half-mode cavities. In step 4 on Fig. 2.2, the cavity is excited by a coaxial probe feed. Therefore, as shown in Fig. 2.3, the inner and outer conductor of the coaxial feed are connected to the antenna slot plane and back plane, respectively. Well-chosen and optimized positioning of the coaxial feed ensures that a loop is made, which creates a magnetic field inside the cavity that couples to the magnetic fields of both subcavity modes. As such, the E-field of the antenna element lies within the XZ-plane, and the H-field lies within the YZ-plane. This results in an antenna that is linearly polarized along the X-axis. Meanwhile, it has to be kept in mind that mechanical bending causes a solid electrotextile wall to

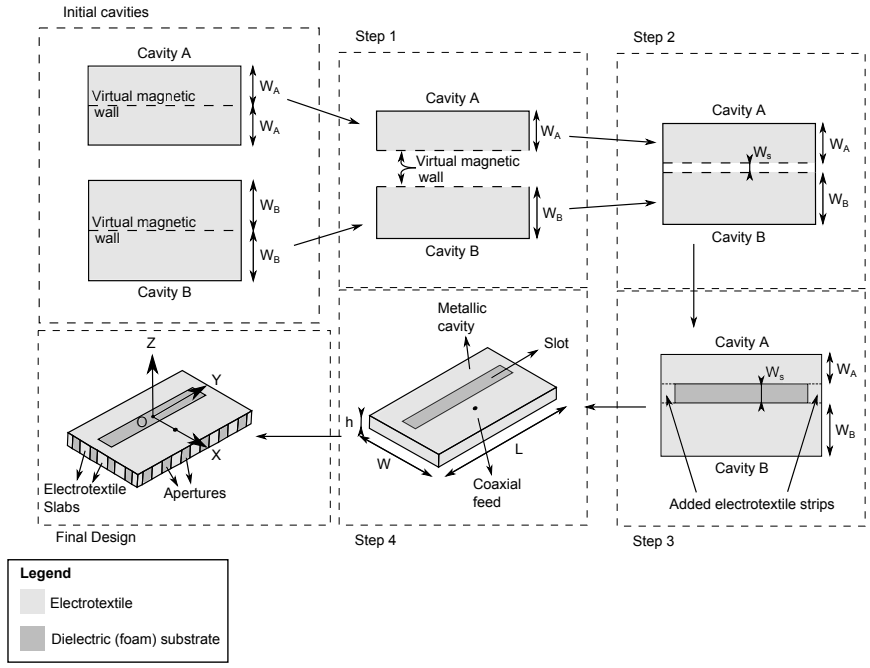

Figure 2.2: Coupled half-mode cavity design steps.

crumple. This undesirable effect is avoided by implementing vertical walls of the cavity as a series of closely spaced electrotextile slabs, instead of solid metal vertical walls commonly used in cavities. This results in the final flexible cavity-backed slot antenna design.

2.2.2 Antenna Materials

As a dielectric foam substrate, a closed-cell expanded rubber, commonly used as a protective foam in firefighter jackets, is chosen and placed in the antenna as shown in Figs. 2.2 and 2.3 [21]. This substrate is flexible, fire-resistant, water-repellent, recovers easily from compression and has a thickness of 4 mm, which is sufficient to achieve the desired bandwidth based on the proposed antenna topology. As a conductive textile, a copper-plated Pure Copper Taffeta electrotextile with a surface resistivity of $0.05\Omega/\square$ is used [8], [22]. A low surface resistivity is necessary to reduce conductive losses in the cavity, and thus contributes to a high antenna efficiency [11]. The electrotextile is glued to the substrate using a thermally-activated adhesive sheet that attaches to the coated fabric, as used in [8].

As displayed in Fig. 2.3, two different types of connectors are investigated to implement the coaxial feed probe. SMA connectors are commonly used in textile designs [8], [9], [11], and have the immediate advantage that they already possess a pin,

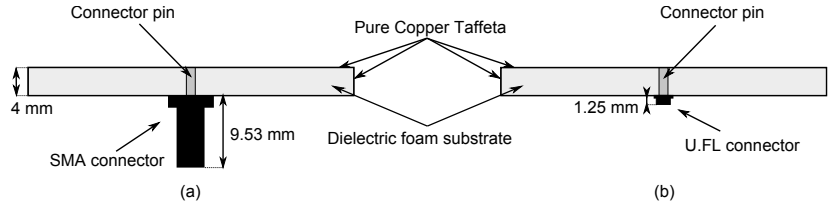

Figure 2.3: Cross-section of the textile ultra-wideband SIW antenna with SMA connector (a) and U.FL connector (b).

which will serve as a feed via to generate the excitation in the cavity [10], as is explained earlier. Yet, as shown in Fig. 2.3, SMA connectors are rather bulky compared to the rest of the design. Because of the importance of miniaturization in wearable electronics, the small size and lightweight properties of U.FL connectors justify investigating the use of this connector type on the antenna. Choosing a U.FL connector over an SMA connector decreases the antenna mass from 3.3 g to only 1.3 g, implying a weight reduction by 60%. However, in that case, a connector pin needs to be soldered to the U.FL connector first. For this, a 1-mm-diameter brass-gold pin is chosen.

2.3 Manufacturing process

The manufacturing process mainly consists of four steps, further explained below. First, the electrotextile is vacuum laminated to the adhesive sheet, after which both are laser cut. The substrate is laser cut as well, albeit in a different form. Then, a judicious alignment procedure is used to attach and wrap the electrotextile-adhesive patch around the substrate. In a final step, a connector with feed pin is inserted into the cavity.

2.3.1 Vacuum Lamination

To ensure that the electrotextile attaches to the substrate in a uniform way, a thermally-activated adhesive sheet has been used. To guarantee uniform adhesion to both the substrate and the electrotextile without glue absorption in either the electrotextile or the substrate, controlled process conditions are required. A Hotronix® Air Fusion heat press is applied to thermally activate the glue with a homogeneously applied pressure of 138 kPa at a temperature of 90°C during 8 seconds. In a first step, the adhesive sheet is thermally activated for attachment to the Pure Copper Taffeta electrotextile. Next, the carrier sheet is removed, leaving behind the glue attached to the electrotextile. Later on, in a final step, the adhesive is activated once more to glue the electrotextile to the substrate.

2.3.2 Laser-Cutting

Patterning fabrics through manual cutting offers insufficient accuracy to yield reproducible antennas. In addition, this approach is too labor-intensive and not suitable for mass production. Furthermore, scalpel cutting induces a significant risk of leaving loose filaments of the fabric, which is especially harmful to antenna performance when the apertures provided for the connector contain electrotextile frays, or when implementing slots which may be short-circuited by these frays. The use of an automatic laser cutter provides computerized sub-millimeter accuracy and not only prevents the cut edges from fraying, but also avoids misalignment between the slot and ground planes. A Pure Copper Taffeta patch, now glued to the adhesive on one side, is laser cut by a BRM90130 100W CO_2 laser cutter in the shape shown in Fig. 2.4 with a laser power of 25 W, at a speed of 100 mm/s, as it melts easier than the substrate, which is cut with a laser power of 80 W at a speed of 20 mm/s.
Depending on the applied connector, a different aperture is cut out for the via connection on the back plane (see Fig. 2.4), above which the applied connector is placed. In order to accommodate an SMA connector, a cylindrical hole with a diameter of 5 mm is cut out. For a U.FL connector, a 1.94 mm to 2.85 mm rectangular hole is chosen instead. The U.FL connector is placed such that the connector's side pin, which is connected to the connector's center conductor (as shown on the top part of Fig. 2.6a), remains separated from the back plane of the antenna cavity.
Making use of the textile slabs shown in Fig. 2.4 avoids the use of bulky and rigid tubelets as in [9], [10], [19]. Using electrotextile slabs instead of tubelets is also a necessity to achieve a low weight, as one single tubelet has a mass of 0.3 g and antennas for comparable operating frequencies easily require more than fifteen such tubelets [8], [9], [13]. Furthermore, the use of tubelets may cause ripping of the electrotextile and may hamper the integration possibilities of the antenna system. Textile slabs also avoid substrate compression due to tubelet punching [10]. Moreover, they guarantee that the sheet resistivity of the vertical walls is known in an exact and reproducible way. In contrast, vertical walls manufactured through embroidery exhibit a sheet resistance that is significantly higher than 0.05 Ω/□, as provided by the electrotextile applied in this work [22]. In addition, embroidered wires may also cause substrate compression [11], [23].

2.3.3 Alignment Procedure

The location of the feed D_f and the dimensions of the connector slot (see H_{aux} and W_{aux} in the enlargement for U.FL and D_{aux} in the enlargement for SMA in Fig. 2.4) for antenna feed placement are important design parameters. Therefore, it is imperative that a robust and straightforward alignment technique is used. Since the electrotextile patch is laser cut in one single piece, potential alignment errors are significantly more visible and thus less likely to happen compared to alignment procedures previously described in literature [6]. Furthermore, the novel workflow increases the ease of fabrication. As shown schematically in Fig. 2.5a, to fix

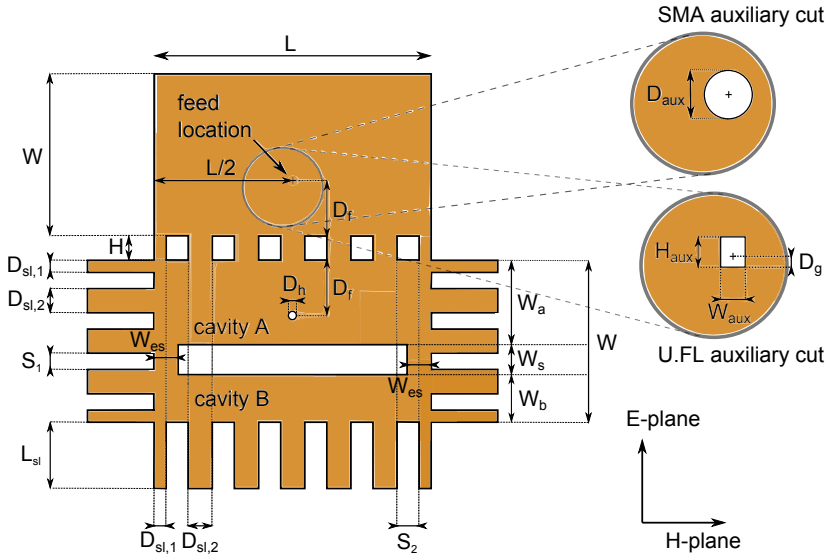

Figure 2.4: Optimized dimensions of the laser cut shape: $H = 4mm, W = 26.8mm, L = 45.9mm, W_a = 14mm, W_b = 7.8mm, W_{es} = 4mm, W_s = 5mm, D_f = 9.2mm, D_h = 0.7mm, D_{aux} = 5mm, H_{aux} = 2.9mm, W_{aux} = 1.9mm, D_g = 0.9mm, L_{sl} = 11mm, D_{sl,1} = 2mm, D_{sl,2} = 4mm, S_1 = 2.7mm, S_2 = 3.7mm$.

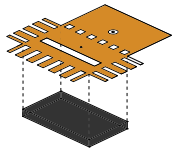

(a) Attachment of top (antenna slot) plane to substrate.

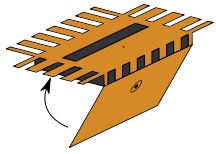

(b) Folding around substrate.

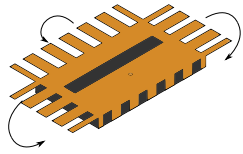

(c) Folding electrotextile around substrate and attachment of slabs.

Figure 2.5: Antenna alignment procedure: steps 1 to 3.

the antenna's slot plane (coming from paragraph 2.3.2) to the substrate, the slot plane part of the electrotextile is thermally activated and connected to one side of the substrate, making use of the adhesive sheet connected to the electrotextile as described in paragraph 2.3.1. In the next step, the back plane is carefully folded around the substrate (Fig. 2.5b), such that it precisely fits the back plane of the substrate. In Fig. 2.5c, the electrotextile ribbons protruding the slot plane are folded around the substrate by a hot surface, thereby activating the adhesive and gluing the ribbons to the back plane.

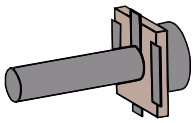

(a) Model of U.FL connector with mounted pin, bottom side.

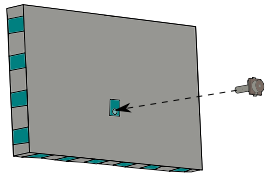

(b) Already perforated cavity, insertion of U.FL connector with mounted pin into cavity.

(c) U.FL connector with soldered pin.

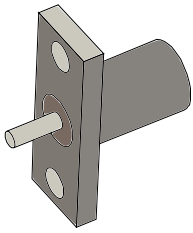

(d) Model of SMA connector with trimmed pin, bottom side.

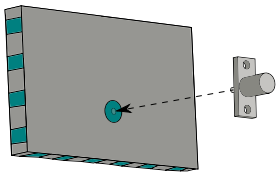

(e) Already perforated cavity, insertion of SMA connector with mounted pin into cavity.

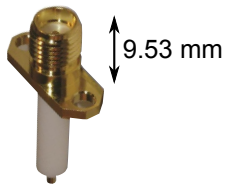

(f) SMA connector.

Figure 2.6: Final step of the fabrication process: Connector placement.

2.3.4 Connector placement

In the final step, the connector is placed. A U.FL connector requires an additional production step. Here, the 1-mm-diameter brass-gold pin is soldered to the inner conductor at the bottom side of the U.FL connector (see Figs. 2.6a and 2.6c). This additional production step is unnecessary for SMA connectors, as they already possess an extruding pin as their center conductor. Instead, the dielectric around the SMA connector's extruding pin is removed, as visible in Fig. 2.6d. Next, the connector is positioned onto the prototype. The pin of the connector is trimmed to an appropriate size, after which it is punched through the substrate, which has been pierced previously. When the connector is in place, its ground pads are soldered to the back plane, after which the other end of the connector pin (which is now slightly protruding from the hole in the slot plane) is soldered to the slot plane, resulting in the final prototypes shown in Fig. 2.7.

2.4 Simulation and Optimization

CST Microwave studio has been used for computer-aided electromagnetic simulation and optimization of the dimensions of the antenna. This has been done by performing a parametric analysis, allowing the design goals to be fulfilled. By optimizing the cavity widths W_a and W_b, the locations of the resonance frequencies

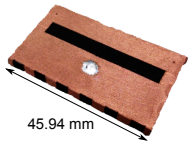

(a) Final design: slot plane.

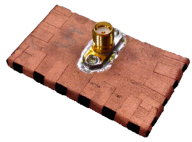

(b) Final design: back plane with SMA connector.

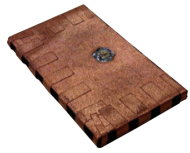

(c) Final design: back plane with U.FL connector.

Figure 2.7: Final design.

can be placed such that the antenna achieves a sufficiently large bandwidth. The length of the cavity L and the placement of the feed D_f are selected for optimal impedance matching. Moreover, the length of the nonresonant slot and, hence, the dimensions of the additional electrotextile strips W_{es}, fixing the actual slot length to $L-2W_{es}$, (highlighted in step 3 of Fig. 2.2) play the role of an additional parameter for tuning the coupling between both half mode cavities. All the aforementioned parameters are optimized to reach an optimal impedance match, while still fulfilling the predetermined impedance bandwidth and radiation goals. The optimized parameter values can be found in Fig. 2.4. The widths $D_{sl,1}$ and $D_{sl,2}$ of the electrotextile slabs are chosen to be sufficiently large, whereas the optimized spacings S_1 and S_2 in between these slabs are small enough such that the fields are contained within the cavity, and lateral radiation losses become negligible. In the meantime, this choice of parameters keeps the antenna cavity mechanically flexible enough to satisfy the wearability constraints.

In Fig. 2.8, we demonstrate the effect of the main dimensions of cavity A (W_a and L) and cavity B (W_b and L) on the antenna's reflection coefficient. Two distinct resonance frequencies can be observed, of which the lowest resonance frequency is related to cavity A and the highest resonance frequency is related to cavity B. Note that the resonance frequency of a cavity is inversely proportional to its dimensions [24]. The design requirements dictate that at least 90% of the maximal power available at the generator should be injected into the antenna over the complete frequency band of operation. This is indicated by the grey rectangular exclusion zone shown in the different subfigures, requiring that the power reflected by the antenna remains below 10%, or -10 dB, between 5.15 GHz and 5.85 GHz. To satisfy these requirements, both resonance frequencies should be carefully selected. Figs. 2.8a and 2.8b show the influence of the half-mode cavity widths W_a and W_b on the resonance frequencies of the antenna, respectively. Since W_a only affects the size of cavity A, by increasing W_a, the lowest resonance frequency decreases while the highest resonance frequency remains unaltered (Fig. 2.8a). A similar behavior can be seen in Fig. 2.8b, where an increase of W_b leads to a downward shift of the highest resonance frequency, while the lowest resonance frequency remains constant. Also, Fig. 2.8c shows that increasing the cavity length L lowers the frequency of operation of the antenna. Indeed, increasing L causes both cavities A and B to increase in size, thereby shifting their respective resonance frequencies

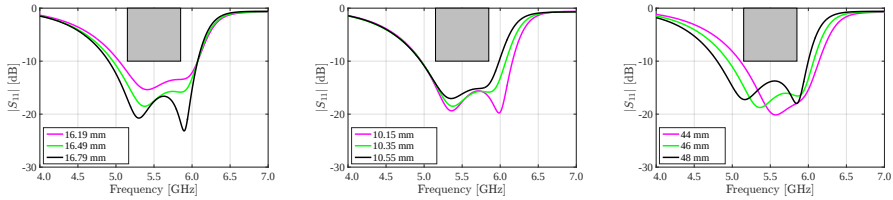

(a) Influence of W_a. (b) Influence of W_b. (c) Influence of L.

Figure 2.8: Simulated influence of cavity dimensions on the magnitude of the reflection coefficient $|S_{1,1}|$ of the antenna.

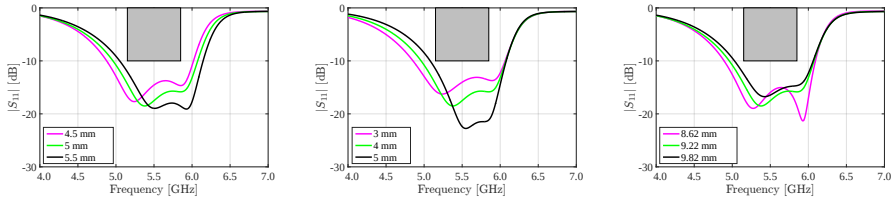

(a) Influence of slot width W_s. (b) Influence of electrotextile strip width W_{es}. (c) Influence of feed position D_f.

Figure 2.9: Influence of coupling and feed position on the magnitude of the reflection coefficient $|S_{1,1}|$ of the antenna.

downwards. However, for all considered variations on W_a, W_b and L, the design requirements remain satisfied, proving the resilience of the antenna design with respect to fabrication tolerances.

In Fig. 2.9, the influences of the nonresonant slot and the feed placement are demonstrated. Decreasing the spacing W_s between both half-mode cavities increases the degree by which they are coupled. As such, the mode bifurcation effect is amplified. This is clear from Fig. 2.9a, where the cavity resonances move further apart indeed. Moreover, it can be noted that decreasing W_s while keeping the total antenna width W constant causes both half-mode cavities to become larger, which lowers their resonance frequencies. This explains the frequency shift visible on Fig. 2.9a. Figs. 2.9b and 2.9c show the influence of W_{es} and D_f, respectively, on the matching of the antenna. Hereby, a trade-off is made between keeping sufficient margins in terms of bandwidth, on the one hand, and maintaining a sufficient impedance match, on the other hand. Fig. 2.9 proves that none of its three discussed dimensions are critical, as the margins on the deviations of the discussed parameters are sufficiently large. The same conclusions were made for Fig. 2.8.

The width of the slabs is the primary parameter controlling the containment of the electromagnetic field inside the cavity. As elaborated in [12], proper field contain-

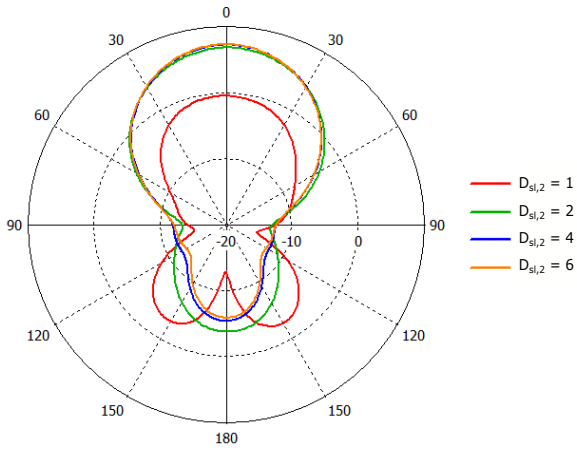

Figure 2.10: Simulated 4.7424 GHz radiation pattern as a function of $D_{sl,2}$ (as defined in Figure 2.4). Smaller values for $D_{sl,2}$ result in larger back lobes of the antenna, since the field containment inside the cavity is worse. The extreme value of $D_{sl,2} = 1$ mm causes the cavity's field containment to fail altogether, which can be seen in the innermost (red) radiation pattern.

ment is achieved when the slabs are as wide as the apertures that separate them. In this way, the radiation will only leave the antenna through the slot in the top plane, which agrees to the intended operation of the antenna. Furthermore, the slab width proves to be the only parameter that exhibits a significant impact on the front-to-back-ratio (FTBR) of the antenna. From the simulations in Figure 2.10, it can be seen that a decreasing slab width results in an increase in the magnitude of the antenna's back lobe. This is demonstrated by the green radiation pattern (corresponding with $D_{sl,2} = 2$ mm, as defined on Figure 2.4), which unmistakably separates from the other radiation patterns corresponding with higher values of $D_{sl,2}$. The exceptionally deviant red pattern however, is obtained for $D_{sl,2} = 1$ mm. Clearly, with such narrow slabs, the cavity fails to contain the field.

2.5 Experimental results

This section discusses the measured figures of merit of the antenna prototypes in free space, as well as when the prototypes are subject to bending in a free space environment. Furthermore, the influence of humidity content and the proximity of the human body is measured.

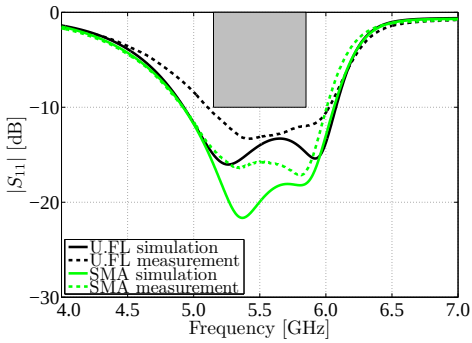

Figure 2.11: Magnitude of the reflection coefficient $|S_{1,1}|$ of the measured antennas in free space, with respect to a 50Ω reference impedance.

2.5.1 Antenna Validation

Figures of merit in free space

The reflection loss and radiation performance of the proposed antenna have been measured in a full-anechoic chamber using an Agilent N5242A PNA-X Microwave Network Analyzer [25] and an Orbit/FR DBDR antenna positioning system. As seen in Fig. 2.11, both the SMA and U.FL antennas clearly exhibit two separate resonances, whereby those of the antenna with SMA connector correspond best to the resonance frequencies as predicted by simulations. It is seen that the broadband design of the measured antenna indeed provides complete coverage of the desired frequency band. Moreover, the bandwidth of the SMA antenna is very similar to the simulated bandwidth. The model using the U.FL connector exhibits a reduced bandwidth as a result of an upwards shifted lower resonance frequency. This is the result of fabrication tolerances. Still, the U.FL prototype covers the desired frequency band. The prototypes of the U.FL antenna and the SMA antenna exhibit a -10 dB bandwidth of 920 MHz and 1.09 GHz, respectively, which categorizes them as UWB antennas [26]. In general, the small differences between measured and simulated results in Fig. 2.11 are due to production tolerances as well as variations in material properties and in the environmental deployment conditions. Although laser patterning and the simplified and improved alignment procedure yield a significantly improved accuracy over hand cutting [27] and alignment, some small manufacturing and alignment errors remain that affect antenna performance. Moreover, the substrate and electrotextile's material properties will slightly vary from batch to batch and with changing environmental conditions [27], [28], giving rise to slightly different antenna characteristics.

The measured antennas maintain a stable gain over the desired frequency band. However, the antenna gain slightly drops off for higher frequencies, as seen in

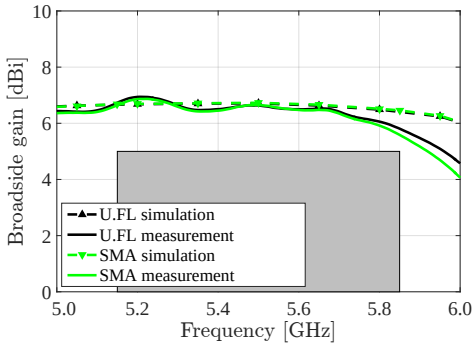

Figure 2.12: Comparison between simulated and measured gain of the measured antennas in free space.

Fig. 2.12. This is due to an increase of the substrate's dielectric losses and the electrotextile's conductor losses. This results in a lower radiation efficiency (see Tables 2.1 and 2.2) and, hence, smaller antenna gain at higher frequencies. Yet, the measured broadside gain remains larger than 5 dBi over the entire frequency band under study. Furthermore, there is a good correspondence between measurements and simulations. Also, it is to be noted that the impact of the chosen connector remains small.

Figs. 2.13 and 2.14 show the radiation patterns in the H-plane and E-plane of the U.FL antenna and the SMA antenna, respectively. As predicted by simulations, both antennas exhibit very similar radiation patterns (see Fig. 2.15) that remain stable over the desired band. The antenna efficiency, gain and front-to-back ratio of both antennas are evaluated at 5.15 GHz, 5.50 GHz and 5.85 GHz, as summarized in Tables 2.1 and 2.2. Both antennas exhibit an efficiency higher than 70% and a gain above 5 dBi. It is thus proven that the antenna meets the free-space design goals formulated in Section 2.2.1.

Table 2.1: Radiation efficiency, broadside gain and front-to-back ratio (FTBR) of the antenna with the U.FL connector.

Frequency [GHz]	5.15	5.50	5.85
Simulated total radiation efficiency [%]	91	89	82
Measured total radiation efficiency [%]	94	90	74
Simulated maximum gain [dBi]	6.72	6.83	6.62
Measured maximum gain [dBi]	6.73	6.64	5.81
Simulated FTBR [dB]	10.47	11.99	14.38
Measured FTBR [dB]	8.39	8.50	7.85

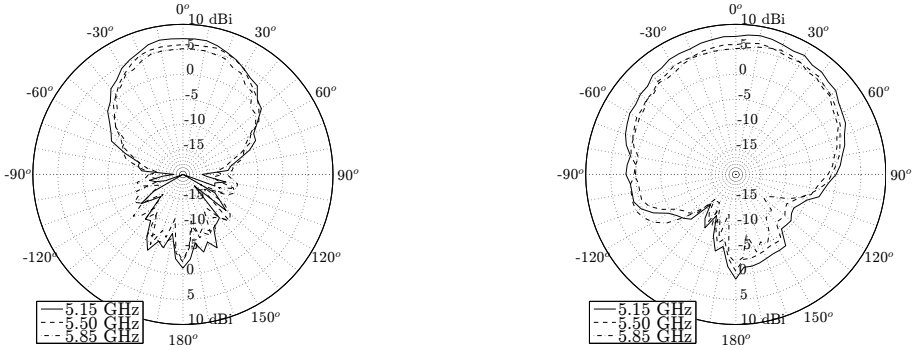

(a) H-plane (b) E-plane

Figure 2.13: Free space radiation pattern of the U.FL antenna.

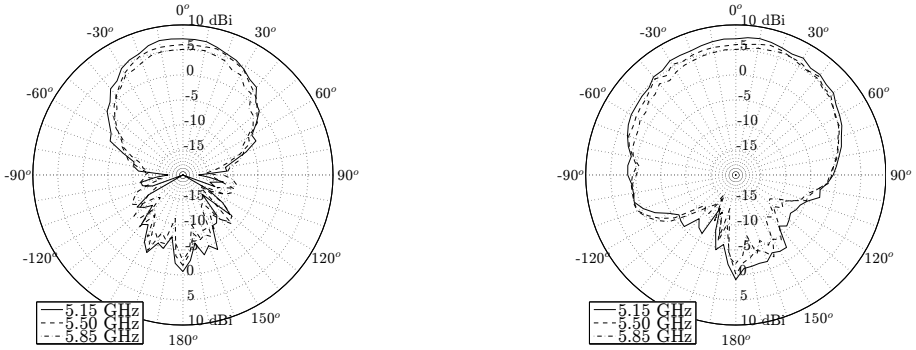

(a) H-plane (b) E-plane

Figure 2.14: Free space radiation pattern of the SMA antenna.

Table 2.2: Radiation efficiency, broadside gain and front-to-back ratio (FTBR) of the antenna with the SMA connector.

Frequency [GHz]	5.15	5.50	5.85
Simulated total radiation efficiency [%]	90	92	87
Measured total radiation efficiency [%]	92	90	70
Simulated maximum gain [dBi]	6.71	6.79	6.60
Measured maximum gain [dBi]	6.65	6.66	5.59
Simulated FTBR [dB]	10.09	11.65	13.69
Measured FTBR [dB]	7.90	7.97	7.93

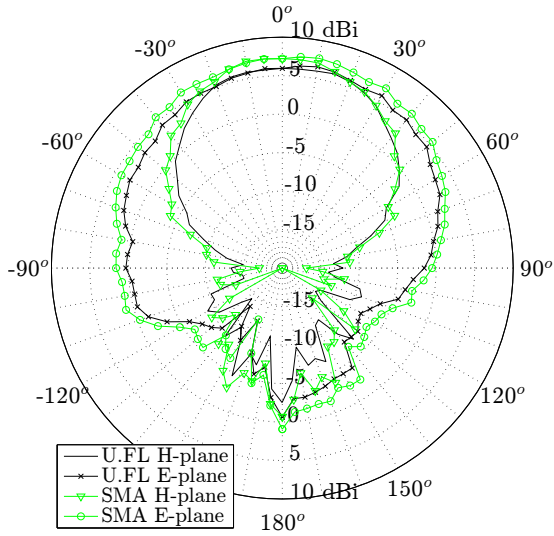

Figure 2.15: Measured radiation patterns of the U.FL antenna and the SMA antenna.

(a) Measured on-body placements of the antenna.

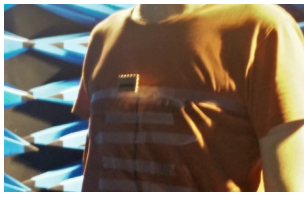

(b) Torso measurement.

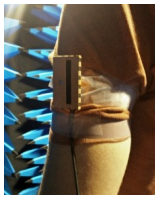

(c) Upper right arm measurement.

Figure 2.16: On-body measurement experimental setup.

Figures of merit on body

Besides free-space measurements, the antenna performance was also evaluated in an on-body deployment scenario. Therefore, the antenna has been measured while worn on the torso of an average adult person of size 1m90 and weight: 85 kg, as well as on the upper left arm of the test subject (see Fig. 2.16). Fig. 2.17 shows a very good antenna performance for all measurements, whether the antenna was characterized in free space, on torso or on the upper left arm. In all measured scenarios, the desired frequency band remains covered.

Fig. 2.18 shows the radiation patterns of all aforementioned scenarios. Note the good correspondence with the simulated free space radiation pattern. Nevertheless, it is important to notice that the broadside gain reduces to some degree and

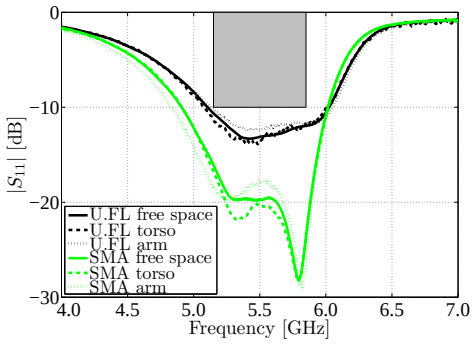

Figure 2.17: Magnitude of the reflection coefficient $|S_{1,1}|$ of the measured antennas in free space compared to measurement on torso and on the left arm, again with respect to a 50Ω reference impedance.

the 3 dB-beamwidth slightly enlarges when deploying the antenna on the human torso. This effect can be attributed to the wider ground plane formed by the presence of the human body [29]. Yet, both measurements in which the antenna is placed on torso and on the upper left arm, exhibit a broadside gain larger than 4 dBi and a 3 dB-beamwidth larger than 60°. Observe that, when the antenna is deployed on the body, most of its backward radiation is suppressed due to body shadowing. Most electromagnetic fields radiated by the antenna towards the body are absorbed and dissipated as heat in the lossy body tissues. This effect also reduces the antenna's radiation efficiency. Note that, thanks to the high antenna-body isolation of the adopted antenna topology, the reduction in radiation efficiency and gain remains small when deploying the antenna on body.

Effects of humidity content

The influence of varying relative humidity conditions on the performance of the antenna has also been investigated. Therefore, between every measurement, the antenna has been exposed to a specified relative air humidity in a climate test cabinet (WK 350 from Weiss Technik) for at least 16 hours. The relative humidity of 0% was achieved by placing the antenna in a closet filled with a constant nitrogen gas flow, as this gas has a relative permittivity that is identical to that of dry air, but it contains no water vapor. Fig. 2.19 shows that the humidity content of the antenna has little influence on antenna behavior. Under all measured circumstances, the antenna bandwidth and impedance matching remain stable. Given the low moisture regain of the selected materials, this is an expected result.

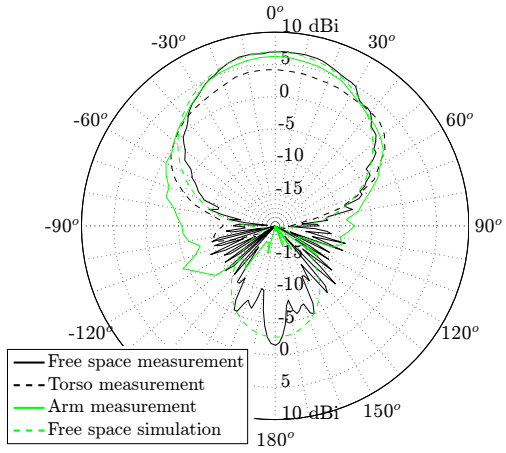

Figure 2.18: Measured vs. simulated 5.50 GHz H-plane radiation patterns of the U.FL antenna, free space vs. on body.

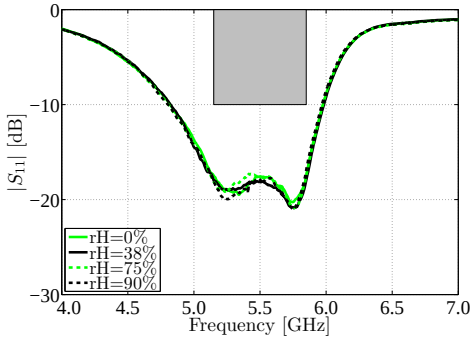

Figure 2.19: Magnitude of the reflection coefficient of the measured antenna for different relative humidities, with respect to a 50Ω reference impedance.

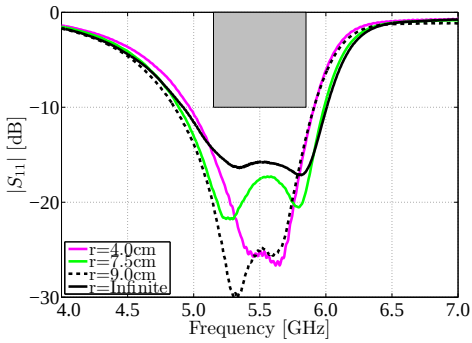

Figure 2.20: Magnitude of the reflection coefficient $|S_{1,1}|$ of the SMA antenna in free space (r= Infinite) compared to the magnitude of the reflection coefficient $|S_{1,1}|$ of the same antenna subject to bending around the X-axis, under different curvature radii r.

2.5.2 Effects of antenna deformation

In a last set of tests, we have evaluated the effect of mechanical bending on the SMA antenna. Here, the antenna has been subjected to a selection of bending radii common to deployment at various locations on the human body. The magnitude of the reflection coefficient $|S_{1,1}|$ of the antenna has been investigated when bending the antenna around its X-axis. Fig. 2.20 shows that under each of these circumstances, the antenna still covers the desired frequency band in terms of impedance match. The small variations in the antenna's reflection coefficient are due to changes in antenna geometry, which may also result in substrate compression and a subsequent increase in substrate permittivity, as demonstrated in [30].

Both H-plane and E-plane radiations pattern of the antenna still meet the design goals when the antenna is bent. It can be observed from Fig. 2.21 that both the -3 dB-beamwidth of the antenna and its antenna gain remain unaffected when the antenna is subjected to the investigated bending conditions.

2.6 Conclusions

A novel production process for wearable high-performance substrate integrated waveguide (SIW) cavity-backed textile antennas was proposed. The production process has been applied to fabricate two novel wearable and flexible cavity-backed SIW antennas for ultra-wideband operation in the [5.15-5.85] GHz band. To construct these antennas, materials commonly found in firefighter suits have been used. The resulting antenna prototypes benefit from an increased mechanical flexibility, while they maintain their radiation and impedance matching properties

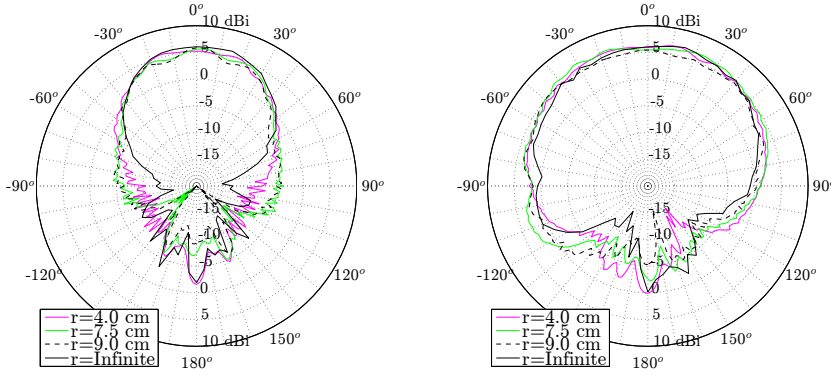

(a) H-plane. (b) E-plane.

Figure 2.21: Measured 5.50 GHz free space radiation pattern of the SMA antenna bent around the X-axis, under different curvature radii r.

over the entire investigated band. Furthermore, the antenna is produced more accurately and requires fewer production steps than previous production methods, thereby resulting in an easier and faster fabrication procedure. The process creates smaller, lighter and mechanically more flexible antennas than cavity-backed SIW antennas fabricated using tubelets. Moreover, it produces more efficient antennas with more precisely known sheet resistivities than similar antennas produced by embroidery. This process may result in the production of actual unobtrusive and discretely wearable textile antenna systems on an industrial scale. Measurements show that the realized antennas continue to meet the predetermined specifications within the entire [5.15 - 5.85] GHz band, when they are subject to mechanical bending as well as when they are exposed to varying relative humidity conditions. This proves that the new manufacturing procedure allows for an accurate and swift way to realize robust, wearable high-performance antennas that are suitable as a wireless node in on-body communication systems.

References

[1] P. Vanveerdeghem, P. Van Torre, C. Stevens, J. Knockaert, and H. Rogier, "Synchronous Wearable Wireless Body Sensor Network Composed of Autonomous Textile Nodes", *Sensors*, vol. 14, pp. 18 583–18 610, 2014.

[2] A. Dierck, S. Agneessens, F. Declercq, B. Spinnewyn, G.-J. Stockman, P. Van Torre, L. Vallozzi, D. Vande Ginste, J. Vanfleteren, T. Vervust, and H. Rogier, "Active Textile Antennas in Professional Garments for Sensing, Localisation and Communication", *International Journal of Microwave and Wireless Technologies*, vol. 6, no. 3-4, pp. 331–341, 2014.

[3] T. Yilmaz, R. Foster, and Y. Hao, "Detecting Vital Signs with Wearable Wireless Sensors", *Sensors*, no. 10, pp. 10 837–10 862, 2010.

[4] J. van den Brand, M. de Kok, M. Koetse, M. Cauwe, R. Verplancke, F. Bossuyt, M. Jablonski, and J. Vanfleteren, "Flexible and Stretchable Electronics for Wearable Health Devices", *Solid-State Electronics*, vol. 113, pp. 116–120, 2015.

[5] J. Lilja, V. Pynttäri, T. Kaija, R. Mäkinen, E. Halonen, H. Sillanpää, J. Heikkinen, M. Mäntysalo, P. Salonen, and P. de Maagt, "Body-Worn Antennas Making a Splash: Lifejacket-Integrated Antennas for Global Search and Rescue Satellite System", *IEEE Antennas and Propagation Magazine*, vol. 55, no. 2, pp. 324–341, 2013.

[6] A. Dierck, H. Rogier, and F. Declercq, "A Wearable Active Antenna for Global Positioning System and Satellite Phone", *IEEE Transactions on Antennas and Propagation*, vol. 61, no. 2, pp. 532–538, 2013.

[7] C. Loss, R. Gonçalves, C. Lopes, P. Pinho, and R. Salvado, "Smart Coat with a Fully-Embedded Textile Antenna for IoT Applications", *Sensors*, vol. 16, pp. 1–13, 2016.

[8] S. Lemey, T. Castel, P. V. Torre, T. Vervust, J. Vanfleteren, P. Demeester, D. Vande Ginste, and H. Rogier, "Threefold Rotationally Symmetric SIW Antenna Array for Ultra-Short-Range MIMO Communication", *IEEE Transactions on Antennas and Propagation*, vol. 64, no. 5, pp. 1689–1699, 2016.

[9] S. Lemey and H. Rogier, "SIW Textile Antennas as a Novel Technology for UWB RFID Tags", in *2014 IEEE RFID Technology and Applications Conference (RFID-TA)*, Sep. 2014, pp. 256–260.

[10] R. Moro, S. Agneessens, H. Rogier, A. Dierck, and M. Bozzi, "Textile Microwave Components in Substrate Integrated Waveguide Technology", *IEEE Transactions on Microwave Theory and Techniques*, vol. 63, no. 2, pp. 422–432, Feb. 2015.

[11] T. Kaufmann and C. Fumeaux, "Wearable Textile Half-Mode Substrate-Integrated Cavity Antenna Using Embroidered Vias", *IEEE Antennas and Wireless Propagation Letters*, vol. 12, pp. 805–808, 2013.

[12] M. Bozzi, A. Georgiadis, and K. Wu, "Review of Substrate-Integrated Waveguide Circuits and Antennas", *IET Microwaves, Antennas & Propagation*, vol. 5, no. 8, pp. 909–920, Jun. 2011.

[13] S. Agneessens and H. Rogier, "Compact Half Diamond Dual-Band Textile HMSIW On-Body Antenna", *IEEE Transactions on Antennas and Propagation*, vol. 62, no. 5, 2374–2381, 2014.

[14] T. Kaufmann, I. M. Fumeaux, and C. Fumeaux, "Comparison of Fabric and Embroidered Dipole Antennas", in *2013 7th European Conference on Antennas and Propagation (EuCAP)*, Apr. 2013, pp. 3252–3255.

[15] R. Seager, S. Zhang, A. Chauraya, W. Whittow, Y. Vardaxoglou, T. Acti, and T. Dias, "Effect of the Fabrication Parameters on the Performance of Embroidered Antennas", *IET Microwaves, Antennas Propagation*, vol. 7, no. 14, pp. 1174–1181, 2013.

[16] *Ultra Small Surface Mount coaxial Connectors*, Hirose Electric Co., Ltd.

[17] Y. Wang and Y. Lu, "The Strip-Ground Rectangular Patch Antenna", *International Journal of Antennas and Propagation*, vol. 2017, p. 7, 2017.

[18] Q. Van den Brande, S. Lemey, J. Vanfleteren, and H. Rogier, "Highly Efficient Impulse-Radio Ultra-Wideband Cavity-Backed Slot Antenna in Stacked Air-Filled Substrate Integrated Waveguide Technology", *IEEE Trans. Antennas Propag.*, vol. 66, no. 5, pp. 2199–2209, 2018.

[19] G. Q. Luo, Z. F. Hu, L. X. Dong, and L. L. Sun, "Planar Slot Antenna Backed by Substrate Integrated Waveguide Cavity", *IEEE Antennas and Wireless Propagation Letters*, vol. 7, 236–239, 2008.

[20] J.-S. Hong and M. J. Lancaster, "Couplings of Microstrip Square Open-Loop Resonators for Cross-Coupled Planar Microwave Filters", *IEEE Trans. Microw. Theory Tech.*, vol. 44, no. 11, pp. 2099–2109, Nov. 1996.

[21] *Closed Cell Expanded Rubber NBR 41-42*, Javaux.

[22] *Pure Copper Polyester Taffeta Fabric*, Less EMF Inc.

[23] F. X. Liu, T. Kaufmann, Z. Xu, and C. Fumeaux, "Wearable Applications of Quarter-Wave Patch and Half-Mode Cavity Antennas", *IEEE Antennas and Wireless Propagation Letters*, vol. 14, pp. 1478–1481, 2015.

[24] D. Pozar, *Microwave Engineering*. Wiley, 2004.

[25] *N5242A PNA-X Microwave Network Analyzer, 26.5 GHz*, Keysight Technologies, 2017.

[26] D. Dardari, R. D'Errico, C. Roblin, A. Sibille, and M. Z. Win, "Ultrawide Bandwidth RFID: The Next Generation?", *Proceedings of the IEEE*, vol. 98, no. 9, pp. 1570–1582, Sep. 2010.

[27] M. Rossi, A. Dierck, H. Rogier, and D. Vande Ginste, "A Stochastic Framework for the Variability Analysis of Textile Antennas", *IEEE Transactions on Antennas and Propagation*, vol. 62, no. 12, pp. 6510–6514, Dec. 2014.

[28] M. Rossi, S. Agneessens, H. Rogier, and D. Vande Ginste, "Assembly-Line-Compatible Electromagnetic Characterization of Wearable Antenna Substrates", *IEEE Antennas and Wireless Propagation Letters*, vol. 16, pp. 1365–1368, 2017.

[29] F. Declercq, A. Georgiadis, and H. Rogier, "Wearable Aperture-Coupled Shorted Solar Patch Antenna for Remote Tracking and Monitoring Applications", in *Proceedings of the 5th European Conference on Antennas and Propagation (EUCAP)*, Apr. 2011, pp. 2992–2996.

[30] F. Boeykens, H. Rogier, and L. Vallozzi, "An Efficient Technique Based on Polynomial Chaos to Model the Uncertainty in the Resonance Frequency of Textile Antennas due to Bending", *IEEE Transactions on Antennas and Propagation*, vol. 62, no. 3, pp. 1253–1260, Mar. 2014.

3

Foldable All-Textile Cavity-Backed Slot Antennas for Personal UWB Localization

Dries Van Baelen, Quinten Van den Brande, Sam Lemey, Jo Verhaevert and Hendrik Rogier

Published in Radio Science

An all-textile multi-moded cavity-backed slot antenna has been designed and fabricated for body-worn impulse radio ultra-wideband (IR-UWB) operation in the [3744-4742.4] MHz frequency band, thereby covering Channels 2 and 3 of the IEEE 802.15.4a standard. Its light weight, mechanical flexibility and small footprint of 35 *mm* × 56 *mm facilitate integration into textile for radio communication equipment for first aid responders, personal locator beacons and equipment for localization and medical monitoring of children or the elderly. The antenna features a stable radiation pattern and reflection coefficient in diverse operating conditions such as in free space, when subject to diverse bending radii, and when deployed on the torso or upper right arm of a test person. The high isolation towards the wearer's body originates from the antenna's hemispherical radiation pattern with a -3 dB beamwidth of* 120° *and a front-to-back-ratio (FTBR) higher than 11 dB over the entire band. Moreover, the antenna exhibits a measured maximum gain higher than 6.3 dBi and a radiation efficiency over* 75%*. In addition, orientation-specific pulse distortion introduced by the antenna element is analyzed by means of the System Fidelity Factor (SFF). The SFF of the communication link between two instances of this antenna is higher than 94% for all directions within the antenna's -3 dB beamwidth. This easily wearable and deployable antenna is suitable to support IR-UWB localization with an accuracy in the order of 5 cm.*

3.1 Introduction

The promising ascent of the Internet of Things (IoT) includes an increasing demand for reliable and integrable Wireless Body Area Network (WBAN) systems [1]. To achieve a market breakthrough, these systems should be wearable in an unobtrusive and comfortable way [2], [3]. Given their mechanical flexibility and the possibilities for unobtrusive on-body integration, textile implementations are promising candidates to fill in a WBAN system's antenna role [4]. In the last decade, a significant amount of research has been invested in the development of textile antennas, enabling applications for first aid responders [5]–[7], healthcare [8]–[11], sports [12], space [13], military [14], [15], RFID [16] and by extension the Internet of Things (IoT) [17]–[19]. The opening of the 3.1-10.6 GHz UWB band along with the publication of the IEEE 802.15.4 standard [20] creates possibilities which recently are being picked up by textile electronics developers.

UWB allows for very high data rates for close-range communication with excellent resilience against multipath effects [21], [22], while using power levels close to the noise floor, thereby avoiding interference with narrowband systems [23]. This low power use is particularly favorable for body-worn systems considering their often limited availability of power [2]. Furthermore, the high available bandwidth enables impulse radio ultra-wideband (IR-UWB) systems to use very narrow time-domain pulses, which allows for ranging at centimeter-scale accuracy [24], [25] with a high immunity against multipath fading [23]. Examples of applications include cyclist positioning systems using the Decawave's DW1000 IC [26], systems for respiration and heartbeat monitoring [27], drone localization [28] and breathing detection of victims buried under building rubble [29]. To allow localization algorithms to provide accurate results, special care must be taken by the designer to mitigate the pulse distortion introduced by the antenna [30].

In the most recent years, numerous UWB textile antennas have been developed, of which many target the IEEE 802.15.4 frequency bands [31]–[36]. However, these antennas do not meet all applicable criteria for antenna deployment in a body-worn scenario for IR-UWB operation. From the time domain perspective, the pulse distortion introduced by the antenna should be reduced to the bare minimum [30]. As of today, this issue is still underexposed in IR-UWB design for wearables. From the perspective of wearability, the antenna must exhibit a small footprint and should be mechanically flexible [37], [38]. In addition, effects such as bending and the presence of the human body should not adversely affect antenna performance [39], [40]. Furthermore, the aforementioned limited availability of power in body-worn systems requires a high radiation efficiency [41]. Moreover, the antenna's radiation pattern should remain stable over the targeted frequency band to mitigate orientation-specific pulse distortion [42]. Finally, in textile antenna design, the moisture regain of the materials applied as substrates should be limited to 3%, to avoid significant deviations in the substrate's dielectric permittivity [43]. The design of a textile antenna system for reliable and high-accuracy IR-UWB applications should take all aforementioned specifications in account.

In this chapter, the bandwidth enhancement technique proposed by Van den Brande et al. (2018) is combined with time and frequency co-simulation to design a wearable all-textile cavity-backed slot antenna for use in on-body IR-UWB systems. The antenna is developed on a substrate with a low moisture regain and manufactured using an accurate and reliable fabrication methodology for textile-based cavity-backed slot antennas [44], to ensure stable behavior of the antenna materials and a reliable, accurate and automated fabrication process. This results in a small and flexible antenna in which only the connector is rigid. Measurements on a fabricated prototype show that the antenna's reflection coefficient with respect to 50 Ω remains below -10 dB over the 3744 MHz - 4742.4 MHz band when deployed in free space, when deployed on diverse locations on the human body and when subjected to diverse bending radii. Moreover, the antenna's radiation pattern is directed away from the wearer's body and remains stable over the entire frequency band for all investigated scenarios. Finally, for all relevant directions, the antenna's orientation specific pulse distortion is low, demonstrated by a System Fidelity Factor (SFF) higher than 94% as discussed in Section 3.4.2.

This chapter is structured as follows. In Section 3.2, the design specifications are put forward, together with a discussion of the chosen antenna topology and its operation principle. Section 3.3 elaborates on the dedicated fabrication method for the production of all-textile cavity-backed Substrate Integrated Waveguide (SIW) antennas, and more specifically how it is applied to implement this design. Simulations have been performed in both time and frequency domain to meet the design goals. Time domain results and the final antenna dimensions are shown in Section 3.4. In Section 5, the results of the measurements, both in free space and on a human body, are discussed.

3.2 Antenna Design

This section discusses the antenna's design specifications in both frequency and time domain, along with the antenna topology chosen to meet these goals. Furthermore, the utilized antenna materials are briefly discussed.

3.2.1 Design specifications

The antenna is designed to cover both Channels 2 (3744 MHz - 4243.2 MHz) and 3 (4243.2 MHz - 4742.4 MHz) of the IEEE 802.15.4 standard for personal IR-UWB-based localization applications with an accuracy of at least 5 cm. Therefore, over both frequency ranges, the magnitude of the reflection coefficient of the antenna with respect to 50 Ω should stay below -10 dB. Moreover, the radiation pattern and the gain should remain stable in these channels. Over the targeted frequency band, the broadside gain should vary no more than by 3 dB and the radiation efficiency should be at least 70%. These characteristics should be maintained when the antenna is deployed on the human body or when it is subjected to

mechanical bending, which often occurs during deployment on the human body. In addition, a front-to-back-ratio (FTBR) higher than 6 dB is recommended to minimize absorption of antenna radiation by the human body. Increasing the FTBR not only decreases the wearer's radiofrequency-field exposure, but also improves the antenna's radiation efficiency. This is especially desirable because of the limited available power in body-worn applications. Minimizing coupling between the antenna and the wearer's body also results in a more stable radiation pattern and offers more options in terms of suitable antenna deployment on the body.

Furthermore, IR-UWB applications require minimal pulse distortion introduced by the transmit and receive antenna. Otherwise, the deformation of the received pulse may affect the localization algorithms, resulting in an inaccurate location estimation. Given that the propagation channel acts as a dispersive medium, pulse distortion should be considered at the system level, taking into account both transmit and receive antennas, as well as the wireless channel [45]. A useful figure of merit to express pulse distortion in the total localization system is the System Fidelity Factor [46]. For localization purposes, the SFF of the IR-UWB system is generally required to be larger than or equal to 90% for all relevant orientations of the receive antenna, with respect to the transmit antenna.

3.2.2 Antenna topology and materials

A cavity-backed slot antenna is adopted to satisfy all imposed design requirements and to facilitate an all-textile implementation. To implement such an antenna, a slot is cut out in a coaxially fed metallic cavity that is filled by a dielectric material. The metal cavity walls ensure that the slot is the only radiating part of the antenna, thereby directing the antenna radiation away from the human body. As radiating cavities typically exhibit a narrowband behaviour, the bandwidth enhancement technique proposed by Van den Brande et al. (2018), is applied to ensure that the antenna covers the entire frequency band, as elaborated in Section 3.2.3.

The complete implementation of the antenna in textile materials offers the mechanical flexibility necessary in body-worn systems and allows for integration into the garments of the user. As a conductive material, copper-plated Pure Copper Taffeta electrotextile by Less EMF (`lessemf.com`) is used. This material has excellent handling characteristics facilitating antenna fabrication, and offers a very low sheet resistivity of $0.05\Omega/\square$, which reduces the conductivity losses of the antenna and thus favorably impacts the radiation efficiency. The dielectric substrate is implemented in a closed-cell expanded rubber material by Javaux (`javaux.com`). With a thickness of 4 mm and excellent recovery from mechanical compression it offers a sufficiently large and stable thickness required for reliable broadband cavity antenna design. Furthermore, its low moisture regain makes its electromagnetic characteristics very resistant against humidity variations. This material is commonly applied as a protective foam in firefighter jackets owing to its resistance against water, heat, fire and a diverse spectrum of chemical compounds.

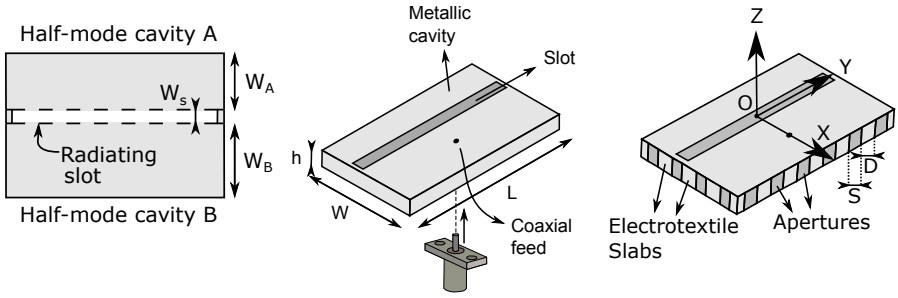

Figure 3.1: Coupled half-mode cavity design.

3.2.3 Operation principle

Since radiating cavities are typically very narrowband, we apply the bandwidth enhancement technique proposed by Van den Brande et al. (2018). In this approach, the open sides of two half-mode cavities with comparable resonance frequencies are brought in close proximity, as shown in Figure 3.1a. Thereby, both half mode cavity resonators are coupled, resulting in mode bifurcation, which distinctly moves both resonances apart [47]. By thorough computer-aided optimization of the half-mode cavity dimensions, along with an adjustment of the separation between both and, thus, the coupling between them, a precise control of the location of both resonance frequencies can be obtained. This allows for a complete coverage of the frequency band of operation. The cavity is excited by a coaxial feed, judiciously placed into one of the half mode cavities (Figure 3.1b). By connecting the cavity's top and bottom plane to the feed's central and outer conductors respectively, a loop is formed, creating a magnetic field in the cavity that couples to the resonant modes of both half-mode subcavities [41]. Therefore, the antenna's E-field lies in the XZ-plane, as shown in Figure 3.1c, and the H-field lies in the YZ-plane. As such, the antenna is linearly polarized.

In a realistic deployment scenario, the electrotextile forming the SIW cavity tends to crumple when it is subject to bending, causing delamination of the electrotextile and the substrate. To avoid this, apertures have been introduced in the vertical cavity walls to ensure that the bending of the vertical cavity walls occurs only along these apertures, thereby reducing stress on the electrotextile. This is illustrated in Figure 3.1c. To minimize radiation losses, the recommended ratio S/D between the width of the apertures and the width of the electrotextile slabs should be equal to or lower than 1 [48].

To accommodate the need for fabrication convenience and automation, together with demanding requirements for wearability and, hence, textilization of the design, the dedicated fabrication process proposed by Van Baelen et al. (2018), is applied, as further elaborated in Section 3.3.

3.3 Fabrication method

The accurate fabrication process can be summarized in four main steps. First, the electrotextile is vacuum laminated to a thermally activated sheet adhesive. Next, both the substrate and the electrotextile are laser cut into their respective shapes. A laser cutter offers the computerized sub-millimeter accuracy unachievable by hand. Furthermore, cutting with scissors or scalpels involves a significant risk of leaving loose strands of the electrotextile fabric. This is especially harmful when these strands would be left in critical areas such as the radiating slot or the connector aperture, not to mention the possibility of short circuits caused by the filaments. Note that, as the electrotextile is cut in one single piece, it can simply be folded around the substrate in a later step, thereby significantly reducing potential misalignments of the top and bottom planes. The 4 mm thick substrate is laser cut in a rectangular patch of 56 mm × 35 mm. The shape of the electrotextile cut is displayed in Figure 3.2. Next, the glue carrier sheet is removed, leaving the glue behind on the laser-cut electrotextile patch. After careful alignation, the substrate and the electrotextile patch slot plane are glued together by a textile heat transfer press, which activates the glue. Then, the rest of electrotextile can be wrapped around the substrate, which forms the final cavity as shown in Figure 3.1c. Note that in this way, the vertical walls of the cavity contain evenly spaced apertures, thereby creating a rectangular SIW cavity. In a final step, the assembly of the antenna is concluded by placing the connector. Suitable apertures in the electrotextile were implemented during the laser cutting process, allowing to punch an appropriately trimmed SMA connector through the substrate. Now, the ground pads of the connector are soldered to the antenna back plane and the center conductor is soldered to the slot plane. This results in the final prototype shown in Figure 3.3.

3.4 Simulation and Optimization

To fulfill the design requirements specified in Section 3.2, both frequency-domain optimizations and time-domain simulations have been carried out. In Section 3.4.1, the influence of the antenna parameters on impedance matching and the location of the resonance frequencies is discussed. Section 3.4.2 elaborates on the time domain pulse distortion caused by the antenna and discusses the simulated distance estimation errors.

3.4.1 Frequency domain simulations

The antenna has been simulated and optimized by using CST Microwave Studio. By performing a thorough parametric analysis, the design goals as stated in Section 3.2.1 are met, as will be shown in Section 3.5. The width of both subcavities (ie. W_a and W_b as seen in Figure 3.2) are the primary parameters to fix the antenna resonance frequencies, along with the length of the cavity L. The latter and the placement of the feed D_f are used to match the antenna to the required

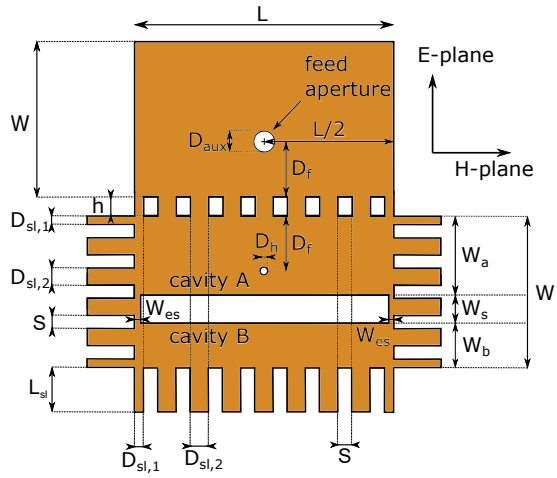

Figure 3.2: Electrotextile dimensions: L = 56 mm, W = 35 mm, W_a = 20 mm, W_b = 10.5 mm, W_s = 4.5 mm, h = 4 mm, D_f = 15 mm, D_{aux} = 5 mm, D_h = 1.27 mm, $D_{sl,1}$ = 2 mm, $D_{sl,2}$ = 4 mm, S = 3 mm, L_{sl} = 10 mm, W_{es}= 1 mm.

Figure 3.3: Final antenna design. Left: Slot plane. Right: Back plane.

impedance level over the entire operating band. To achieve the required bandwidth, the amount of coupling between both half-mode cavities is optimized via the slot parameters W_s and W_{es}. Although lower values of W_{es} cause a larger impedance matching bandwidth, a trade-off must be made to ensure the mechanical integrity of the antenna, since setting W_{es} to zero would remove a necessary support structure keeping some vertical electrotextile walls in place. Therefore, a sufficiently large value for W_{es} should be selected. For this, W_{es} = 1 mm is chosen.

All the aforementioned parameters have been optimized to comply with impedance matching goals, while maintaining a stable desired radiation pattern over the target frequency band and meeting the time domain requirements described in Section 3.4.2. Well-considered dimensions for $D_{sl,1}$, $D_{sl,2}$ and S ensure that radiation losses through the vertical cavity walls are negligible while guaranteeing mechanical flexibility. The resulting simulated reflection coefficient and radiation pattern of the proposed antenna are shown in Section 3.5 together with the measurement results.

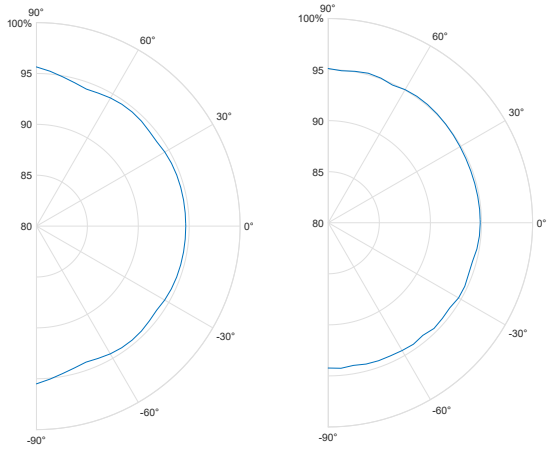

Figure 3.4: SFF using the pulse measured on a DW1000 IC operating in Channel 2. Left: SFF [%] in H-plane. Right: SFF [%] in E-plane.

3.4.2 Time domain simulations

Next, the orientation-specific pulse distortion of our all-textile antenna element is analyzed by means of the SFF, defined by Quintero et al. (2011) as:

$$SFF = \max_{t} \left| \frac{\int_{t_0}^{t_n} T_s(\tau) R_s(\tau + t) d\tau}{\sqrt{\int_{t_0}^{t_n} T_s^2(\tau) d\tau \int_{t_0}^{t_n} R_s^2(\tau) d\tau}} \right|,$$

where T_s(t) and R_s(t) represent the pulse at the transmit antenna's port and the receive antenna's port, respectively, and this for all $n+1$ timestamps t_0 to t_n. As such, the antenna is analyzed in a complete transmit-receive antenna system. In this chapter, our all-textile UWB antenna element is used both as a transmit and receive antenna. Then, the procedure outlined in Quintero et al. (2011) is exploited to calculate the antenna system's SFF when the receive antenna is rotated in its E- and H-plane, respectively, while the transmit antenna is transmitting along broadside. As an input pulse, the default output pulse of the Decawave DW1000 chipset when operating in Channel 2 is used. The resulting SFF in the relevant hemisphere is displayed in Figure 3.4, which is indeed larger than 90% for all relevant orientations of the receive antenna. As such, the pulse distortion due to the antenna characteristics is small enough to enable localization algorithms to provide accurate location estimations. In a subsequent step, the distance estimation error is determined to be in the order of magnitude of 5 cm as can be seen in Figure 3.5.

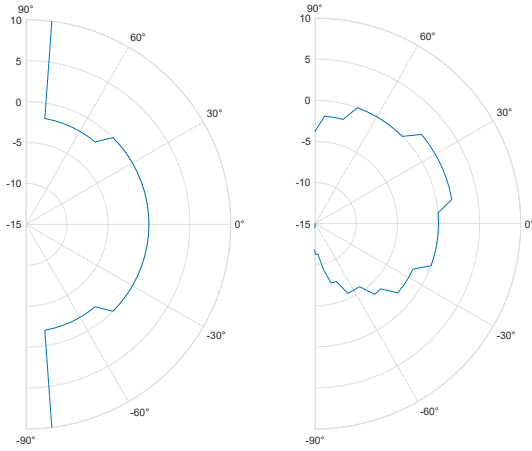

Figure 3.5: Distance estimation error. Left: DEE [cm] in H-plane. Right: DEE [cm] in E-plane.

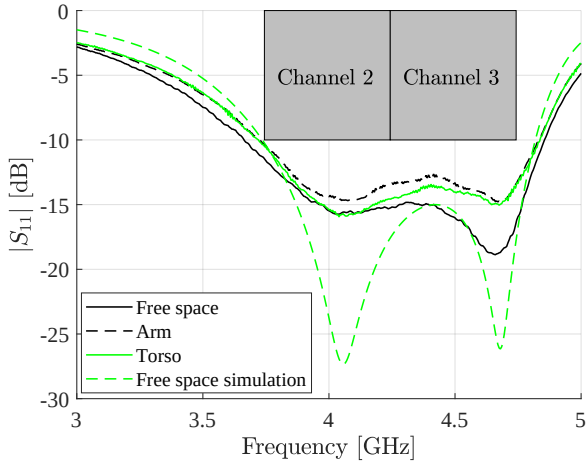

Figure 3.6: Magnitude of the measured reflection coefficient $|S_{1,1}|$ of the antenna in different deployment scenarios, in comparison to the simulated free space reflection coefficient.

3.5 Measurements

This section discusses the measured figures of merit of a fabricated prototype both in free space and in two human body deployment scenarios. Furthermore, the impact of mechanical bending on antenna performance has been investigated.

Both the reflection coefficient and the radiation pattern measurements were performed using an Agilent N5242A PNA-X Microwave Network Analyzer (Agilent Technologies, `https://www.agilent.com/`). For the radiation pattern measurements the antenna has been mounted on a Orbit/FR DBDR antenna positioning system (`http://www.orbitfr.com/`) in a full anechoic chamber.

In Figure 3.6, the simulated reflection coefficient is compared to the measured reflection coefficients in a stand-alone free space environment and in an on-body deployment scenario. Here, the antenna has been outfitted on a test person, having a size of 1.90 m and a mass of 85 kg. Measurements were performed when the antenna was placed on the torso and the upper right arm of the test person, respectively.

Both in simulations and measurements, the two resonances are clearly visible, providing an impedance bandwidth spanning the entire targeted frequency band. The measured free space fractional bandwidth of 27.9% qualifies this antenna as an UWB antenna. Furthermore, there is good correspondence between the resonance frequencies of the free space measurement and the resonance frequencies of the on-body measurements. Differences between simulation and measurements originate from fabrication tolerances and deployment conditions that slightly differ from the exact free space conditions assumed by the simulator. Furthermore, the electromagnetical properties of the applied materials vary slightly from batch to batch. Comparison between the measured scenarios proves that the influence of the human body on the antenna's reflection coefficient is indeed very limited.

Figure 3.7 shows the measured free space radiation patterns in the E-plane and H-plane, respectively. Table 3.1 summarizes the most important figures of merit related to the radiation pattern. Both the antenna's maximum gain and FTBR remain stable over the entire frequency band. Moreover, the measured radiation efficiency is higher than 75%. Owing to a large FTBR and a 3 dB-beamwidth of 120° centered around broadside, the radiation pattern experiences little influence from the proximity of the human body, as seen in Figure 3.8. Here, the radiation patterns at 4243.2 MHz, resulting from simulation in free space stand-alone conditions, measurement in free space conditions and when deployed on body show good agreement. Figure 3.9 shows the radiation patterns of the antenna while deployed on the torso and the arm of the test person, respectively. Because the positioning accuracy of a test person is prone to small errors, the maxima of the main lobes have slightly shifted.

Additional free space measurements have been performed while the antenna was subjected to mechanical bending, as is displayed in Figure 3.10. The antenna has

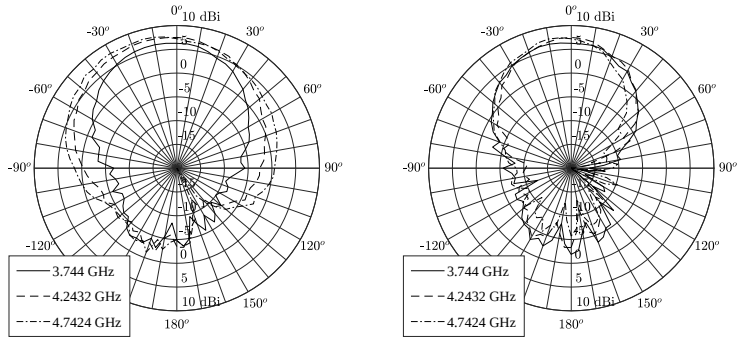

Figure 3.7: Free space radiation pattern. Left: E-plane, Right: H-plane.

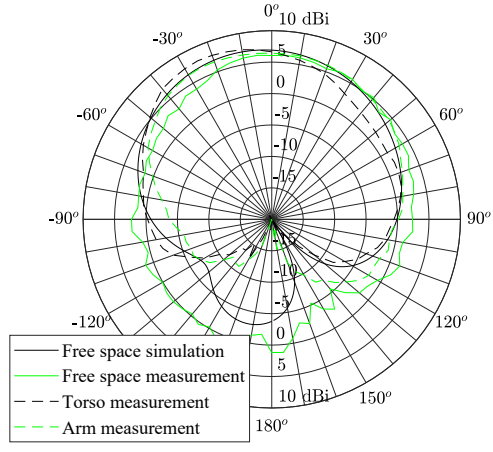

Figure 3.8: E-plane radiation pattern in different deployment scenarios, at 4243.2 MHz

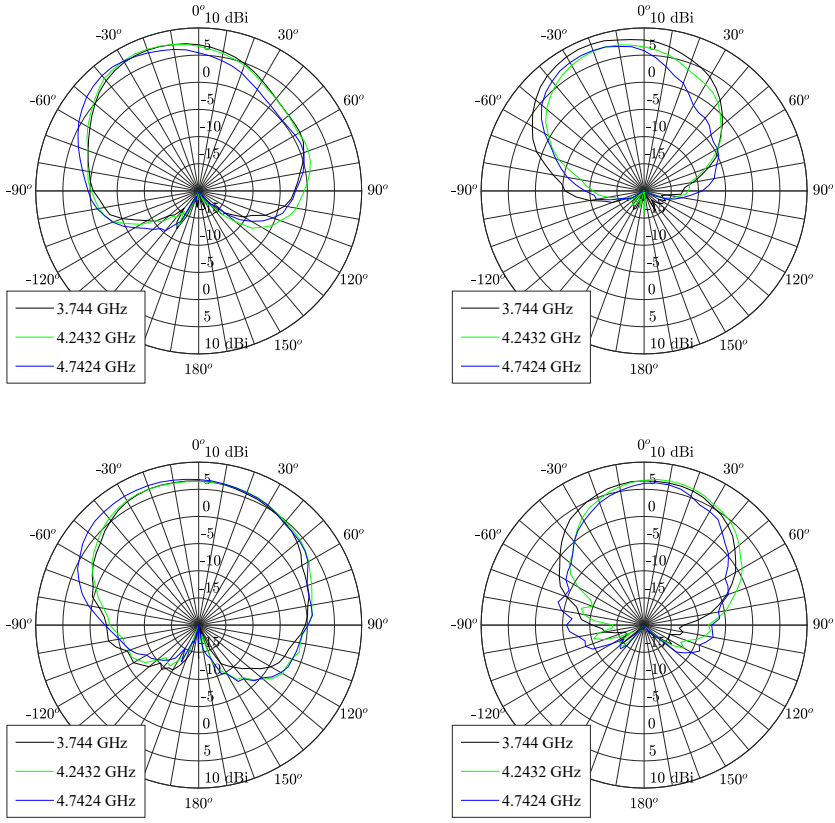

Figure 3.9: Radiation pattern on body. Top left: Torso E-plane, top right: Torso H-plane. Bottom left: upper right arm E-plane, bottom right: upper right arm H-plane.

been bent around the X-axis shown in Figure 3.1c, which lies in the antenna's E-plane. Figure 3.11 compares the reflection coefficient of the antenna when it is subject to diverse bending radii which are commonly encountered on the human body. The influence of bending on the radiation pattern can be seen in Figure 3.12. These figures show that the antenna characteristics remain stable under bending. Only under the small bending radius of 4 cm, the resonance frequencies shift such that the complete UWB frequency band is no longer fully covered.

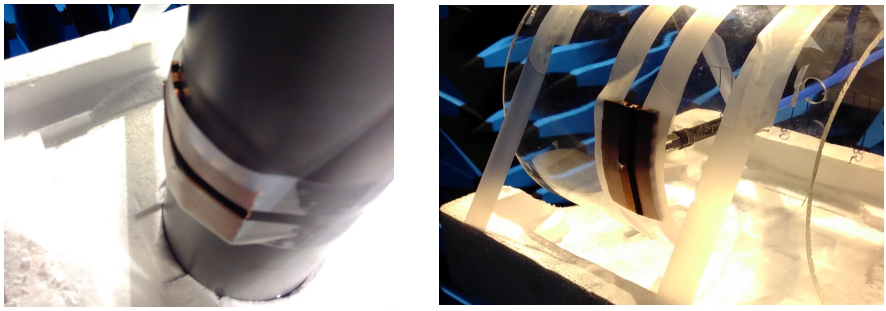

Figure 3.10: Radiation pattern measurement setup subjecting antennas to mechanical bending.

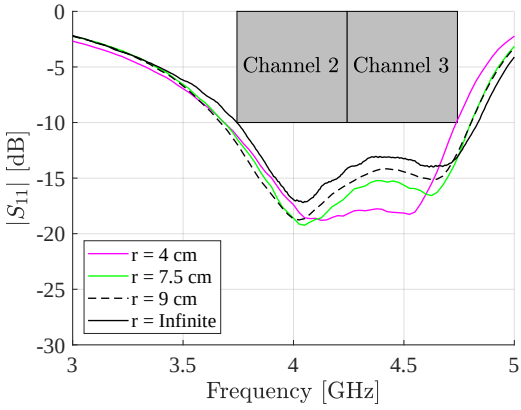

Figure 3.11: Magnitude of the measured reflection coefficient $|S_{1,1}|$ of the antenna while subject to mechanical bending, for different bending radii r, along the E-plane axis.

Table 3.1: Free space figures of merit of the measured prototype.

Frequency [MHz]	3744	4243.2	4742.4
Simulated maximum gain [dBi]	6.6	7.0	6.5
Measured maximum gain [dBi]	6.4	7.6	8.0
Simulated FTBR [dB]	9.8	11.4	13.2
Measured FTBR [dB]	11.2	11.0	12.2
Simulated radiation efficiency [%]	96	97	88
Measured radiation efficiency [%]	78	91	87

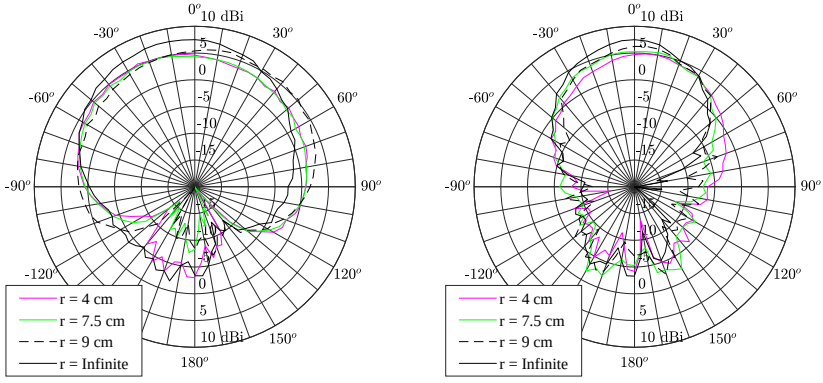

Figure 3.12: Measured radiation pattern under diverse bending radii, at 4243.2 MHz. Left: E-plane, Right: H-plane

3.6 Conclusions

An all-textile multi-moded cavity-backed slot antenna that covers channels 2 and 3 of the IEEE 802.15.4 standard has been proposed for on-body deployment in personal IR-UWB-based localization applications. The magnitude of the reflection coefficient with respect to 50 Ω remains lower than -10 dB over a fractional bandwidth of 27.9%, thereby qualifying the antenna as an UWB antenna. The measured FTBR of 11 dB indicates that the antenna's radiation pattern is directed away from the wearer's body. Therefore, less power is dissipated in the wearer's body in comparison with more omnidirectional antennas, resulting in a more efficient use of available power and reducing the wearer's radio field exposure. The antenna's reflection coefficient and radiation pattern have been investigated in free space, when the antenna was deployed on the torso and upper right arm of a test person, respectively, and in free space when bent over diverse bending radii. Measurements show that both the reflection coefficient and the radiation pattern experience limited influence from bending or proximity of the human body, illustrating the low coupling between the antenna and the human body. Simulations in the time-domain show the antenna's suitability for IR-UWB localization systems.

References

[1] S. Chatterjee, S. Chatterjee, S. Choudhury, S. Basak, S. Dey, S. Sain, K. S. Ghosal, N. Dalmia, and S. Sircar, "Internet of Things and Body Area Network-an Integrated Future", in *2017 IEEE 8th Annual Ubiquitous Computing, Electronics and Mobile Communication Conference (UEMCON)*, Oct. 2017, pp. 396–400.

[2] S. Agneessens, S. Lemey, T. Vervust, and H. Rogier, "Wearable, Small, and Robust: The Circular Quarter-mode Textile Antenna", *IEEE Antennas and Wireless Propagation Letters*, vol. 14, pp. 1482–1485, 2015.

[3] S. Lemey, S. Agneessens, and H. Rogier, "Wearable Smart Objects: Microwaves Propelling Smart Textiles: A Review of Holistic Designs for Wireless Textile Nodes", *IEEE Microw. Mag.*, vol. 19, no. 6, 83–100, 2018.

[4] A. K. Skrivervik and G. Marrocco, "Guest Editorial: Special Cluster on Antennas for Wireless Body Area Networks", *IEEE Antennas and Wireless Propagation Letters*, vol. 14, pp. 1471–1473, 2015.

[5] T. Castel, S. Lemey, S. Agneessens, P. Van Torre, H. Rogier, and C. Oestges, "Reliable Communication Between Rescuers During Interventions Using Textile Antenna Systems", in *2015 IEEE 20th INTERNATIONAL WORKSHOP ON COMPUTER AIDED MODELLING AND DESIGN OF COMMUNICATION LINKS AND NETWORKS (CAMAD)*, Guildford, ENGLAND: IEEE, 2015, pp. 135–139.

[6] A. Dierck, H. Rogier, and F. Declercq, "A Wearable Active Antenna for Global Positioning System and Satellite Phone", *IEEE Transactions on Antennas and Propagation*, vol. 61, no. 2, pp. 532–538, 2013.

[7] J. Lilja, P. Salonen, T. Kaija, and P. de Maagt, "Design and Manufacturing of Robust Textile Antennas for Harsh Environments", *IEEE Transactions on Antennas and Propagation*, vol. 60, no. 9, pp. 4130–4140, Sep. 2012.

[8] S. Agneessens, T. Castel, P. Van Torre, E. Tanghe, G. Vermeeren, W. Joseph, and H. Rogier, "A Wearable Repeater Relay System for Interactive Real-time Wireless Capsule Endoscopy", in *2013 Proceedings of the International Symposium on Antennas and Propagation*, vol. 1, Nanjing, China: IEEE, 2013, pp. 597–600.

[9] M. M. Bait-Suwailam, I. I. Labiano, and A. Alomainy, "Effect of Textile Properties on a Low-Profile Wearable Loop Antenna for Healthcare Applications", in *2019 13th European Conference on Antennas and Propagation (EuCAP)*, Mar. 2019, pp. 1–4.

[10] R. Bharadwaj, S. Swaisaenyakorn, C. G. Parini, J. C. Batchelor, and A. Alomainy, "Impulse Radio Ultra-Wideband Communications for Localization and Tracking of Human Body and Limbs Movement for Healthcare Applications", *IEEE Transactions on Antennas and Propagation*, vol. 65, no. 12, pp. 7298–7309, Dec. 2017.

[11] H. Rogier, S. Agneessens, T. Castel, S. Lemey, F. Declercq, P. Vanveerdeghem, P. Van Torre, L. Vallozzi, and W. Joseph, "Novel Wearable Antenna Systems for High Datarate Mobile Communication in Healthcare", eng, in *2014 EAI 4TH INTERNATIONAL CONFERENCE ON WIRELESS MOBILE COMMUNICATION AND HEALTHCARE (MOBIHEALTH)*, Athens, GREECE, 2014, pp. 188–191.

[12] B. Mandal, B. Mukherjee, A. Chatterjee, and S. K. Parui, "Design of Printed Body Wearable Textile Antenna for Broadband Application", in *2013 IEEE Applied Electromagnetics Conference (AEMC)*, Dec. 2013, pp. 1–2.

[13] T. F. Kennedy, P. W. Fink, A. W. Chu, N. J. Champagne, G. Y. Lin, and M. A. Khayat, "Body-Worn E-Textile Antennas: The Good, the Low-Mass, and the Conformal", *IEEE Transactions on Antennas and Propagation*, vol. 57, no. 4, pp. 910–918, Apr. 2009.

[14] T. Kaija, J. Lilja, and P. Salonen, "Exposing Textile Antennas for Harsh Environment", in *2010 - MILCOM 2010 MILITARY COMMUNICATIONS CONFERENCE*, Oct. 2010, pp. 737–742.

[15] H. Lee, J. Tak, Y. Hong, and J. Choi, "Design of an All-Textile Antenna Integrated in Military Beret for GPS/RFID Applications", in *2016 International Symposium on Antennas and Propagation (ISAP)*, Oct. 2016, pp. 982–983.

[16] Z. Khan, X. Chen, H. He, J. Xu, T. Wang, L. Cheng, L. Ukkonen, and J. Virkki, "Glove-Integrated Passive UHF RFID Tags—Fabrication, Testing and Applications", *IEEE Journal of Radio Frequency Identification*, vol. 3, no. 3, pp. 127–132, Sep. 2019.

[17] H. Lee and J. Choi, "A Compact All-Textile On-Body SIW Antenna for IoT Applications", in *2017 IEEE International Symposium on ANTENNAS and Propagation USNC/URSI National Radio Science Meeting*, Jul. 2017, pp. 825–826.

[18] S. Lemey and H. Rogier, "SIW Textile Antennas as a Novel Technology for UWB RFID Tags", in *2014 IEEE RFID TECHNOLOGY AND APPLICATIONS CONFERENCE (RFID-TA)*, Tampere, Finland: IEEE, 2014, pp. 256–260.

[19] C. Loss, R. Gonçalves, C. Lopes, P. Pinho, and R. Salvado, "Smart Coat with a Fully-Embedded Textile Antenna for IoT Applications", *Sensors*, vol. 16, pp. 1–13, 2016.

[20] "IEEE Standard for Local and Metropolitan Area Networks–Part 15.4: Low-Rate Wireless Personal Area Networks (LR-WPANs)", *IEEE Std 802.15.4-2011 (Revision of IEEE Std 802.15.4-2006)*, pp. 1–314, Sep. 2011.

[21] G. Adamiuk, T. Zwick, and W. Wiesbeck, "UWB Antennas for Communication Systems", *Proceedings of the IEEE*, vol. 100, no. 7, pp. 2308–2321, Jul. 2012.

[22] Y. Luo and C. Look Law, "Robust Ultra-Wideband Direction Finding in Dense Cluttered Environments", *IEEE Transactions on Wireless Communications*, vol. 14, no. 9, pp. 4772–4782, Sep. 2015.

[23] R. Kshetrimayum, "An Introduction to UWB Communication Systems", *IEEE Potentials*, vol. 28, no. 2, pp. 9–13, Mar. 2009.

[24] A. Alarifi, A. Al-Salman, M. Alsaleh, A. Alnafessah, S. Al-Hadhrami, M. A. Al-Ammar, and H. S. Al-Khalifa, "Ultra Wideband Indoor Positioning Technologies: Analysis and Recent Advances", *Sensors*, vol. 16, no. 5, p. 36, 2016.

[25] M. Ridolfi, S. Vandermeeren, J. Defraye, H. Steendam, J. Gerlo, D. De Clercq, J. Hoebeke, and E. De Poorter, "Experimental Evaluation of UWB Indoor Positioning for Sport Postures", *SENSORS*, vol. 18, no. 1, 2018.

[26] K. Minne, N. Macoir, J. Rossey, Q. Van den Brande, S. Lemey, J. Hoebeke, and E. De Poorter, "Experimental Evaluation of UWB Indoor Positioning for Indoor Track Cycling", *Sensors*, vol. 19, p. 17, 2019.

[27] H. Shen, C. Xu, Y. Yang, L. Sun, Z. Cai, L. Bai, E. Clancy, and X. Huang, "Respiration and Heartbeat Rates Measurement Based on Autocorrelation Using IR-UWB Radar", *IEEE Transactions on Circuits and Systems II: Express Briefs*, vol. 65, no. 10, pp. 1470–1474, Oct. 2018.

[28] F. Lazzari, A. Buffi, P. Nepa, and S. Lazzari, "Numerical Investigation of an UWB Localization Technique for Unmanned Aerial Vehicles in Outdoor Scenarios", *IEEE Sensors Journal*, vol. 17, no. 9, pp. 2896–2903, May 2017.

[29] H. Lv, W. Li, Z. Li, Y. Zhang, T. Jiao, H. Xue, M. Liu, X. Jing, and J. Wang, "Characterization and Identification of IR-UWB Respiratory-Motion Response of Trapped Victims", *IEEE Transactions on Geoscience and Remote Sensing*, vol. 52, no. 11, pp. 7195–7204, Nov. 2014.

[30] L. Zwirello, L. Reichardt, X. Li, and T. Zwick, "Impact of the Antenna Impulse Response on Accuracy of Impulse-Based Localization Systems", in *2012 6th European Conference on Antennas and Propagation (EUCAP)*, 2012, pp. 3520–3523.

[31] M. Klemm and G. Troester, "Textile UWB Antennas for Wireless Body Area Networks", *IEEE Transactions on Antennas and Propagation*, vol. 54, no. 11, pp. 3192–3197, Nov. 2006.

[32] P. B. Samal, P. J. Soh, and G. A. E. Vandenbosch, "UWB All-Textile Antenna With Full Ground Plane for Off-Body WBAN Communications", *IEEE Transactions on Antennas and Propagation*, vol. 62, no. 1, pp. 102–108, Jan. 2014.

[33] S. Yan, L. A. Y. Poffelie, P. J. Soh, Xuezhi Zheng, and G. A. E. Vandenbosch, "On-Body Performance of Wearable UWB Textile Antenna with Full Ground Plane", in *2016 10th European Conference on Antennas and Propagation (EuCAP)*, Apr. 2016, pp. 1–4.

[34] L. A. Yimdjo Poffelie, P. J. Soh, S. Yan, and G. A. E. Vandenbosch, "A High-Fidelity All-Textile UWB Antenna With Low Back Radiation for Off-Body WBAN Applications", *IEEE Trans. Antennas Propag.*, vol. 64, no. 2, pp. 757–760, Feb. 2016.

[35] J. Zhong, A. Kiourti, T. Sebastian, Y. Bayram, and J. L. Volakis, "Conformal Load-Bearing Spiral Antenna on Conductive Textile Threads", *IEEE Antennas and Wireless Propagation Letters*, vol. 16, pp. 230–233, 2017.

[36] S. Zhu and R. Langley, "Dual-Band Wearable Textile Antenna on an EBG Substrate", *IEEE Transactions on Antennas and Propagation*, vol. 57, no. 4, pp. 926–935, Apr. 2009.

[37] M. Osman, M. Rahim, N. A. Samsuri, M. Elbasheer, and M. Ali, "Textile UWB Antenna Bending and Wet Performances", *International Journal of Antennas and Propagation*, vol. 2012, May 2012.

[38] B. Sanz-Izquierdo, J. Batchelor, and M. Sobhy, "Compact UWB Wearable Antenna", May 2007, pp. 121 –124.

[39] Y. Hong, J. Tak, and J. Choi, "An All-Textile SIW Cavity-Backed Circular Ring-Slot Antenna for WBAN Applications", *IEEE Antennas and Wireless Propagation Letters*, vol. 15, pp. 1995–1999, 2016.

[40] F. Liu, Z. Xu, D. C. Ranasinghe, and C. Fumeaux, "Textile Folded Half-Mode Substrate-Integrated Cavity Antenna", *IEEE Antennas and Wireless Propagation Letters*, vol. 15, pp. 1693–1697, 2016.

[41] D. Van Baelen, S. Lemey, J. Verhaevert, and H. Rogier, "A Novel Manufacturing Process for Compact, Low-Weight and Flexible Ultra-Wideband Cavity Backed Textile Antennas", *Materials*, vol. 11, no. 1, p. 17, 2018.

[42] M. H. Rabah, D. Seetharamdoo, R. Addaci, and M. Berbineau, "Novel Miniature Extremely-Wide-Band Antenna With Stable Radiation Pattern for Spectrum Sensing Applications", *IEEE Antennas and Wireless Propagation Letters*, vol. 14, pp. 1634–1637, 2015.

[43] C. Hertleer, A. Van Laere, H. Rogier, and L. Van Langenhove, "Influence of Relative Humidity on Textile Antenna Performance", *Textile Research Journal*, vol. 80, no. 2, pp. 177–183, 2010.

[44] D. Van Baelen, S. Lemey, J. Verhaevert, and H. Rogier, "Improved Fabrication Methodology for Foldable All-Textile Cavity-Backed Slot Antennas", in *2019 URSI Asia Pacific Radio Science Conference (AP-RASC)*, 2019, pp. 1–4.

[45] Q. Van den Brande, S. Lemey, J. Vanfleteren, and H. Rogier, "Highly-Efficient Impulse-Radio Ultra-Wideband Cavity-Backed Slot Antenna in Stacked Air-Filled Substrate-Integrated-Waveguide Technology", *IEEE Transactions on Antennas and Propagation*, vol. 66, no. 5, pp. 2199–2209, May 2018.

[46] G. Quintero, J.-F. Zürcher, and A. K. Skrivervik, "System Fidelity Factor: A New Method for Comparing UWB Antennas", *IEEE Trans. Antennas Propag.*, vol. 59, no. 7, pp. 2502–2512, 2011.

[47] J.-S. Hong and M. J. Lancaster, "Couplings of Microstrip Square Open-Loop Resonators for Cross-Coupled Planar Microwave Filters", *IEEE Trans. Microw. Theory Tech.*, vol. 44, no. 11, pp. 2099–2109, Nov. 1996.

[48] M. Bozzi, A. Georgiadis, and K. Wu, "Review of Substrate-Integrated Waveguide Circuits and Antennas", *IET Microwaves, Antennas & Propagation*, vol. 5, no. 8, pp. 909–920, Jun. 2011.

4

Fully Flexible Textile Antenna-Backed Sensor Node for Body-Worn UWB Localization

Dries Van Baelen, Nicola Macoir, Quinten Van den Brande, Eli De Poorter, Sam Lemey, Jo Verhaevert and Hendrik Rogier

Published in Sensors

A mechanically flexible textile antenna-backed sensor node is designed and manufactured, providing accurate personal localization functionality by application of Decawave's DW1000 Impulse Radio Ultra-Wideband (IR-UWB) Integrated Circuit (IC). All components are mounted on a flexible polyimide foil, which is integrated on the backplane of a wearable cavity-backed slot antenna designed for IR-UWB localization in Channels 2 and 3 of the IEEE 802.15.4-2011 standard (3744 MHz–4742.4 MHz). The textile antenna's radiation pattern is optimized to mitigate body effects and to minimize absorption by body tissues. Furthermore, its time-domain characteristics are measured to be adequate for localization. By combining the antenna and the bendable Printed Circuit Board (PCB), a mechanically supple sensor system is realized, for which the performance is validated by examining it as a node used in a complete localization system. This shows that six nodes around the body must be deployed to provide system coverage in all directions around the wearer. Even without using sleep mode functionalities, measurements indicate that the system's autonomy is 13.3 hours on a 5 V 200 mAh battery. Hence, this system acts as a proof of concept for the joining of localization electronics and other sensors with a full-textile antenna into a mechanically flexible sensor system.

4.1 Introduction

Wireless Body Area Network (WBAN) systems are indispensable for the integration of a plethora of useful body-centric functionalities into the Internet of Things (IoT). Currently, they have given rise to healthcare systems providing measurement of life signs, such as blood glucose levels or electrocardiograms (ECGs) [1]–[3]; systems that provide fall detection in the elderly [4], [5]; and environmental sensing systems measuring the temperature, gas and dust concentrations, and relative humidity of the surrounding environment for, for example, emergency responders and mining personnel [6]. Among the myriads of possible functionalities, localization is of particular interest to WBAN systems.

Over the years, a multitude of positioning methodologies has been developed, each with their own benefits and disadvantages [7], [8]. Among those, the ultra-wideband (UWB) technology described in the IEEE 802.15.4-2011 standard [9] is the most interesting candidate. Here, a very-low-power broadband pulse is applied to provide communication between the tag and anchor. Due to the nature of its signal type and the very wide bandwidth used, the system exhibits high immunity to narrowband signal interference [8]. Furthermore, owing to the very low power present in the signal, which is spread over a large bandwidth, and given the signal's pseudo-random nature, UWB causes little interference with other wireless technologies [10]–[12]. The high data rate and short packet time cause few opportunities for collisions, allowing for a high node density of the applied system [10], [13]. Since the use of large bandwidths causes a very steep flank in the time domain, localization devices can provide very accurate time-of-arrival estimations, down to 10 cm [14]. Finally, because of the very short time-domain pulses, UWB has a high immunity against multipath effects [15], [16]. These properties promote UWB technology as a prime candidate for both indoor and outdoor real-time localization systems.

Applications of UWB technology include person proximity detection [17], tracking of cattle [18]–[20] and industrial assets [21], sports analysis [22], [23], and many others. Although all these positioning systems use UWB technology, they are still rigid and bulky and, just as is often observed in UWB antenna development, they typically do not take human body proximity into account. To attain true market and customer acceptation, wearable WBAN sensor systems need to be comfortable, discrete, and unobtrusive. This means that they should be low profile and mechanically flexible and that they should spend energy in a responsible, efficient way, since (flexible) battery capacity is a limiting factor in a body-worn system, in particular, when the aforementioned wearability constraints need to remain satisfied.

In this chapter, UWB technology is applied to realize accurate localization functionality as a part of a complete mechanically flexible WBAN sensor system, featuring Decawave's DW1000 localization IC [14]. The system provides sensor data for temperature, relative humidity, and air pressure, which, together with the ranging

data, can be stored on-board in a discrete flash memory. The system is implemented on a polyimide foil to provide maximal mechanical flexibility. The bottom of this polyimide foil is then connected to the backplane of a cavity-backed slot antenna, which serves as an integration platform for the discrete electronic components.

The fabrication process in [24] was applied to create a mechanically flexible, full textile cavity-backed slot antenna. Since such low-profile antennas are notoriously narrowband, the broadbanding technique described in [25] was applied. The resulting antenna exhibits a reflection coefficient with respect to 50 Ω lower than −10 dB over both Channels 2 and 3 of the IEEE 802.15.4-2011 standard (3744 MHz–4243.2 MHz and 4243.2 MHz–4742.4 MHz, respectively). Furthermore, the results from [26] indicate that the selected antenna topology is a suitable choice to reduce the phase center shift as a function of incident angle as much as possible, as is required for accurate localization applications. Moreover, [26] proves the feasibility of this antenna topology for on-body deployment, as both its reflection coefficient with respect to 50 Ω and its radiation pattern remain stable under diverse deployment circumstances, such as in free space with and without mechanical bending or when worn on the torso or on the upper right arm of a test person.

To achieve accurate localization performance, both the pulse distortion and the phase center shift of the antenna should be minimized. The former impedes accurate reception of the signal, whereas the latter causes a distance estimation error (DEE). Both parameters are functions of the incident angle of the wave and, hence, must be investigated for all directions relevant for body-worn scenarios. For this, only angles up to 60° from the antenna's broadside are considered due to body shadowing effects in directions approaching or exceeding 90° away from the antenna's broadside.

The main innovations presented in this chapter are as follows:

- Co-design of a mechanically flexible textile antenna for UWB localization and a mechanically flexible PCB featuring both digital and time-domain-sensitive analog parts, and combination of the textile antenna and the PCB into a functional system.
- Proof of the suitability of the full-textile cavity-backed slot antenna for localization purposes by characterizing both the antenna's pulse distortion and phase center shift.
- Proof of concept of the integration of a textilized unobtrusive body-worn sensor node in an existing UWB localization infrastructure under the presence of body shadowing and proximity.

This chapter is structured as follows. Section 4.2 lists the requirements of the sensor system and the antenna. It specifically highlights the consequences of wearability and of requirements pertinent to localization on a system and antenna design.

Furthermore, some feasible localization methodologies are discussed. Section 4.3 elaborates on various investigated figures of merit. The time-domain behavior of the standalone antenna is discussed, along with the free space power pattern and power consumption of the complete sensor system. Furthermore, the UWB connectivity between the body-worn sensor system and existing localization infrastructure are evaluated. Conclusions are provided in Section 4.4.

4.2 System Requirements and Design

This section discusses the requirements of the system and elaborates on the design choices made to meet them. The implications for both the antenna and the backbone electronics are investigated. Furthermore, a suitable localization methodology is selected.

4.2.1 System Requirements

WBAN systems should possess a high degree of wearability. This implies that the system should be unobtrusive to the user: it should be lightweight, should have a small footprint, and should be mechanically flexible to interfere as little as possible with the user's movements. This requirement is also translated into the power source, so frugal use of the available power is essential.

From an electromagnetic point of view, the system should comply with all requirements for efficient and accurate localization in accordance with the IEEE 802.15.4-2011 standard. For this, its antenna is selected to operate in Channels 2 and 3 (3744 MHz–4243.2 MHz and 4243.2 MHz–4742.4 MHz, respectively) of the aforementioned standard. Over both channels, the antenna's reflection coefficient with respect to 50 Ω should remain below −10 dB while a radiation efficiency of at least 70% should be maintained. Both the radiation pattern and the impedance matching should remain stable over the entire targeted frequency band, and they should not deteriorate when the antenna is deployed on the body. This implies that coupling with the human body should be minimized as much as possible. Not only will this low coupling result in more stable antenna characteristics, remaining comparable to the antenna's standalone behavior in free space, but also it minimizes the energy absorbed by the wearer's body. In any practical scenario, external nodes should be able to connect and communicate with the system at all times and for all orientations of the wearer's body with respect to the surrounding localization infrastructure.

Moreover, the angle-dependent phase difference between a wave received along broadside and a wave incoming from another incident angle introduces a distance estimation error (DEE) when performing flank detection of an incoming pulse. A different way to state this is that the antenna's phase center shifts as a function of incident angle. For the antenna to be suitable for use in UWB localization systems, it is imperative that the DEE is kept sufficiently small. In other words, the phase

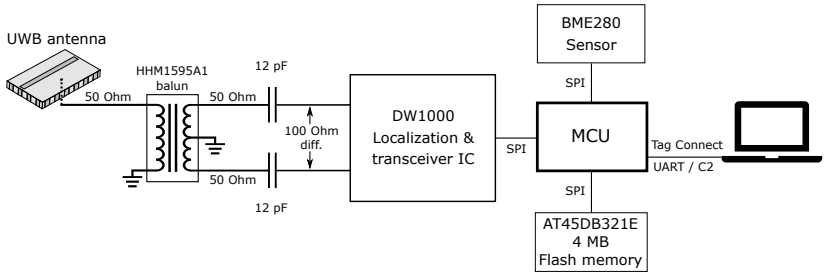

Figure 4.1: System architecture of the sensor system. The RF path of the signal from the antenna towards the localization IC is elaborated in detail.

center shift as a function of incident angle should remain small. The DEE should remain below 10 cm for all directions relevant to a body-worn scenario defined in Section 4.1, as this keeps the ranging error introduced by the antenna in the same range as the adopted localization Integrated Circuit's (IC's) positioning accuracy.

4.2.2 System Overview

Figure 4.1 outlines the system architecture of the proposed sensor system. The system's assembly of sensor functionalities may be refitted or expanded at will. To demonstrate this, a basic sensor such as the Bosch Sensortec BME280 temperature, air pressure, and relative humidity sensor [27] is integrated on the board, together with Decawave's DW1000 localization IC [14], which also hosts a built-in transceiver. Furthermore, the DW1000 module is fully compliant with the IEEE 802.15.4-2011 standard and it can be configured to operate in multiple UWB channels specified in this standard. Both the BME280 sensor and the DW1000 IC are controlled by an ultra-low-power Silicon Labs C8051F921 microcontroller [28].

An Adesto AT45DB321E 4 MB flash memory [29] is included, allowing application-dependent storage of, for example, sensor data. All communication between the aforementioned components occurs via the Serial Peripheral Interface (SPI) protocol.

Since the use of bulky connectors conflicts with the wearability constraints, a landing pad for a Tag Connect [30] interface was provided. The Tag Connect plug features spring-loaded pins to ensure reliable electric contact with the landing pads present on the target PCB. In this way, both the C2 programming interface and the UART bus for runtime communication with a PC are provided.

Finally, the signal from the DW1000 is injected into a cavity-backed slot antenna by a probe feed, as further elaborated in Section 4.2.3.

4.2.3 Antenna Design

The results from [24]–[26] prove that the cavity-backed slot antenna topology is suitable for the goals stated in Section 4.2.1. The antenna topology allows for low pulse distortion, and its distance estimation errors induced by a phase-center shift are in the order of 5 cm in all directions when considering a body-worn scenario [26], causing it to qualify for the 10 cm criterion. Furthermore, the frequency-domain characteristics of the topology remain stable when such an antenna is subject to bending or when placed in proximity of a human body [24].

Since the system is designed for smooth integration into clothing, it is desirable for the complete system to be mechanically flexible to hamper the wearer's motions as little as possible. Therefore, the fabrication procedure and the materials described in [24] are used to create a mechanically flexible, full-textile cavity-backed slot antenna in substrate integrated waveguide (SIW) technology.

The antenna is based on the coupled half-mode cavity-backed slot antenna design in [26]. In this topology, the open ends of two differently dimensioned SIW half-mode cavities are placed in close proximity. Together with a sufficiently small separation between the half-mode cavities' natural resonance frequencies, this close proximity causes both cavities to experience a strong mutual coupling, which triggers mode splitting, as explained in [31]. Through thorough computer-aided design, a suitable choice for the half-mode cavity dimensions and their mutual spacing is found, causing the coupled half-mode cavities to cover the entire desired frequency range. A minor redesign is performed on the antenna from [26], since the integration of the electronics required a comparatively smaller pin diameter. The resulting antenna dimensions are specified in the caption of Figure 4.2.

The results from [24]–[26] show that the antenna topology exhibits a directive radiation pattern oriented away from the human body, with a measured front-to-back ratio (FTBR) higher than 11 dB within the IEEE 802.15.4-2011 Channels 2 and 3. These results also demonstrate that this antenna topology exhibits low coupling with the human body, thereby reducing the wearer's Specific Absorption Rate (SAR) discussed in Section 4.3.2 and limiting the influence of human body proximity on the radiation pattern and impedance matching of the antenna.

4.2.4 Circuit Design

To provide mechanical flexibility, the electronics forming the backbone functionality of the system are implemented on a flexible polyimide foil, as shown in the side view on Figure 4.2. The upper part of this schematic concerns the flexible PCB. The lower part of this schematic consists of the textile antenna, bounded by its electrotextile (orange) backplane and slot plane (orange and black). These are surrounded by vertical electrotextile slabs, thus forming the substrate integrated waveguide cavity described in [24] and visualized in the top of Figure 4.1.

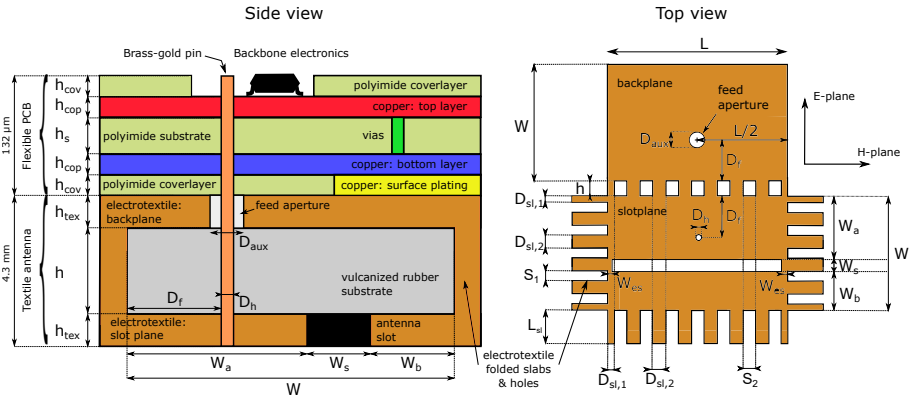

Figure 4.2: Stackup of the finished sensor node (side view, left) and shape of the unassembled electrotextile patch (top view, right). Dimensions: L = 56 mm, W = 34 mm, W_a = 20 mm, W_b = 10.5 mm, W_s = 4.5 mm, D_f = 15 mm, D_{aux} = 5 mm, D_h = 1 mm, $D_{sl,1}$ = 2 mm, $D_{sl,2}$ = 4 mm, S_1 = 2.8 mm, S_2 = 4 mm, L_{sl} = 10 mm, W_{es} = 1 mm, h = 4 mm, h_{tex} = 0.15 mm, h_{cov} = 25 μm, h_{cop} = 16 μm, and h_s = 50 μm. This model is based on the design from [26], accommodating a different feed pin size.

The connection between the antenna and the DW1000 IC is schematically represented in Figure 4.1, according to the design rules specified in [13]. As prescribed by the DW1000 manufacturer, the RF output of the localization IC is connected to two 12 pF capacitors by means of a 100 Ω differential transmission line. Then, a 50 Ω single-ended transmission line is used to connect each capacitor to a pin of the balanced port of a TDK HHM1595A1 balun [32]. Another 50 Ω single-ended transmission line then connects the balun's unbalanced port to the antenna feed pin, which is soldered to the transmission line. For this, a trimmed Multi-Contact 42.0001 brass-gold pin with a diameter of 1 mm was selected. The antenna and the circuit's feed pin structure are co-optimized to provide a 1.8-mm diameter ground clearance, together with an aperture in the backplane of the antenna cavity. Then, the probe feed structure was realized by fitting the feed pin through the middle of this hole, after which the antenna was completed by soldering the pin's other end to the antenna's top plane.

When designing mechanically flexible PCBs, care must be taken to distribute the mechanical stress applied to the copper and solder seams as a result of bending. Given that isolated vias and soldering joints are common failure points on flexible substrates, we combined their individual stiffness by aligning vias and component edges to form rigid lines. If sufficient well-positioned bending spaces are implemented in between the rigid lines, the PCB concentrates its bending along those directions in which it is allowed to do so. The result of this design rule is illustrated in Figure 4.3a, where component edges and vias are aligned as much as possible,

while the large footprint provided to the PCB by the back side of the textile antenna provides sufficient spacing to layout the components such that bending lines are realized along which no rigid elements are present. For example, the via rows in between the flash memory and the DW1000 IC are clearly aligned, and sufficient spacing is available in between these components, providing multiple lines over which the PCB can bend. Some examples of these bending lines are highlighted by the orange dash-dotted lines in Figure 4.3a. Furthermore, bending of the PCB induces mechanical stress that concentrates on the inner corners of the copper planes and on the transitions between signal lines and vias. The ensuing metal fatigue causes a significant risk for the copper to tear at these weak points. This effect is particularly detrimental to the performance of the system, since the cracks may cause signal lines to snap altogether. Therefore, gradual bends in copper sheets are preferred over abrupt inner corners, and the transition between signal lines and vias should be realized in a gradual droplet-like shape. For the same reason, signal lines need to bend smoothly instead of the sharp 90° or 45° corners commonly encountered in a conventional PCB design [33]. A correct example is shown in the inset of Figure 4.3a. Here, the top plane (red) containing all electronics is shown, together with the via layout (green) and the PCB's ground plane, displayed in blue. Note the gradual bends of the signal lines and the gradual tapering of signal lines approaching a via. In addition, the inner corners of copper surfaces are smoothed to gradual bends.

The connection between the ground plane and the back side of the antenna is realized by electroless nickel plated gold (ENIG) surface plating (yellow), which is patterned in a honeycomb structure to maintain mechanical flexibility while keeping sufficient electrical contact with the electrotextile beneath it, as is illustrated in the side view on Figure 4.2. Figure 4.3b reveals that the left side of the ground plane lacks surface plating. Instead, the 25 μm polyimide coverlayer and the trench visible in the middle of the figure isolate the analog circuitry's ground plane from noise originating from the digital electronics such as the microcontroller, the sensor, or the flash memory. In addition, these digital components also require protection from the sharp pulses emitted by the DW1000 IC, justifying thorough electromagnetic compatibility (EMC) measures taken concerning and surrounding the DW1000 IC. A via fence was implemented around the DW1000 and its peripheral components, such as the IC's crystal, decoupling capacitors, and radio-frequency (RF) connection to the antenna to provide additional EMC safety. Over the entire PCB, numerous vias were applied to implement a proper RF system reference plane. The resulting assembled sensor system is shown in Figure 4.4.

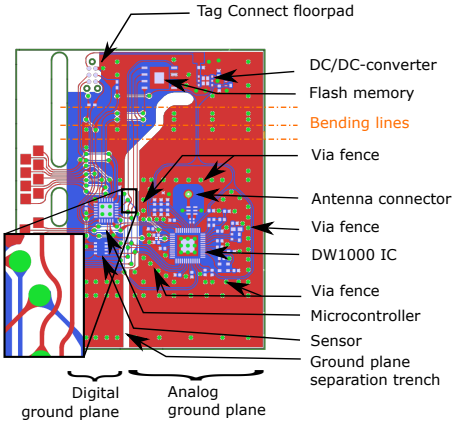

(a) Top plane (red) and ground plane (blue). Some horizontal bending lines are highlighted in orange.

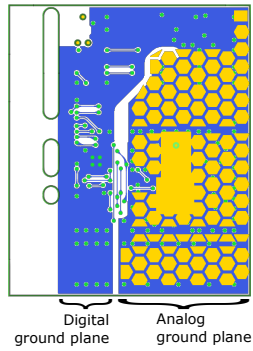

(b) Ground plane (blue) with conductive surface plating (yellow).

Figure 4.3: Layout of the Printed Circuit Board (PCB), top view.

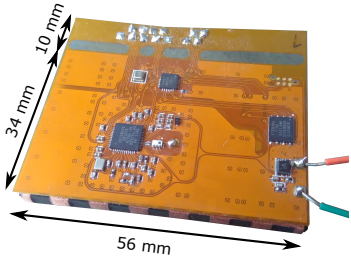

(a) Sensor node, flexible PCB side.

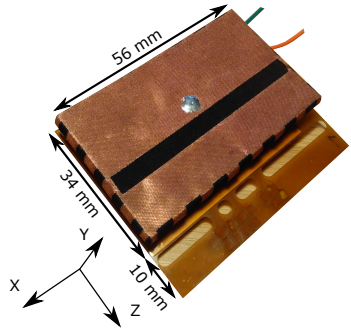

(b) Sensor node, antenna side.

Figure 4.4: Assembled sensor node. The flexible PCB is attached to the back of the antenna. The H-plane corresponds with the XY-plane, and the E-plane is oriented along the YZ-plane. The size of the antenna is 56 mm × 34 mm. An appendage of width 10 mm has been provided for testing purposes.

4.2.5 Localization Methodologies

As of today, a multitude of localization algorithms exist. To localize mobile tags, the Two-Way Ranging (TWR) approach is the preferred choice. Here, the mobile tag initiates communication by sending the first message to the anchor, which replies

with a message at a set amount of time after reception of the first packet. Based on the time between the transmission of the first packet and reception of the second packet (the so-called round trip delay), the distance between the tag and the anchor node can be calculated. Repeating this process with different anchor nodes provides multiple distance measurements, which in turn can be used to localize the mobile tag. In contrast to, for example, the Time-Difference of Arrival (TDoA) or Time of Arrival (ToA) [8], TWR does not require accurate synchronization between the sensor node and the other localization infrastructure to produce a suitable localization result. By measuring the round-trip delay, TWR avoids this issue, which would otherwise be highly impractical for body-worn localization. TWR has as a further advantage that two nodes can range with each other (proximity detection) without using any external infrastructure. Furthermore, TWR schemes such as Symmetric Double-Sided TWR (SDS-TWR) exhibit excellent resistance against clock-induced ranging errors [13], [34]. A disadvantage of TWR in comparison to TDoA- or ToA-based methods is that more messages are required and more complex hardware are needed at the target node. However, this is not prohibitive, and since the need for synchronization between tag and anchor nodes is nonexistent, multi-antenna TWR-based schemes are the preferred choice for body-worn UWB localization.

TWR schemes are perfectly compatible with the IEEE802.15.4-2011 standard used by the DW1000 IC. The standard is an attractive choice for wireless sensor networks (WSNs), since these networks are generally deployed with a large number of nodes (hundreds or even thousands). In addition, having low-cost nodes with long battery lifetime is even more attractive in body-worn systems than it already was for WSNs in general.

4.3 Results

This section discusses the experiments that validate the performance of both the antenna and the complete sensor system with the flexible PCB integrated on the antenna's backplane. Section 4.3.1 elaborates on measurements relevant to localization performance that can only be acquired by investigating the antenna itself, such as system fidelity factor (SFF) and distance estimation error. They are therefore performed in free space. Other system parameters can be obtained from the complete sensor system and are presented in Section 4.3.2. Here, the influence of the presence of a PCB is illustrated by measurement of the power pattern of the PCB, which employs the textile antenna to transmit in continuous wave mode. The system's performance in body-worn scenarios was then validated by deploying the wireless sensor node in a body-worn positioning experiment. Finally, the system's power use and the consequences for body-worn design were investigated.

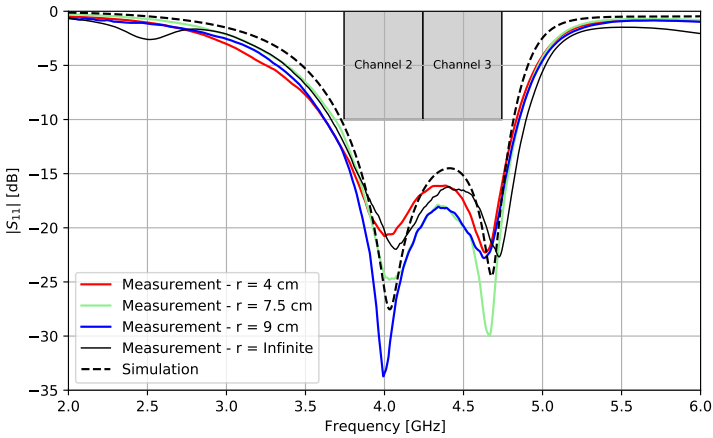

Figure 4.5: Magnitude of the simulated and measured reflection coefficient S_{11} of the cavity-backed slot antenna as a function of the frequency while subject to mechanical bending along the x-axis in the H-plane and for different bending radii r, frequently encountered on the human body.

4.3.1 Standalone Antenna

A prototype of the cavity-backed slot antenna was realized, containing an SMA connector through which its reflection coefficient S_{11} was measured. Figure 4.5 compares the magnitude of the free-space-measured reflection coefficient with the simulated one as a function of the frequency. The antenna was also measured under mechanical bending along the x-axis in the H-plane and with bending radii r, frequently encountered on the human body. It can be concluded that the antenna is mechanically flexible because the antenna characteristics under bending are similar to the case without bending (indicated as r = infinite). In both the measurements and the simulation, Channels 2 and 3 of the IEEE 802.15.4-2011 were also entirely covered.

Electromagnetic field-based UWB link simulations from [26] showed that a system in which this antenna is used both as transmitter and receiver provides a system fidelity factor larger than or equal to 90% for all directions within 60° of the antenna's broadside. This means that the pulse distortion introduced by this system remains sufficiently low to allow the localization IC to accurately timestamp the incoming pulse. Furthermore, simulations from [26] predicted that, for these directions, the DEE as a function of incident angle remains in the order of 5 cm. Novel free-space measurements on this antenna confirm that these criteria were met. To prove this, the Orbit/FR DBDR antenna positioning system (MVG, 75005 Paris, France, `http://www.orbitfr.com/`, accessed on 12 November 2020) and an Agilent N5242A PNA-X Microwave Network Analyzer (Agilent Technologies, Santa

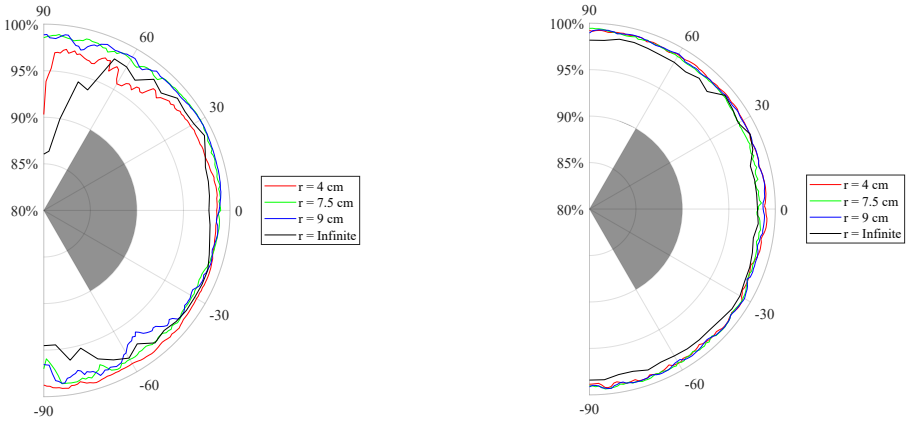

(a) Azimuth plane (XY-plane).

(b) Elevation plane (YZ-plane).

Figure 4.6: Measured System Fidelity Factor (SFF) of the standalone antenna as a function of the respective angle. Different bending radii r, frequently encountered on the human body, are applied. As a reference, the SFF $>$ 90% goal is marked in grey.

Clara, CA 95051, USA, `https://www.agilent.com/`, accessed on 12 November 2020) [35] were used to obtain the transfer function of the measurement setup, where one port was set at the input connector of the transmit antenna under test and the other port was positioned at the output connector of an identical receive antenna.

The receive antenna was rotated in its H-plane and E-plane, as shown in the top view on Figure 4.2, to record the transfer function of the entire system for every investigated position in a frequency band stretching from 1 GHz to 18 GHz with a step size of 50 MHz. The system impulse response was then found by Fourier transforming this transfer function. Next, as an input signal $T_s(t)$, the default output pulse of the DW1000 localization IC when operating in Channel 2 was selected. This input signal was then convoluted with the impulse response obtained from the aforementioned measurements, resulting in the pulse $R_s(t)$ as obtained at the port of the receive antenna. Finally, the SFF was obtained by taking the maximum of the normalized cross correlation of both signals, as described in [36]. Figure 4.6 shows the resulting SFF as a function of the respective rotation angle. To prove the mechanical flexibility, the antenna was subjected to mechanical bending along the x-axis in the H-plane and with different bending radii r, frequently encountered on the human body. It is clear that, for all directions within 60° of the antenna's broadside, the SFF stays well above 90%.

The time index at which the maximum of the normalized cross correlation of both signals is obtained depends on the relative orientation between the transmit and

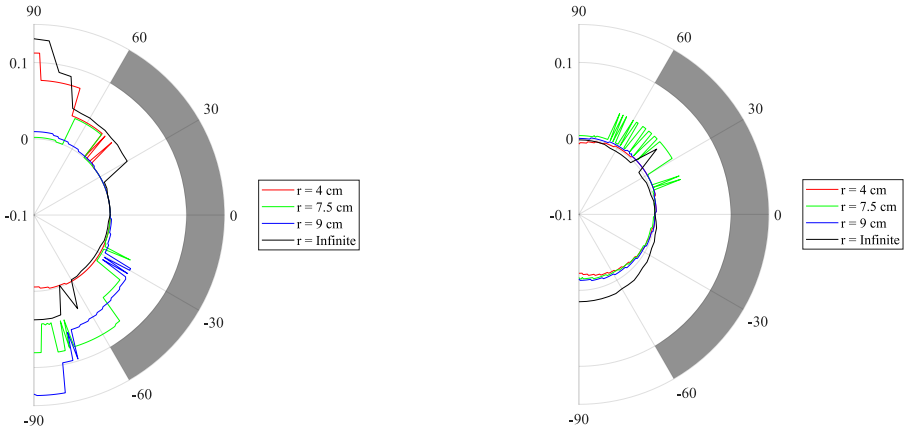

(a) Azimuth plane (XY-plane).

(b) Elevation plane (YZ-plane).

Figure 4.7: Measured Distance Estimation Error (DEE) (m) of the standalone antenna as a function of the respective angle. The broadside of the antenna radiation pattern is defined as having 0 cm deviation. Different bending radii r, frequently encountered on the human body, are applied. As a reference, the DEE $<$ 10 cm goal is marked in grey.

receive antennas. Therefore, as this time index defines the time of arrival of the signal pulse, the antenna orientation causes a distance estimation error. Figure 4.7 reveals that, in both investigated slices, for all directions within 60° of the antenna's broadside and for the same bending radii r, the maximum distance estimation error introduced by the antenna remains below the 5 cm predicted by simulations, which is smaller than the targeted 10 cm positioning error as generated by the DW1000 IC itself [13].

A comparison of UWB textile antennas is provided in Table 4.1. This table shows conventional antenna parameters as well as system-level parameters relevant to positioning, such as the pulse distortion, quantified by either the fidelity factor or the System Fidelity Factor (SFF) [37], dependent on the originally provided parameter. The proposed antenna has a lower impedance matching bandwidth in comparison to the other cited works, which are designed to cover the entire Federal Communications Commission (FCC) band. Nevertheless, it is sufficient to cover two IEEE802.15.4 UWB channels, while the antenna's radiation efficiency is significantly better and exhibits a stable radiation pattern in proximity of the human body. Furthermore, the proposed antenna features excellent pulse distortion behavior.

Table 4.1: Comparison with other UWB antennas throughout literature.

Ref.	Antenna topology	Maximum gain	Impedance match [GHz]
[38]	Arc-shaped patch	6 dBi	3.8–6, 6.6–8.3, 8.6–9.8
[39]	Octagonal monopole	1.1–7.2 dBi	3.2 –>11
[40]	Annular slot	not evaluated	3.2–9.9
[41]	Splined monopole	5 dBi	3 –>16
This antenna	Cavity-backed slot antenna	>6.4 dBi	3.7–4.8
Ref.	**Fidelity in free space**	**Approx. -3dB beamwidth**	**Antenna efficiency**
[38]	0.78–0.92 (SFF)	30°–60°	20–40%
[39]	>96% (SFF)	<20°–70°	not evaluated
[40]	80–100% (FF)	60°–140°	not evaluated
[41]	not evaluated	80°– omnidirectional	5–40%
This antenna	>97% (SFF)	75°–95°	78–91%

4.3.2 System Performance

This section examines the measurements where the flexible PCB is integrated on the backplane of the adjusted textile antenna discussed in Section 4.2.3. Section 4.3.2 elaborates on the measured power pattern of the system and compares it to the radiation pattern of the standalone antenna. The results of the body-worn positioning experiment are shown in Section 4.3.2. Finally, the measured energy consumption of the system and the effect of power saving measures on battery life are discussed in Section 4.3.2.

Radiated power pattern

The measurement results from [26] show that the standalone antenna possesses a single-lobe directional radiation pattern with a front-to-back ratio (FTBR) between 11.0 dB and 11.2 dB over the 3744 MHz to 4243.2 MHz band, which forms

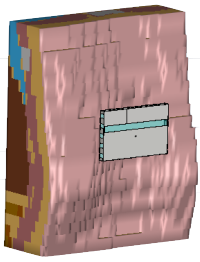

(a) Selected Gustav human body model slice.

(b) Complete Gustav human body model. The location of the selected slice is outlined in dark blue.

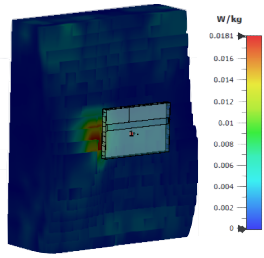

(c) Simulated SAR in the selected slice.

Figure 4.8: SAR simulation on CST's Gustav human body model [42]. As can be seen from Figure 4.8c, the maximum SAR value (red) amounts 0.0181 W/kg, which is well below the legal 2 W/kg limit.

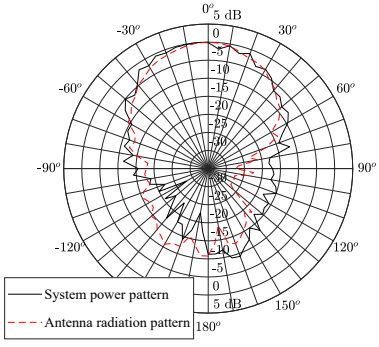

(a) Azimuth plane (XY plane).

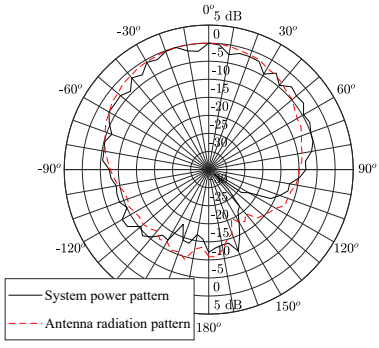

(b) Elevation plane (YZ plane).

Figure 4.9: Received radiation pattern (black line) when the DW1000 is configured in continuous wave mode in Channel 2 overlayed with the measured radiation pattern published in [26] (dashed red line). For comparison, both patterns are normalized to 0 dB broadside gain.

Channel 2 of the IEEE 802.15.4-2011 standard. A body-worn antenna design should strive for a high FTBR, since increasing the antenna's FTBR reduces the amount of energy which is directed towards the wearer's body. Therefore, it also reduces the amount of energy which is absorbed into bodily tissues, as expressed by the SAR. The maximum energy transmitted by the DW1000 localization IC is legally constrained to -41.3 dBm/MHz [43], which results in the IC emitting a maximum total power of 0.037 mW in one channel. Figure 4.8 shows the result of a SAR simulation performed on a slice of the CST Gustav human body model. The system's power pattern and its total radiated power already indicate that the SAR value of this system will be adequately low. The maximum SAR value found in this simulation equals 0.0181 W/kg, which is distinctly below the legal 2 W/kg SAR benchmark. We now verify whether the radiation pattern of the sensor system integrated on the backplane of the adjusted textile antenna possesses a similar FTBR, which is most desirable in WBAN systems, as motivated in Section 4.2.3. Therefore, the DW1000 IC was configured to transmit in continuous wave mode in Channel 2. The system is then placed on the rotor mount of an Orbit/FR DBDR antenna positioning system and measured using a R&S 1093.44995K07 FSV spectrum analyzer, resulting in the normalized power pattern shown in Figure 4.9. The power pattern is directive with a maximum along the (−5°;0°) azimuth-elevation direction, with a FTBR of 11.2 dB. The smoothed beam pattern's 3 dB beamwidth measures 90° in the elevation slice and 55° in the azimuth slice. Figure 4.9 further exhibits a clear similarity between the normalized power pattern of the complete system, shown in Figure 4.4b, and the normalized radiation pattern of the standalone textile antenna in [26]. Combined with the limited influence of human body proximity on the radiation pattern of cavity-backed slot antennas [24], this similarity leads to the conclusion that the system is suitable for deployment on a human body. Therefore, the system should be able to reliably connect to any external localization infrastructure, which is further investigated in Section 4.3.2.

Body-Worn Positioning Experiment

A body-worn localization system should be able to provide adequate quality-of-service, regardless of the user's orientation with respect to the surrounding localization infrastructure. Inevitably, due to the body shadowing effect and given that the system employs a directional antenna optimized to counter this effect, not all anchor positions can be reached simultaneously by the same antenna. Therefore, multiple antenna positions on the wearer's body should be used [44], as every direction around the user's body must be serviced by at least one body-worn antenna element for all positions and orientations that the user might be in. To investigate this, a system consisting of multiple wearable sensor nodes was deployed at diverse locations around the waist of a male test person having a size of 1.90 m and a mass of 85 kg. This is described in Figure 4.10. Figure 4.10a shows the layout of the experimental setup. Note that both anchor nodes positioned on the bottom of the figure each contain two anchor nodes, located on top of each other, approximately 2.2 m apart. The precise locations of all anchor nodes, in-

Table 4.2: The positions of the anchor nodes shown in Figure 4.10a with respect to the measurement space center.

Device	x [mm]	y [mm]	z [mm]
Anchor Wall Bottom Right	-3980	5302	440
Anchor Wall Bottom Left	3886	5318	439
Anchor Wall Top Right	-3980	5302	2647
Anchor Wall Top Left	3886	5318	2653
Anchor Tripod Mounted	-164.6	1504.6	1205.4
Device	x [mm]	y [mm]	z [mm]
Sensor system, body-worn	-100	-3000	1200

cluding the tripod mounted anchor, are constant throughout all experiments and have been determined using the MOCAP system [45]. They are described in Table 4.2. Figure 4.10b elaborates on the angles used to describe the positioning experiment. The angle between the user's anterior direction and the direction of the tripod is given by α. The position of the textile antenna on the user's body is characterized by the angle ϕ between the user's anterior direction and the textile antenna's broadside direction.

To facilitate testing, the system is attached to a belt, as shown in Figure 4.11a, allowing it to be shifted around the test person's waist between the different body-deployment locations under study visualized in Figure 4.11b. At a distance of 4.53 m to the test person, an anchor node was mounted on a tripod. The sensor system was then implemented as a tag in the WiPos (Wireless Positioning) system [46]. It periodically transmited a packet every 67 ms using the configurations listed in Table 4.3.

Practical scenarios often involve anchor nodes that are deployed close to the ground or above its users' heads. Table 4.2 shows that, in the WiPos test setup, anchor nodes were deployed at such locations. If the vertical plane beamwidth of the textile antenna of the body-worn wireless sensor node are too narrow, approaching these anchor nodes could induce connectivity loss since it would set up a wireless link with the anchor nodes along a direction where the textile antenna's gain is low. Therefore, the antenna is deployed such that its E-plane, with a smoothed beamwidth of 90°, coincides with the vertical plane, since Figure 4.9 shows that the antenna's E-plane beamwidth is larger than its H-plane beamwidth, which equals 55°. The measurements reveal that the minimum horizontal distance between the sensor system and the aforementioned anchor nodes in which a connection can be maintained equals zero.

Furthermore, in a practical application, every wireless sensor node's position is responsible for covering an azimuthal section of the wearer's surroundings. The nodes' deployment positions should be chosen such that these sections provide connectivity with external hardware over the full 360° of azimuthal coverage around

Table 4.3: Settings used in the on-body positioning experiment.

Parameter	Setting
UWB Channel	2
Bitrate	850 kbps
Pulse Repetition Frequency (PRF)	64 MHz
Preamble length	1024
Preamble code	10

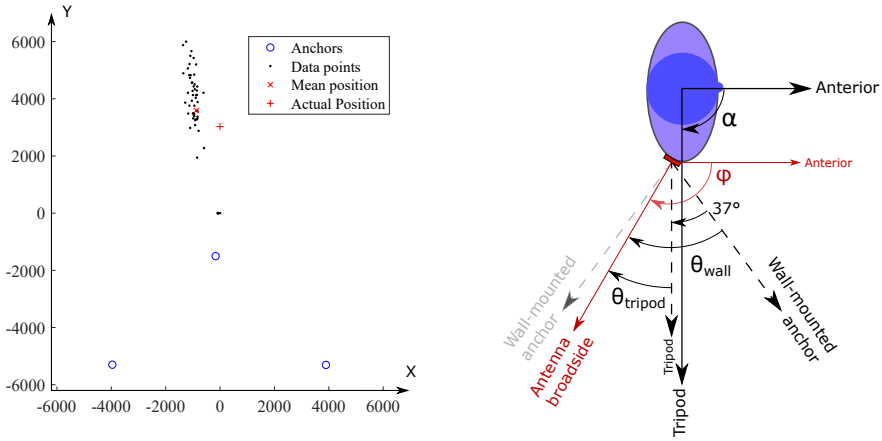

(a) (b)

Figure 4.10: Body-worn positioning experiment. α is the angle between the user's anterior direction and the direction of the tripod. ϕ is the angle between the user's anterior direction and the textile antenna's broadside orientation. (**a**) Anchor and test subject (not to scale) positions in mm with the anchor positions displayed as blue circles. Both anchors at the highest Y coordinate consists of two anchor nodes stacked on top of each other. For exact coordinates, please refer to Table 4.2. (**b**) Investigation of connectivity between the tripod mounted anchor and the sensor module. The sensor module was deployed at the body position characterized by $\phi = 120°$. The tripod mounted anchor is located in the azimuthal direction for which $\alpha = 90°$. The antenna's broadside deflection with respect to the tripod mounted anchor is therefore $\theta_{tripod} = +30°$. The precise locations of the anchors are given in Table 4.2.

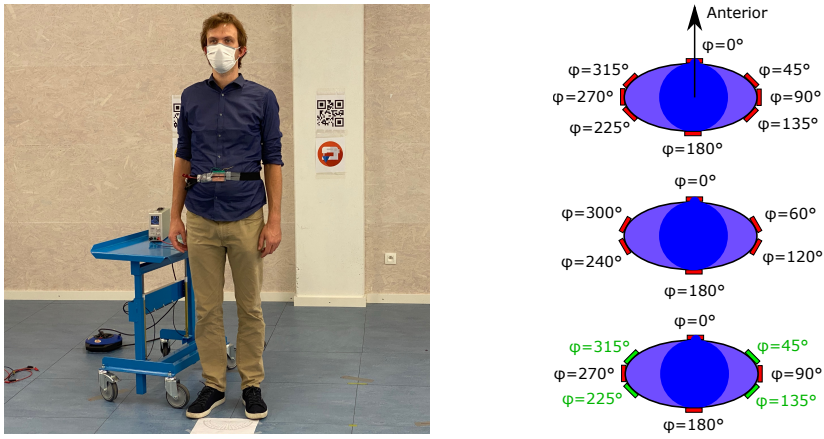

(a) (b)

Figure 4.11: Deployment on the user's body. (**a**) Test subject fitted with the belt hosting the sensor node. This is the on-body deployment position for $\phi = 0°$. The system is powered by an external power source for measurement purposes. (**b**) Some scenarios for 8 (top), 6 (middle), and 4 (bottom) body-deployment positions. Two possible configurations for 4 body-deployment positions are provided.

the wearer. To verify this for any chosen deployment position, the connectivity should be investigated not only for the case in which the antenna's broadside is directed towards the tripod-mounted anchor but also for when the broadside points away from the tripod's direction at an azimuthal deflection angle θ_{tripod}, as displayed in Figure 4.10b. In this experiment, a value $\theta_{tripod} = 30°$ in both directions is investigated. When the sensor system is placed at a position for which $\phi = 0°$, as illustrated in Figure 4.11b, the maximum value for θ at which connectivity is maintained is found to be slightly larger than 60°.

To quantify the number of body-deployment positions necessary to provide connectivity in all directions around the user, the fraction of packets received by the tripod mounted anchor with respect to the packets sent by the sensor node was investigated. Therefore, the wireless sensor node was deployed at the different body positions shown in Figure 4.11b. Table 4.4 lists the percentage of packets received by the tripod mounted anchor when the textile antenna's broadside was directed towards the tripod ($\theta_{tripod} = 0°$) or was azimuthally deflected 30° away from it ($\theta_{tripod} = \pm 30°$). For every measurement, the test subject was moved to ensure that the wireless sensor node was located at the coordinates specified in Table 4.2. As Table 4.4 shows, the user's arms shadow the sensor node for the body positions associated with $\phi = 120°$ and $\phi = 240°$, although connectivity data for the positions associated with $\phi = 135°$ and $\phi = 225°$ strongly suggests the viability of solutions with only 6 deployment positions. However, using 8 body-deployment positions distributed evenly around the test person's waist is sufficient to provide

Table 4.4: Percentage of packets received by the anchor on the fixed tripod mount for different body-deployment positions characterized by ϕ and for different deflections θ_{tripod} between the textile antenna's broadside orientation with respect to the direction of the tripod mount. As visualized in Figure 4.10b, the test person was oriented such that $\alpha = \phi - \theta_{tripod}$.

	6 Body positions					
	Percentage of packets received			Number of sent packets		
ϕ \ θ_{tripod}	-30°	0°	30°	-30°	0°	30°
0°	100.00%	100.00%	100.00%	184	334	152
60°	100.00%	100.00%	100.00%	112	200	149
120°	62.89%	0.00%	0.00%	97	69	101
180°	100.00%	100.00%	100.00%	114	115	175
240°	0.00%	100.00%	100.00%	141	123	123
300°	100.00%	100.00%	100.00%	132	157	129

	8 Body positions					
	Percentage of packets received			Number of sent packets		
ϕ \ θ_{tripod}	-30°	0°	30°	-30°	0°	30°
0°	100.00%	100.00%	100.00%	184	334	152
45°	100.00%	100.00%	100.00%	148	189	140
90°	0.00%	100.00%	100.00%	117	150	145
135°	100.00%	100.00%	100.00%	81	79	116
180°	100.00%	100.00%	100.00%	114	115	175
225°	100.00%	100.00%	100.00%	131	140	90
270°	100.00%	100.00%	99.24%	161	108	131
315°	100.00%	100.00%	100.00%	171	164	164

coverage in all directions. Indeed, Table 4.4 shows that all deployment positions with a broadside direction in which the sensor system fails to connect with the tripod mounted anchor are backed up by a successful connection from the neighboring deployment position. For example, an anchor node positioned such that $\alpha = 120°$ is not serviced by a sensor node placed at the body position associated with $\phi = 90°$, since in this position, Table 4.4 reveals that, for $\theta_{tripod} = -30°$, no packets have been received. However, the neighboring body-deployment position, where $\phi = 135°$, provides coverage over all investigated θ angles, which include the direction for which $\alpha = 120°$. Therefore, it covers this direction, which was shadowed for the $\phi = 90°$ body-deployment position.

When considering solutions with fewer than 6 body-deployment locations, the azimuthal sections that need to be covered by each body-deployment position become wider than the 60° coverage, represented by the data provided in Table 4.4.

Table 4.5: Percentage of transmitted packets received by the two wall-mounted anchor nodes located in the opposite direction of the textile antenna's broadside rotation for different body-deployment positions. With respect to the user's anterior direction, the connectivity directions α represented by these wall anchors are given by $\alpha = \phi - \theta_{wall}$, as can be seen on Figure 4.10b. The table shows that no combination of fewer than 6 body-deployment locations ϕ can be found in which the node can make a reliable connection with the anchors deployed in all investigated elevation angles.

	Percentage of packets received			
θ_{wall}	$-67°$		$67°$	
Receiving anchor / ϕ	Top Right	Bottom Right	Top Left	Bottom Left
0°	1,11%	95,58%	0,00%	0,00%
45°	21,92%	97,26%	0,00%	12,50%
60°	0,00%	17,27%	0,00%	0,00%
90°	0,00%	0,00%	80,28%	100,00%
120°	3,19%	56,38%	0,00%	0,00%
135°	90,91%	98,70%	0,00%	0,00%
180°	0,00%	0,90%	0,00%	85,55%
225°	0,00%	0,00%	0,00%	96,51%
240°	0,00%	0,00%	95,83%	100,00%
270°	0,00%	30,82%	0,00%	0,00%
300°	78,46%	99,23%	0,00%	0,00%
315°	36,53%	97,62%	0,00%	32,92%

However, Table 4.2 and Figure 4.10 reveal the presence of four other anchor nodes in the Y direction at an azimuth angle of ±37° from the tripod direction. Therefore, the azimuthal difference between the antenna's broadside direction and the direction of these wall-mounted anchor nodes visualized in Figure 4.10b totals $\theta_{wall} = \theta_{tripod} + 37°$. This provides extra connectivity data, presented in Table 4.5. Here, for all investigated body-deployment locations, the fraction of the amount packets received on the two wall-mounted anchor nodes located at an azimuthal deflection $\theta_{wall} = 67°$ with respect to the textile antenna's broadside direction, is displayed. From Table 4.5, no suitable combination of fewer than 6 body-deployment locations can be found that provide coverage for all directions around the user. To qualify a body-deployment position for a certain ϕ as suitable, the connectivity between the anchor nodes and the sensor system should be reliable for all investigated elevation angles.

Power Use

Since battery capacity takes up a lot of the available weight and space budget in a body-worn scenario, efficient power use is of great importance. Given that the DW1000 localization IC also acts as a transceiver, this component will be the most important consumer of power. Considering that the DC/DC converter exhibits an efficiency higher than 90% under the operating conditions [47] and that the other components' power consumptions are dwarfed by that of the DW1000's transceiver [27]–[29], it is primarily the duty cycle at which the DW1000's transceiver is active, for example, by sniffing for packets, which determines the system battery's lifespan. It is, therefore, necessary that a practical system would employ a timeslot-based communication schedule, as is required by the IEEE 802.15.4a standard.

To provide a few measured indicative values for autonomy of the system, the system was configured in some representative scenarios, which are summarized in Table 4.6. In all scenarios, the DW1000 localization IC is configured according to the settings listed in Table 4.3. The device operates in Channel 2 of the IEEE 802.15.4-2011 standard. In the first scenario from Table 4.6, the system was configured in its most power-hungry state. Intentionally, none of the power-conserving mechanisms and methods suggested by the manufacturer were applied, which results in the microcontroller returning the localization IC to the receive mode immediately after it completed a packet reception. In this worst-case setting, the system spends 700 mW of power. Currently, available flexible batteries [48] with a capacity of 200 mAh and a footprint comparable to this system would make the system last for only 1.42 h. Clearly, a degree of power conservation should be applied for practical application of the system. The second scenario from Table 4.6 is the standby situation: all peripheral components are powered up but idle. The microcontroller internally performs operations. Table 4.6's third scenario constitutes a basic use of the localization IC, where it periodically transmits dummy payloads of 17 bytes long at an interval of 16 packets per second. The table shows that the difference in the system's measured average current is below 1 mA, as measured on the power supply. On a 200 mAh battery, this provides to the system an autonomy of 13.3 h, even without the use of any component's sleep mode. To further limit power use, UWB Medium Access Control (MAC) protocols such as [49] can be applied, which further save power by periodically disabling the UWB radio. As such, 13.3 h is still a pessimistic value, leading to the conclusion that the system's power use is suitable for a WBAN system.

4.4 Conclusion

A complete and mechanically flexible wireless body area network sensor system was proposed. The system consists of a full-textile cavity-backed slot antenna designed for use in Channels 2 and 3 of the IEEE 802.15.4-2011 standard. By measuring the impulse response of the measurement setup containing two standalone

Table 4.6: System power use in various scenarios and associated lifetime on a 5 V, 200 mAh battery.

Scenario	Measured average current	Battery power use	Battery lifetime
Continuous RX	140 mA	700 mW	1.42 hrs
Microcontroller active, DW1000 idle	15 mA	75 mW	13.3 hrs
Microcontroller active, DW1000 transmitting at 16 packets/s	15 mA	75 mW	13.3 hrs

antennas, the system fidelity factor was proven to be well above the 90% criterion commonly used in localization. Furthermore, the distance estimation error, resulting from the angle-dependent phase difference between a wave incoming from broadside with respect to a wave incoming from a given incident angle, proves to be below 5 cm in both the azimuth plane and the elevation plane of the antenna. This is lower than the error introduced by the localization IC. The antenna was modified slightly to enable on its feed plane the integration of a mechanically flexible PCB, which hosts a temperature, relative humidity, and air pressure sensor; a DW1000 Impulse-Radio Ultra-Wideband localization IC; and a 4 MB flash memory. Measurements in which the transceiver was configured in continuous wave mode prove that the presence of the PCB on the feed plane of the antenna has little influence on the antenna's radiation pattern. A directive power pattern with a front-to-back ratio of 11.2 dB was obtained. Its shape is very similar to the radiation pattern of the standalone textile antenna. The antenna's directive radiation pattern requires it to be deployed at multiple deployment locations on the wearer's body. By relying on eight deployment positions, coverage in all directions is provided with ample redundancy. The measurements suggest that six deployment positions suffice as well if these positions are chosen carefully, to avoid shadowing by the wearer's arms. Configurations with fewer deployment positions were proven not to be feasible. Analysis of the localization accuracy of a system employing multiple collaborating nodes, along with a formal investigation of optimal body-deployment positions are outside the scope of this chapter. They will be considered in future research. The power use of the complete sensor system heavily depends on the duty cycle at which the transceiver is activated. In a worst-case testing scenario in which 16 packets per second were sent, the measurements indicate that a system autonomy of 13.3 h can be obtained from a 5 V, 200 mAh flexible battery. The innovations in this chapter include the co-design of a low-power, comprehensive mechanically flexible PCB featuring both digital and time-domain-sensitive analog parts with a mechanically flexible textile antenna for UWB localization. Furthermore, the suitability of full-textile cavity-backed slot antennas for localization purposes was demonstrated by measurement of both the antenna's pulse distortion and phase center shift. This system acts as a proof of concept for

the implementation of electronics for localization in a complete and fully flexible sensor system in textile.

References

[1] M. U. H. Al Rasyid, F. A. Saputra, and A. Christian, "Implementation of Blood Glucose Levels Monitoring System Based on Wireless Body Area Network", in *In Proceedings of the 2016 IEEE International Conference on Consumer Electronics-Taiwan (ICCE-TW)*, Nantou, Taiwan, 27-29 May 2016, pp. 1–2.

[2] M. Hadjem, O. Salem, and F. Naït-Abdesselam, "An ECG Monitoring System for Prediction of Cardiac Anomalies Using WBAN", in *In Proceedings of the 2014 IEEE 16th International Conference on e-Health Networking, Applications and Services (Healthcom)*, Natal, Brazil, 15–18 October 2014, pp. 441–446.

[3] M. Roşu and S. Paşca, "A WBAN-ECG Approach for Real-Time Long-Term Monitoring", in *2013 8TH INTERNATIONAL SYMPOSIUM ON ADVANCED TOPICS IN ELECTRICAL ENGINEERING (ATEE)*, 2013, pp. 1–6.

[4] S. K. Gharghan, S. S. Fakhrulddin, A. Al-Naji, and J. Chahl, "Energy-Efficient Elderly Fall Detection System Based on Power Reduction and Wireless Power Transfer", *Sensors*, vol. 19, no. 20, p. 4452, Oct. 2019.

[5] C. Kamyod, "Low-Cost Falling Detection System", in *In Proceedings of the 2018 15th International Conference on Electrical Engineering/Electronics, Computer, Telecommunications and Information Technology (ECTI-CON)*, Chiang Rai, Thailand, 18–21 July 2018, pp. 784–787.

[6] M. Cicioğlu and A. Çalhan, "Performance Analysis of IEEE 802.15.6 for Underground Disaster Cases", *Comput. Stand. Interfaces*, vol. 66, p. 103 364, 2019.

[7] R. Mautz, *Indoor Positioning Technologies*, Habilitation Thesis, Eidgenössische Technische Hochschule (ETH) Zürich, Switzerland.

[8] F. Zafari, A. Gkelias, and K. K. Leung, "A Survey of Indoor Localization Systems and Technologies", *IEEE Communications Surveys Tutorials*, vol. 21, no. 3, pp. 2568–2599, 2019.

[9] "IEEE Standard for Local and Metropolitan Area Networks–Part 15.4: Low-Rate Wireless Personal Area Networks (LR-WPANs)", *IEEE Std 802.15.4-2011 (Revision of IEEE Std 802.15.4-2006)*, pp. 1–314, Sep. 2011.

[10] R. Kshetrimayum, "An Introduction to UWB Communication Systems", *IEEE Potentials*, vol. 28, no. 2, pp. 9–13, Mar. 2009.

[11] M. Sharma, *Ultra Wideband Wearable Sensors for Motion Tracking Applications*, Ph.D. Thesis, Queen Mary University of London, London, UK, 2015.

[12] M. Delamare, R. Boutteau, X. Savatier, and N. Iriart, "Static and Dynamic Evaluation of an UWB Localization System for Industrial Applications", *Science*, vol. 2, no. 2, p. 23, 2020.

[13] Decawave, "APS003 Application Note Real Time Location Systems An Introduction", Decawave Ltd, Adelaide Chambers, Peter Street, Dublin 8, Tech. Rep. 1.00, 2014.

[14] *DW1000 IEEE802.15.4-2011 UWB Transceiver*, 2.19, Decawave Limited, Adelaide Chambers, Peter Street, Dublin, D08 T6YA, Ireland, 2017.

[15] D. Dardari, A. Conti, U. Ferner, A. Giorgetti, and M. Z. Win, "Ranging With Ultrawide Bandwidth Signals in Multipath Environments", *Proc. IEEE*, vol. 97, no. 2, pp. 404–426, 2009.

[16] M. Z. Win and R. A. Scholtz, "On the Robustness of Ultra-Wide Bandwidth Signals in Dense Multipath Environments", *IEEE Commun. Lett.*, vol. 2, no. 2, pp. 51–53, 1998.

[17] Lopos. (Jul. 2020). "Social Distancing Under Control with UWB Localisation", [Online]. Available: `http://www.lopos.be/en/`.

[18] P. Hindermann, S. Nuesch, D. Fruh, A. Rust, and L. Gygax, "High Precision Real-Time Location Estimates in a Real-Life Barn Environment Using a Commercial Ultra Wideband Chip", *Comput. Electron. Agric.*, vol. 170, 1–9, Feb. 2020.

[19] K. Ren, J. Karlsson, M. Liuska, M. Hartikainen, I. Hansen, and G. H. M. Jørgensen, "A Sensor-Fusion-System for Tracking Sheep Location and Behaviour", *Int. J. Distrib. Sens. Netw.*, vol. 16, no. 5, p. 155 014 772 092 177, 2020.

[20] S. Benaissa, F. Tuyttens, D. Plets, J. Trogh, L. Martens, L. Vandaele, W. Joseph, and B. Sonck, "Calving and Estrus Detection in Dairy Cattle Using a Combination of Indoor Localization and Accelerometer Sensors", *Comput. Electron. Agric.*, vol. 168, p. 105 153, 2020.

[21] M.-G. Li, H. Zhu, S.-Z. You, and C.-Q. Tang, "UWB-Based Localization System Aided With Inertial Sensor for Underground Coal Mine Applications", *IEEE Sens. J.*, vol. 20, no. 12, 6652–6669, 2020.

[22] M. Ridolfi, S. Vandermeeren, J. Defraye, H. Steendam, J. Gerlo, D. De Clercq, J. Hoebeke, and E. De Poorter, "Experimental Evaluation of UWB Indoor Positioning for Sport Postures", *Sensors*, vol. 18, no. 2, p. 168, 2018.

[23] K. Minne, N. Macoir, J. Rossey, Q. Van den Brande, S. Lemey, J. Hoebeke, and E. De Poorter, "Experimental Evaluation of UWB Indoor Positioning for Indoor Track Cycling", *Sensors*, vol. 19, no. 9, p. 2041, 2019.

[24] D. Van Baelen, S. Lemey, J. Verhaevert, and H. Rogier, "A Novel Manufacturing Process for Compact, Low-Weight and Flexible Ultra-Wideband Cavity Backed Textile Antennas", *Materials*, vol. 11, no. 1, p. 17, 2018.

[25] Q. Van den Brande, S. Lemey, J. Vanfleteren, and H. Rogier, "Highly Efficient Impulse-Radio Ultra-Wideband Cavity-Backed Slot Antenna in Stacked Air-Filled Substrate Integrated Waveguide Technology", *IEEE Trans. Antennas Propag.*, vol. 66, no. 5, pp. 2199–2209, 2018.

[26] D. Van Baelen, Q. Van den Brande, S. Lemey, J. Verhaevert, and H. Rogier, "Foldable All-Textile Cavity-Backed Slot Antennas for Personal UWB Localization", *Radio Sci.*, vol. 55, no. 3, pp. 1–11, Feb. 2020.

[27] *BME280 Combined Humidity and Pressure Sensor*, Bosch Sensortec.

[28] *C8051F93x-C8051F92x*, 1.4, Silicon Laboratories Inc., 400 West Cesar Chavez Austin, TX 78701 USA, 2016.

[29] *AT45DB321E*, Adesto Technologies, Adesto Headquarters 1250 Borregas Avenue Sunnyvale, CA 94089, 2013.

[30] *Footprint for TC2030-MCP-NL Plug-of-nails (TM) Cable*, Tag-Connect, 433 Airport Blvd, Suite 323 Burlingame, CA 94010 USA, 2010.

[31] J.-S. Hong and M. J. Lancaster, "Couplings of Microstrip Square Open-Loop Resonators for Cross-Coupled Planar Microwave Filters", *IEEE Trans. Microw. Theory Tech.*, vol. 44, no. 11, pp. 2099–2109, Nov. 1996.

[32] *Multilayer Balun - for 3000-8000 MHz HHM1595A1*, TDK, Apr. 2015.

[33] J. Fjelstad, *Flexible Circuit Technology*, 4th ed., Seaside, OR USA: BR Publishing, Inc., 2011.

[34] Nanotron Technologies GmbH, *Symmetrical Multipath Method for Determining the Distance Between Two Transceivers*, 2015.

[35] *N5242A PNA-X Microwave Network Analyzer, 26.5 GHz*, Keysight Technologies, 2017.

[36] G. Quintero, J.-F. Zürcher, and A. K. Skrivervik, "System Fidelity Factor: A New Method for Comparing UWB Antennas", *IEEE Trans. Antennas Propag.*, vol. 59, no. 7, pp. 2502–2512, 2011.

[37] M. Koohestani, A. A. Moreira, and A. K. Skrivervik, "Fidelity Concepts Used in UWB Systems", in *In Proceedings of the 2014 IEEE Antennas and Propagation Society International Symposium (APSURSI)*. Memphis, TN, USA, 2014.

[38] R. B. V. B. Simorangkir, A. Kiourti, and K. P. Esselle, "UWB Wearable Antenna With a Full Ground Plane Based on PDMS-Embedded Conductive Fabric", *IEEE Antennas Wirel. Propag. Lett.*, vol. 17, no. 3, 493–496, 2018.

[39] L. A. Yimdjo Poffelie, P. J. Soh, S. Yan, and G. A. E. Vandenbosch, "A High-Fidelity All-Textile UWB Antenna With Low Back Radiation for Off-Body WBAN Applications", *IEEE Trans. Antennas Propag.*, vol. 64, no. 2, pp. 757–760, Feb. 2016.

[40] M. Klemm and G. Troester, "Textile UWB Antennas for Wireless Body Area Networks", *IEEE Trans. Antennas Propag.*, vol. 54, no. 11, 3192–3197, 2006.

[41] Y. Sun, S. W. Cheung, and T. I. Yuk, "Design of a Textile Ultra-Wideband Antenna with Stable Performance for Body-Centric Wireless Communications", *IET Microw. Antennas Propag.*, vol. 8, no. 15, 1363–1375, 2014.

[42] Dassault Systèmes, *Gustav human body voxel model*.

[43] *DW1000 User Manual*, 2.12, Decawave Limited, Adelaide Chambers, Peter Street, Dublin, D08 T6YA, Ireland, 2017.

[44] S. Lemey, S. Agneessens, and H. Rogier, "Wearable Smart Objects: Microwaves Propelling Smart Textiles: A Review of Holistic Designs for Wireless Textile Nodes", *IEEE Microw. Mag.*, vol. 19, no. 6, 83–100, 2018.

[45] *Qualisys Precision Motion Capture and 3D Positioning Tracking System*, `http://https://www.qualisys.com/`, Accessed: 2020-11-12.

[46] B. Van Herbruggen, B. Jooris, J. Rossey, M. Ridolfi, N. Macoir, Q. Van den Brande, S. Lemey, and E. De Poorter, "Wi-PoS : A Low-cost, Open Source Ultra-wideband (UWB) Hardware Platform with Long Range Sub-GHz Backbone", *Sensors*, vol. 19, no. 7, p. 16, 2019.

[47] *WPMDB1960501XF / 171960501*, 1.0, Wurth Elektronik eiSos GmbH & Co. KG, 2017.

[48] Shenzhen Grepow Battery Co., Ltd. (Aug. 2020). "A Review of Flexible Battery Manufacturers", [Online]. Available: `https://www.grepow.com/article/detail/a-review-of-flexible-battery-manufacturers.html`.

[49] N. Macoir, J. Bauwens, B. Jooris, B. Van Herbruggen, J. Rossey, J. Hoebeke, and E. De Poorter, "UWB Localization with Battery-Powered Wireless Backbone for Drone-Based Inventory Management", *Sensors*, vol. 19, no. 3, p. 467, 2019.

5 Conclusions and Outlook

5.1 General Conclusions

Smart textiles offer valuable opportunities to bridge the gap between the IoT and its human users. However, for the consumer to adopt electronic systems integrated into its garments, such systems need to be comfortable, unobtrusive and context-aware. Wide acceptance furthermore requires body-worn smart textile systems to be inexpensive, so the availability of low-cost production processes that create robust and reliable smart textile systems is essential.

Such a manufacturing methodology for the fabrication of full-textile cavity-backed slot antennas has been presented in Chapter 2. In comparison with previous fabrication methods, the methodology significantly reduces the chance for misalignments of the electrotextile planes. Furthermore, fewer fabrication steps are required, and the resulting antennas are considerably more lightweight and flexible. The manufactured prototypes are highly efficient and experience limited influence from body proximity or from mechanical bending. Therefore, the topology qualifies as a suitable choice for deployment on a human body.

In Chapter 3, the aforementioned fabrication process has been applied to realize a cavity-backed slot antenna for operation in Channels 2 and 3 of the IEEE802.15.4a standard. As could be expected from results from Chapter 2, measurements proved that the antenna has a low coupling with the human body and can be bent over diverse bending radii encountered on a person. Moreover, the antenna qualifies for use in a body-worn impulse-radio ultra-wideband localization system, since over all directions relevant to this scenario, system fidelity factor calculations showed that its orientation-specific pulse distortion is low, and its antenna's phase center is sufficiently stable over these angles. This is verified by measurements presented in Chapter 4. Therefore, this antenna design satisfies wearability constraints, com-

patibility with the body, and localization prerequisites, qualifying it as a suitable choice for body-worn localization.

A complete sensor system in textile has been developed in Chapter 4. The sensor node hosts both basic and more complex sensing electronic devices such as an environmental sensor and Decawave's DW1000 localization IC, with a microcontroller and a flash memory as a backbone. To maintain mechanical flexibility, the PCB has been implemented on a flexible polyimide substrate, which is attached to the back of the textile antenna proposed in Chapter 3 to reduce the surface occupied by the system on the garment. It is shown that the radiation pattern of the antenna experienced very little influence from the presence of the flexible PCB on its back plane. Since a body-worn antenna is unable to service all directions around the user due to body shadowing, multiple locations on the user's body need to be employed. By using six positions around the user's waist, external localization infrastructure is able to connect with the system from all azimuthal directions, without any minimum range. This experimentally proves the feasibility of the antenna for use in body-worn localization. Combining the antenna's favorable time-domain characteristics, its suitability for on-body operation, and the sensor system's already satisfactory power use in a worst-case scenario where no power saving measures have been taken, it can be concluded that this comprehensive sensor node qualifies as a body-worn localization system. Comparable systems enjoy a drastically reduced production cost when entering the stage of mass production. While the cost of such systems is heavily dependent on the desired functionalities, it will probably still be too large to allow commercial adoption of integration into everyday garments. However, prices comparable to present day sports wearables should be feasible, ranging from fifty to some hundreds of euros. This cost would make them perfectly suited for professional garments like those found in sectors such as industry, defense or medicine.

In this work, a practical demonstration of an unobtrusively wearable and energy-efficient sensor node has been discussed. It is a stepping stone, demonstrating the addition of sensor electronics and ultra-wideband localization functionality to the smart fabrics and interactive textiles (SFIT) technology.

5.2 Outlook

This dissertation encompasses one of the efforts that still needed to be undertaken before SFIT could have been adopted as a part of our everyday lives, and to allow it to form the natural link bridging the gap between the IoT and its users.

In this work, the required number of body deployment positions necessary to realize communication in all directions around the user has been discussed. Since using fewer antenna deployment positions results in a reduction in the cost and complexity of the body-worn system, a detailed investigation into optimal body deployment locations is appropriate. Since they experience no shadowing due to

other body parts, but still allow deployment in all azimuthal directions, the shoulders and upper arms of the user are promising candidates for this. It should be noted however that the antenna is linearly polarized. If the user lifts its arms, this might cause a polarization mismatch with the anchor antennas.

Where this work elaborates on the design of textile-compatible, mechanically flexible and complex electronic systems and the application of localization functionality therein, there still is a need for practical methods to integrate these systems and antennas into actual garments. The systems should be integrated such that they are securely affixed to the garment, but also so that they remain unobtrusive and mechanically flexible. Furthermore, the integration procedures should take lasting washability of such complete systems into account, thereby specifically asserting the washability of the electronic circuitry, the antenna, and the interconnects in between them. Possible solutions might include sewing the textile antenna system into the garment, or providing a lockable pocket to the inside of the garment, in which the system can then be placed.

A complete and commercially exploitable SFIT system should draw power from a flexible battery, which should possess an adequate autonomy. Furthermore, this battery should be rechargeable, since the connections required to couple and decouple the battery form extra failure points, and battery removal impedes true unobtrusive integration into the garment. Moreover, disposable batteries cause a lot of waste, which results in a negative environmental impact. Rechargeable batteries might not keep up with the large amount of recharging cycles required for a smart wearable. In this respect, further developments in the topic of flexible supercapacitors are a welcome sight. Power harvesting techniques may be applied to extend battery life, although a meaningful extension still comes at a significant increase in system cost or size. Furthermore, when using solar panels, the dependency on the presence of sunlight limits the applicability of the system. If large surfaces of the garment are required to host this infrastructure, the unobtrusiveness and wearability of the system may be impeded. An interesting option compatible with completely unobtrusive incorporation of all system components, is the integration of wireless power transfer (WPT) infrastructure in the smart textile, for example to allow the user to recharge the garment overnight by putting it in close proximity with a recharging station. Multiple planar WPT designs in textile are already presented in literature, promising the feasibility of integrating these functionalities in a garment.

In the meantime, the flexible electronic components technology is publishing interesting results. With unobtrusiveness and integrability in mind, such components would prove most valuable for application in smart textiles. In this way, the electric components from this dissertation, which are still rigid, could be made flexible as well. However, as long as the state-of-the-art does not yet support the higher frequencies encountered in modern consumer electronics, and until more complex flexible IC's become widely available, the added value of flexible electronic components to smart textile technology will prove to be limited.

The application of millimeter-wave technology also shows great promise for body-worn antenna design. Antennas realized for such frequencies generally exhibit footprints that are small enough to comfortably and unobtrusively fit onto any garment. Furthermore, even modest bandwidths ranging from 5% to 10% result in large bandwidth values in absolute units, which offers opportunities to realize IR-UWB localization systems. Yet, implementation of this is challenging on its own, since dedicated hardware is required, and the achievable range is smaller due to path losses. Under any circumstance, operation on these frequencies would fit in joining the body area network to 5G infrastructure, so its ultra high data rates and low latencies can readily be provided to the wireless body area network.

Finally, the weaving of basic sensor components into textile materials, which is already observed today, should be extended to more advanced electronic components with a comparatively larger footprint, such as microcontrollers.